High Performance, Robust Control
of Flexible Space Structures

(MSFC Center Director's Discretionary Fund Final Report,
Project No. 96–23)

National Aeronautics and
Space Administration

Marshall Space Flight Center

Acknowledgments

TABLE OF CONTENTS

TABLE OF CONTENTS (Continued)

LIST OF FIGURES

LIST OF FIGURES (Continued)

LIST OF TABLES

vii

TECHNICAL MEMORANDUM

HIGH PERFORMANCE, ROBUST CONTROL OF FLEXIBLE SPACE STRUCTURES
(MSFC Center Director's Discretionary Fund Final Report, Project No. 96–23)

1. INTRODUCTION

Where there is no vision, the people perish, Proverbs 29:18.

Throughout history, mankind's ambition has fueled a drive to explore. The last four decades in particular have seen a great expansion of technology brought about by the space program. Along with advances in technology comes the opportunity to expand our understanding of the universe which demands even greater advances in technology. To realize ambitious technical goals requires increasingly sophisticated spacecraft systems. One technology area that is especially challenging is pointing control systems for flexible space structures. Applications include space telescopes and interferometers, Earth-observing spacecraft, communications spacecraft, and military spacecraft such as space-based lasers and tracking systems. Control systems for flexible space structures must meet stringent performance requirements while being robust to model uncertainties. The topic of this dissertation is robust control system design for flexible space structures (FSS's) that achieve high performance on orbit.

1.1 Challenges of Flexible Space Structure Control

Vibration control of flexible spacecraft has motivated intense research in modern and robust control theory. In general, FSS's possess several pathologies that compound the difficulty of controller design. Light-weight, low-stiffness structures coupled with stringent pointing requirements result in numerous closely spaced, lightly damped vibrational modes within the controller bandwidth. A primary difficulty with control of FSS's is that accurate models of the on-orbit system are not typically available a priori. Successful implementation of a high-performance, on-orbit pointing control system requires integration of system identification and control system design in a form that facilitates iterative redesign, or "tuning," of the control system.

Recent experience with the Hubble Space Telescope (HST) serves to illustrate the need for on-orbit system identification and controller tuning.[2] After initial deployment, the HST experienced severe pointing disturbances due to thermal excitation of the solar arrays and the performance degradation was attributed to model errors. On-orbit test data were used to update the control design model for controller redesign. Incremental control augmentation in the form of forward path and inner loop feedback filters was employed with each subsequent retune phase exhibiting increasing levels of performance. However, this redesign effort took considerable time and a very substantial investment of manpower. Considerable savings could have been gained by a more efficient methodology for on-orbit control system redesign.

For many spacecraft, to obtain high-performance pointing control on orbit requires closed-loop system identification and controller refinement to improve performance. A methodical process for on-orbit tuning for flexible spacecraft must consist of five steps: (1) Empirical or analytical model development for initial control design; (2) low authority control design for robust stability; (3) closed-loop system identification to improve knowledge of the on-orbit plant dynamics; (4) controller refinement to increase control authority and improve performance; and (5) performance assessment. Steps (3)–(5) may be iterated until the desired controller performance is obtained.

Closed-loop system identification (step 3) is significant for a number of reasons. Typically, spacecraft cannot be tested on orbit in the open-loop manner. Also, open-loop modeling errors are not necessarily indicative of closed-loop robustness or performance.[3] For control system tuning with flexible spacecraft, the plant model should be obtained from closed-loop excitation in the orbital environment. A new procedure for closed-loop system identification is also presented which tunes the parameters of an open-loop (state space) control design model to better characterize the on-orbit dynamics.

Recent advancements in the field of robust multivariable control have provided a fruitful paradigm for on-orbit controller (step 4) tuning where the competing issues of performance and stability are explicitly addressed. Mixed H_2/H_∞ control theory is well suited to on-orbit controller tuning since the technique generates a set of controllers that trade between robustness and performance. The control formulation is such that the controller parameters are tuned to account for plant changes or varying performance requirements. Successive implementation of these controllers allows the compensator to be selected which achieves maximum performance in the presence of model errors. In this research effort, a homotopy algorithm was developed for synthesis of fixed-order, mixed H_2/H_∞ compensators.

1.2 Contributions

It is the goal of this dissertation to develop a control design and system identification procedure that achieves high performance while providing robust stability guarantees. Contributions of this research effort include the following:

1. This dissertation will present a homotopy algorithm for fixed order, mixed H_2/H_∞ compensator synthesis.

2. To successfully implement this homotopy algorithm required the development of a new algorithm for numerical optimization that is robust to ill-conditioned and indefinite Hessians. The utility of this new optimization algorithm is demonstrated by examples in appendix A.

3. Examples are given that illustrate the significance of mixed-norm design for nominal performance and robust stability. Included is a control design exercise for an experimental flexible space structure that includes open-loop system identification for control design model development.

4. A new method for system identification from closed-loop response data is presented for multi-input, multi-output systems in canonical form. Examples are given to demonstrate the closed-loop system identification and controller redesign process.

2

This dissertation is structured as follows. In section 2, a brief survey of the developments in control design and system identification which relate to controller tuning will be presented. Special attention is given to fixed-order control design for both robustness and performance. Emphasis is also placed on recent developments in closed-loop system identification. The approaches to control design for nominal performance, robust performance, and nominal performance/robust stability are highlighted in section 3. The formulation of the fixed-order mixed H_2/H_∞ control design method is also given. Homotopy methods are introduced in section 4 and a homotopy algorithm developed to synthesize mixed H_2/H_∞ controllers is presented. Section 5 presents mixed-norm control design examples. The new closed-loop system identification procedure is given in section 6 with examples. Conclusions and recommendations are provided in section 7 and appendix A is included to present the details of the numerical optimization procedure developed for ill-conditioned and indefinite Hessians.

2. BACKGROUND

2.1 Fixed-Order Control Design For Stability and Performance

Recent years have seen significant advances in modern control theory with H_2 and H_∞ methods gaining widespread recognition and application. Early work in multivariable control synthesis utilized a quadratic cost functional to minimize the H_2 norm of a system response to white noise inputs. While the H_2 procedure is well suited to design for nominal performance in terms of root-mean-square (RMS) quantities such as minimizing line-of-sight errors or control energy, it is well known that stability and performance cannot be guaranteed in the presence of model uncertainties. Robustness is addressed in H_∞ control theory which guarantees stability and performance (when defined by an H_∞ norm measure) in the presence of unstructured uncertainty models, albeit often resulting in overly conservative designs. μ-analysis and μ-synthesis methods have reduced the conservatism of H_∞ methods by accounting for the structure in the uncertainty and performance specifications.[4–6]

A significant disadvantage of these modern control techniques is that the resulting compensator is the same order as the generalized plant, which is often larger than the original plant due to the inclusion of frequency-dependent weights to achieve the desired performance and robustness characteristics. The consequential large controller order can be indirectly alleviated by reducing the order of the controller or alternatively by reducing the order of the design plant. In either case, indirect methods are suboptimal in performance and do not guarantee closed-loop stability. However, direct methods may be employed which impose constraints on controller order or architecture in the optimization procedure and hence provide stability and performance guarantees. In an optimization-based synthesis procedure, necessary conditions are formulated for the constrained closed-loop system that ensure internal stability.

The Optimal Projection method of Hyland and Bernstein is an H_2 procedure whereby order constraints are imposed on the controller and the necessary conditions for minimizing a quadratic cost functional with respect to the fixed-order controller are derived.[7] The resulting necessary conditions consist of two modified Riccati equations and two modified Lyapunov equations coupled by an oblique projection matrix. However, solution of the necessary conditions for realistic large-order systems is a difficult task. Homotopy methods have been employed to solve the optimal projection equations.[8]

As a means of providing robust stability with RMS-type performance, the mixed H_2 / H_∞ methodology has been developed. Much work has been done with variations of the mixed H_2 / H_∞ problem (for a summary see reference 9). The earliest refereed work was done by Bernstein and Haddad who extended the Optimal Projection approach to (linear-quadratic-Gaussian) LQG control with an H_2 norm constraint.[1] Their formulation minimized an overbound on the H_2 norm from a disturbance input to one output while satisfying an H_∞ norm overbound from the same disturbance input to a second output. This approach is potentially conservative as a result of minimizing an overbound on the H_2 norm. This approach was extended to the general mixed H_2 / H_∞ problem which can be specialized to

4

both full- and fixed-order pure H_2 and pure H_∞ controllers.[10] Reference 11 further extended the mixed H_2 / H_∞ formulation of reference 1 by fully accounting for singularities in the problem formulation. Rotea and Khargonekar formulated the general mixed H_2 / H_∞ problem with independent inputs and outputs for the two transfer functions and minimized the actual H_2 norm based on full state feedback.[12] Ridgely extended the formulation to output feedback including the fixed-order case with either regular or singular H_∞ constraints[9] and provided a numerical solution.[13] Another approach to the general mixed H_2 / H_∞ problem was developed by Sweriduk and Calise[14] who used a differential game formulation with a conjugate gradient algorithm to obtain fixed-order controllers. In this dissertation, a numerical solution of this formulation using a homotopy algorithm is developed and presented in section 4. Based on the formulation of reference 1, homotopy algorithms have also been recently developed for both discrete time and continuous time mixed H_2 / H_∞ design.[15,16]

Ridgely et al. shows the mixed H_2 / H_∞ problem to be a strictly convex optimization problem with a unique solution when the controller is of the order equal to or larger than the underlying H_2 problem.[9] The solution is shown to lie on the boundary of the infinity norm constraint when active (for $\gamma < \bar{\gamma}$ where $\bar{\gamma}$ is the H_∞ norm when the optimal H_2 controller is used) and is just the H_2 controller when $\gamma \geq \bar{\gamma}$. For controllers with order less than the underlying H_2 problem, the possibility of local minima in the unconstrained H_2 problem (Optimal Projection) exists and the solution of the mixed H_2 / H_∞ problem may or may not lie on the boundary of the H_∞ norm constraint. As will be shown in the next section, Sweriduk and Calise[14] begin with the fixed-order H_∞ cost functional and append the fixed-order H_2 cost functional. Reference 9 takes the converse approach by appending the H_∞ norm constraint to the H_2 cost functional. As a consequence, the formulation in reference 9 can handle both regular and singular H_∞ constraints and can be specialized to the H_2 problem. Conversely, the reference 14 formulation can handle both regular and singular H_2 constraints and can be specialized to the H_∞ problem. However, the ability to handle singular constraints on either cost exists as long as one of the cost constraints is regular. Whereas the reference 14 formulation assumes that the plant dynamics (A matrix) of the two transfer functions are the same, reference 9 allows different dynamics in the two separate underlying H_∞ and H_2 problems. Using the canonical compensator with a static gain output formulation presented in section 3, the reference 14 formulation requires the simultaneous solution of five coupled nonlinear matrix equations. Reference 9 presents the necessary conditions in the form of seven coupled, nonlinear matrix equations.

2.2 Closed-Loop System Identification and Control Design

Implicit in the design of high-performance control systems is the availability of an accurate model of the system to be controlled. Although system identification and control design are both critical aspects of high-performance model based control design, the theoretical foundations of these two disciplines have developed distinctly. Developments in system identification have been directed toward obtaining accurate nominal models with bounds on the associated uncertainty. Recognizing the dependence on accurate nominal design models, robust control theory has been developed to accommodate modeling errors. Recently, attention has been drawn to the fact that the issues of system identification and control design must be treated as *mutually dependent*. In reference 3, Skelton points out that since the magnitude and spectrum of excitation forces are controller-dependent, an appropriate model

for control design cannot be determined independent of the controller. The point is made that the validity of the model is dictated by the controller instead of the opposite, as is usually assumed. Since the model that is most appropriate depends on the control design, the open-loop response of a model is not sufficient to indicate the fidelity of the model for control design. Additionally, robust performance requires an accurate model of the plant in the controller crossover frequency range,[17] indicating that the amount of model error that can be tolerated is frequency- and controller-dependent. Hence, the issues of model identification and model-based control design must be treated as a joint problem suggesting an iterative solution.[3, 18]

Closed-loop system identification (i.e., identification of the open-loop plant given closed-loop response data and knowledge of the compensator dynamics) is currently a field of active research. Most of the methods that identify state space models of the open-loop plant are based on identifying the closed-loop Markov parameters from frequency response functions and then extracting the open-loop Markov parameters. A discrete time state space realization is then obtained from these identified Markov parameters. An approach to iterative closed-loop system identification and controller redesign is given by Liu and Skelton where a state space model is estimated using the q-Markov Cover algorithm and a controller is designed using the Output Variance Constraint algorithm.[19] q-Markov Cover theory describes all realizations of a linear system which match the first q-Markov parameters and covariance parameters of the true system generated by pulse responses. First, the entire closed-loop system is estimated and then, using knowledge of the compensator dynamics, the plant is extracted. However, the identified open-loop plant has dimension equal to the controller dimension plus the dimension of the identified closed-loop plant. Model order reduction is used to remove the superfluous states. A similar approach is taken in reference 20 where Phan et al. formulate a method which first obtains the closed-loop Markov parameters and then the open-loop Markov parameters are recovered. A discrete time state space realization is then obtained from the Markov parameters. Other related approaches are given in references 21 and 22.

To provide synergism, an iterative process should match the system identification objectives with the control design objectives. Reference 18 presents an iterative algorithm for frequency-response identification from closed-loop data and robust control design. The identification phase is control-oriented with the objective of providing robust performance by closely approximating the achieved closed-loop performance. The interplay between identification and control design is formalized by specifying a performance metric (norm) for model-based optimal control design and an identification cost function that minimizes the difference in the achieved performance and nominal design performance as defined by the same metric. Many algorithms have been developed based on this general framework which utilize different performance norms and identification algorithms. An excellent survey of this topic is given in reference 23. Most of the work cited therein has been done in the context of single-input, single-output (SISO) systems.

A classical approach to parameter estimation which has been extended to closed-loop system identification is the prediction error approach.[24] This optimization method estimates the parameters of a linear system by minimizing the squared sum of the errors between the actual measurements and the predicted measurements. Zang, Bitmead, and Gevers present an iterative prediction error

6

identification and control design algorithm based on the H_2 norm.[25] The control objective is used to frequency-weight the identification cost functional and the resulting prediction error spectrum is used to frequency-weight the control design. In this manner the control is penalized heavily where the SISO transfer function model fit is poor and the model is weighted to fit best in the regions most critical to performance. Another approach utilizes the dual Youla parameterization of all plants stabilized by a given controller. This approach was introduced by Hansen and Franklin[26] and further elaborated by Hansen et al. in reference 27 as applied to closed-loop experiment design. Schrama applied the dual Youla parameterization to closed-loop system identification in references 28 and 29 as did Anderson and Kosut in reference 30. A related method directed toward identification of the coprime factors of the plant was introduced by Schrama in reference 28 and was further elaborated in references 29 and 31.

In this dissertation the prediction error method is extended to closed-loop identification for multivariable systems. Building on a method developed for estimation of the parameters of an open-loop system in canonical form from open-loop data, a new procedure for closed-loop system identification is developed and demonstrated in section 6.

3. APPROACHES TO CONTROL DESIGN FOR FLEXIBLE SPACE STRUCTURES

H_2 methods are often used when designing control systems to reduce the vibration response of a flexible structure. While H_2 design gives good nominal performance, the controllers are highly tuned to the design model and errors in the design model are not accounted for, typically inducing instability at higher levels of control authority. As a result, the actual performance achievable is limited with H_2 designs. To achieve high levels of performance in the actual system, robustness to model errors must be taken into account in the design process as is done in the H_∞ control design theory. In the following sections, a brief introduction to H_2, H_∞, μ-synthesis, and mixed H_2 / μ control theory is given followed by the problem formulation for fixed-order control design.

3.1 Control Design for Stability and Performance

The generalized plant of a standard control problem is given by

$$\dot{x} = Ax + B_1 w + B_2 u \tag{1}$$

$$z = C_1 x + D_{12} u \tag{2}$$

$$y = C_2 x + D_{21} w + D_{22} u \ , \tag{3}$$

where $x \in R^n$ is the state vector, $w \in R^{nw}$ is the disturbance vector, $u \in R^{nu}$ is the control vector, $z \in R^{nz}$ is the performance vector, and $y \in R^{ny}$ is the measurement vector. The following is assumed:

- (A, B_1, C_1) is stabilizable and detectable

- D_{12} has full column rank

- D_{21} has full row rank.

A general compensator for this system is

$$\dot{x}_c = A_c x_c + B_c y \tag{4}$$

$$u = C_c x_c \ , \tag{5}$$

where $x_c \in R^{nc}$ is the state vector of the controller, the dimension of which can be specified. Closing the loop using negative feedback yields the closed-loop system dynamics

$$\dot{\bar{x}} = \tilde{A}\bar{x} + \tilde{B}w \tag{6}$$

8

$$z = \tilde{C}\tilde{x} \ , \tag{7}$$

where

$$\tilde{x} = \begin{bmatrix} x \\ x_c \end{bmatrix} \tag{8}$$

$$\tilde{A} = \begin{bmatrix} A & -B_2 C_c \\ B_c C_2 & A_c - B_c D_{22} C_c \end{bmatrix} \tag{9}$$

$$\tilde{B} = \begin{bmatrix} B_1 \\ B_c D_{21} \end{bmatrix} \tag{10}$$

$$\tilde{C} = \begin{bmatrix} C_1 & -D_{12} C_c \end{bmatrix} \ . \tag{11}$$

The set of all internally stabilizing compensators is defined as

$$S_c = \left\{ (A_c, B_c, C_c) : \tilde{A} \text{ is asymptotically stable} \right\} \ . \tag{12}$$

3.1.1 Nominal Performance Design

For an H_2 problem, the objective is to minimize the H_2 norm of the closed-loop transfer function from disturbance inputs to performance outputs

$$T_{zw} = \tilde{C}\left(sI - \tilde{A}\right)^{-1}\tilde{B} \ , \tag{13}$$

where the disturbances are confined to the set of signals with bounded power and fixed spectra. If the disturbance is modeled as white noise, the objective is

$$\min_{S_c} \left\{ J(A_c, B_c, C_c) = \lim_{t \to \infty} E\left\{ z(t)^T z(t) \right\} \right\} \ , \tag{14}$$

where $E\{*\}$ is the expectation operator. The cost can be expressed as

$$J(A_c, B_c, C_c) = \mathrm{tr}\left\{ Q\tilde{B}\tilde{B}^T \right\} = \mathrm{tr}\left\{ P\tilde{C}^T\tilde{C} \right\} \ , \tag{15}$$

where

$$\tilde{A}P + P\tilde{A}^T + \tilde{B}\tilde{B}^T = 0 \tag{16}$$

$$\tilde{A}^T Q + Q\tilde{A} + \tilde{C}^T\tilde{C} = 0 \ . \tag{17}$$

P is the controllability grammian of $\left(\tilde{A}, \tilde{B}\right)$ and Q is the observability grammian of $\left(\tilde{C}, \tilde{A}\right)$. An equivalent cost functional also arises for the case of impulsive inputs.

Another approach to design for nominal performance employs the H_∞ norm, which can be interpreted as the gain of the system and is the worst-case amplification over all inputs $w(t)$ of bounded energy L_2 signals. From a frequency domain perspective, the H_∞ norm is defined as the maximum singular value of $T(s)$ over all frequencies, i.e.,

$$\left\| T_{zw} \right\|_\infty = \sup_\omega \left\{ \overline{\sigma} \left(T_{zw}(j\omega) \right) \right\} , \tag{18}$$

where $\overline{\sigma}$ denotes the maximum singular value. H_∞ control design theory, based on references 32 and 33, involves defining (possibly frequency-dependent) weights on the inputs and outputs such that the performance objectives are satisfied by minimizing $\left\| T_{zw} \right\|_\infty$. Because the H_∞ norm is defined with respect to the peak magnitude of the transfer matrix frequency response and the H_2 norm is defined by an integral square quantity (in time or frequency by Parseval's Theorem), the respective closed-loop systems may have considerably different characteristics. Depending on the performance objectives, one design procedure may be preferable to the other. When performance is specified by RMS measures, H_2 design typically yields better nominal performance. The significant benefit of H_∞ theory is that robustness to unstructured model errors is explicitly factored into the design process.

3.1.2 Robust Stability and Robust Performance

In addition to nominal performance, robust stability is an important design consideration. Robust stability requires the closed-loop system to remain stable for bounded model errors. The uncertainty may be modeled in many forms such as multiplicative, inverse multiplicative, additive, parametric, etc., and may be located at various points in the loop. By absorbing all of the scalings and weights into the plant, P, the robust stability problem may be formulated as the linear fractional transformation (LFT) in figure 1. The uncertainties are scaled so that Δ_δ is the set of all stable perturbations, Δ, such that $\left\| \Delta \right\|_\infty \leq \delta$. Assuming that $K(s)$ internally stabilizes the closed-loop for $\Delta = 0$, then a sufficient condition for robust stability for all plants in the set formed by $\Delta \in \Delta_\delta$ is that[34, 35]

$$\left\| T_{zw}(K) \right\|_\infty \leq \frac{1}{\delta} . \tag{19}$$

Thus, like the nominal performance problem, robust stability is characterized by the H_∞ norm of a transfer function.

It is the ability to formulate the performance problem as a robust stability problem that enables design for robust performance in the H_∞ setting. Consider the LFT of an uncertain plant in figure 2 with inputs and outputs defined for performance and an uncertainty model. The conditions for robust performance are:

1. Robust stability (equation (19))

2. Performance maintained for all $\Delta \in \Delta_\delta$.

10
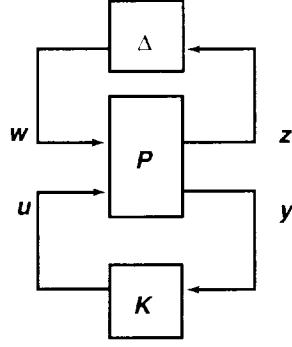
Figure 1. LFT for robust stability analysis.
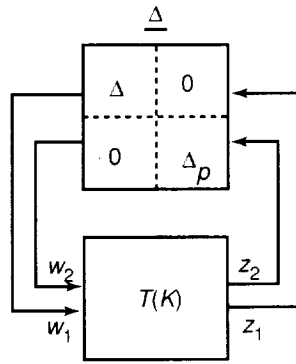
Figure 2. LFT for robust performance design.

Closing the loop from z_2 to w_2 through a fictitious uncertainty block Δ_p recasts the robust performance problem as a robust stability problem, shown in figure 2, where the blocks are scaled to one.

A sufficient condition for robust performance is that

$$\|T(K)\|_\infty < \frac{1}{\delta} \ . \tag{20}$$

Define $\underline{\Delta}_\delta$ to be the set of all stable, bounded, unstructured perturbations $\underline{\Delta}$ such that $\|\underline{\Delta}\|_\infty < \delta$. When $\underline{\Delta} \in \underline{\Delta}_\delta$, equation (20) is necessary and sufficient to ensure robust stability. Designing for robust performance using Δ_p as in figure 2 introduces a block diagonal structure to $\underline{\Delta}$ which results in equation (20) being only sufficient and possibly overly conservative. This conservatism is relaxed in the μ-analysis and μ-synthesis procedures by accounting for the block diagonal structure in $\underline{\Delta}$. The structured singular value, μ, is the inverse of the smallest destabilizing perturbation of a transfer function matrix and is defined as:

$$\mu(T_{zw}(j\omega)) = \frac{1}{min\left\{\overline{\sigma}(\Delta(j\omega)) : \Delta \in \underline{\Delta}_\delta, det\left[I - T_{zw}(j\omega)\Delta(j\omega)\right] = 0\right\}} \ . \tag{21}$$

The structured singular value is used to define the μ-measure, which although not a norm, is given by

$$\|T(j\omega)\|_\mu = \sup_\omega \{\mu(T_{zw}(j\omega))\} \quad . \tag{22}$$

Hence, the sufficient condition for robust performance in equation (20) becomes the necessary and sufficient condition

$$\|T(j\omega)\|_\mu < \frac{1}{\delta} \quad . \tag{23}$$

Although the structured singular value cannot be directly computed, an upper bound can be computed as

$$\mu(T) = \inf_D \left\{ \bar\sigma\left(DTD^{-1}\right)\right\} \quad , \tag{24}$$

where $D = \mathrm{diag}\left[d_j I_j\right]$ has the same structure as Δ and d_j are scalar, positive, real functions of frequency. An iterative scheme is used to solve this optimization problem. In the first step, an H_∞ controller is designed and in the second step, the D-scales are optimized for this controller in accordance with equation (24). A curve-fitting step is used to determine stable, minimum phase rational transfer function fits (in magnitude) to the optimum D-scales. In the next iteration, these D-scales are incorporated into the generalized plant and the control design is repeated, followed again by D-scaling. This iterative process continues until the upper bound in equation (24) cannot be reduced significantly.

3.1.3 Robust Stability and Nominal Performance Design

Although μ-synthesis provides stability and performance in the presence of model errors, the performance is defined by an H_∞ norm measure. The mixed H_2 / H_∞ design procedure has been developed to provide robust stability and nominal (H_2) performance by minimizing the H_2 norm for one set of inputs/outputs while satisfying an H_∞ norm overbound for another set of inputs/outputs. With reference to figure 2, the objective is to satisfy

$$\min_K \|T_{z_2 w_2}\|_2 \quad . \tag{25}$$

subject to

$$\|T_{z_1 w_1}\|_\infty < \gamma \quad . \tag{26}$$

This problem has been solved for controllers of fixed dimension in references 9, 14, and 36–38.

The formulation of reference 14 is presented in the next section and a numerical homotopy algorithm for this formulation of the mixed H_2 / H_∞ control design problem is presented in section 4. The homotopy algorithm is a two-parameter iterative scheme which effectively trades between robust stability and nominal performance by varying the overbound on the H_∞ norm, γ, and the weight on the H_2 cost, λ. For a given γ, λ is increased until the H_∞ norm constraint becomes an active equality constraint (at which point the H_2 norm can no longer be reduced), or until the H_2 norm ceases

to decrease. The set of controllers where the H_∞ norm is equal to the overbound are called the boundary solutions. This set provides an explicit tradeoff between nominal performance and robust stability. By incorporating the D-scales from μ-synthesis into the H_∞ subproblem, the structure of the uncertainty block may be accounted for, resulting in a fixed-order mixed H_2/μ design procedure. Recent developments in robust control theory that avoid this multiplier-controller iteration process include the use of absolute stability theory such as Popov analysis.[37–40] This approach provides a means for simultaneous optimization of a fixed-architecture controller and a fixed-structure multiplier that accounts for both complex and real-structured uncertainty. A homotopy algorithm was developed for synthesis of robust controllers with fixed-structure multipliers.[41]

The conflicting demands of designing for robustness and performance may be explicitly addressed in the mixed H_2/H_∞ design setting. The utility of mixed-norm design is exploited by separating performance and robustness using the H_2 subproblem to design for nominal performance and using the H_∞ subproblem to achieve robust stability. In figure 2 the inputs and outputs associated with the uncertainty model comprise w_1 and z_1, w_2 is associated with disturbance excitations and measurement noise, and z_2 is associated with performance outputs. In this manner, the set of boundary controllers explicitly trade off nominal performance with levels of robustness to uncertainty. As illustrated in figure 3, this set of controllers includes, at one extreme, the lowest authority controller which provides maximum robustness and minimum performance and, at the other extreme, a maximum performance controller with the minimum stability margins. Hence, this paradigm is well suited for tuning a controller on orbit by incrementally increasing control authority.
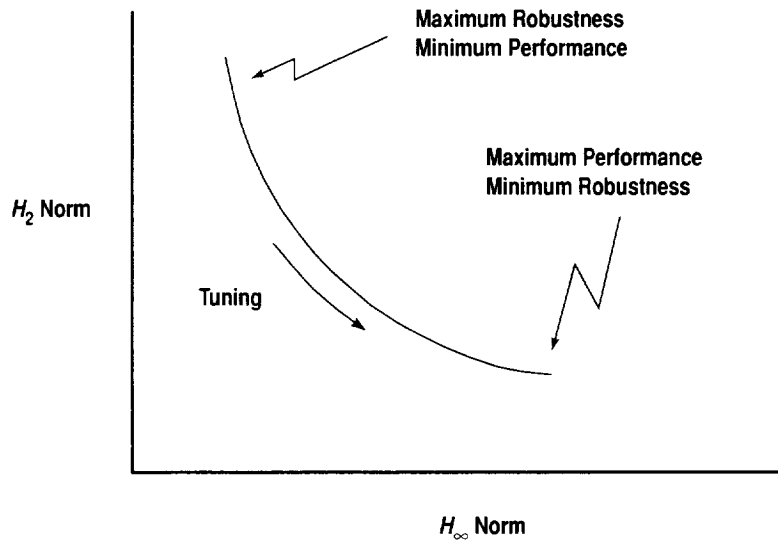
Figure 3. Performance versus robustness trade.

Another significant aspect of this approach is that each controller in the set may be successively implemented to determine the point at which achieved performance begins to deviate from nominal performance. At that point, the maximum achievable performance with robust stability for a given design model is achieved. The same implementation strategy could be applied to H_2 and μ control

design. However, mixed-norm design tends to allow higher performance levels to be attained for a given bounded model error by designing for robust stability. Since H_2 design does not account for model errors, the sensitivity to model errors typically results in achieving lower levels of performance than the mixed-norm designs. On the other hand, μ designs are not optimized for H_2 performance and although robust stability is given, the performance is not comparable to H_2 nominal performance design. These issues are illustrated by design examples in section 5.

In the following section, the problem formulation and necessary conditions for fixed-order H_2, H_∞, and mixed H_2/H_∞ control design are presented. Section 4 presents the homotopy algorithm for fixed-order, mixed-norm synthesis.

3.2 Fixed-Order Control Design Formulation

In order to obtain the H_2-optimal compensator, the Lagrangian is formed by augmenting the cost functional, equation (15), with the constraint, equation (17), yielding

$$L\left(Q,L,A_c,B_c,C_c\right) = \mathrm{tr}\left\{Q\tilde{B}\tilde{B}^T + \left(\tilde{A}^TQ + Q\tilde{A} + \tilde{C}^T\tilde{C}\right)L\right\} ,$$ (27)

where L is a symmetric matrix of Lagrange multipliers. Matrix gradients are taken to determine the first order necessary conditions:

$$\frac{\partial L}{\partial Q} = 0, \quad \frac{\partial L}{\partial L} = 0, \quad \frac{\partial L}{\partial A_c} = 0, \quad \frac{\partial L}{\partial B_c} = 0, \quad \frac{\partial L}{\partial C_c} = 0 .$$ (28)

Hence, computing an H_2-optimal controller of fixed-order $n_c < n$ for the general controller structure given in equations (4)–(5) requires the simultaneous solution of five coupled equations. This is not only computationally expensive, but is also further complicated by the fact that the problem is over-parametrized with such a compensator.

To optimize the controller for a specified controller state dimension, a "controller form" architecture is imposed on the compensator dynamics.[42] This minimal realization avoids the problem of over parametrization and is a canonical form under mild conditions.[43] The internal structure of the compensator is prespecified by assigning a set of feedback invariant indices, v_i. In controller canonical form, the compensator is defined as

$$\dot{x}_c = P^0 x_c + N^0 u_c - N^0 y$$ (29)

$$u_c = -P x_c$$ (30)

$$u = -H x_c ,$$ (31)

14

where $x_c \in R^{nc}$ and $u_c \in R^{ny}$. P and H are free-parameter matrices, and P^0 and N^0 are fixed matrices of zeros and ones determined by the choice of controllability indices. Similarly, a compensator in observer canonical form can be constructed. In this paper only the controller canonical form is employed, which imposes the lower bound $n_c \geq ny$ on the order of the compensator.

By augmenting the generalized plant of equations (1)–(3) with the compensator of equations (29)–(31), the system may be written as

$$\dot{\bar{x}} = \begin{bmatrix} A & 0 \\ -N^0 C_2 & P^0 \end{bmatrix} \bar{x} + \begin{bmatrix} B_1 \\ -N^0 D_{21} \end{bmatrix} w + \begin{bmatrix} B_2 & 0 \\ -N^0 D_{22} & N^0 \end{bmatrix} \bar{u}$$

$$= \bar{A}\bar{x} + \bar{B}_1 w + \bar{B}_2 \bar{u} \ , \tag{32}$$

$$z = \begin{bmatrix} C_1 & 0 \end{bmatrix} \bar{x} + \begin{bmatrix} D_{12} & 0 \end{bmatrix} \bar{u} = \bar{C}_1 \bar{x} + \bar{D}_{12} \bar{u} \ , \tag{33}$$

$$\bar{y} = \begin{bmatrix} 0 & I \end{bmatrix} \bar{x} = C_2 \bar{x} \ , \tag{34}$$

$$\bar{u} = -\begin{bmatrix} H \\ P \end{bmatrix} \bar{y} = -G\bar{y} \ , \tag{35}$$

where the augmented control input is

$$\bar{u} = \begin{bmatrix} u \\ u_c \end{bmatrix} \ . \tag{36}$$

Equations (32)–(35) define a static gain output feedback problem where the compensator is represented by a minimal number of free parameters in the design matrix, G. The closed-loop system is given by

$$\dot{\bar{x}} = (\bar{A} - \bar{B}_2 G \bar{C}_2)\bar{x} + \bar{B}_1 w = \tilde{A}\bar{x} + \tilde{B}w \tag{37}$$

$$z = (\bar{C}_1 - \bar{D}_{12} G \bar{C}_2)\bar{x} = \tilde{C}\bar{x} \ . \tag{38}$$

Minimizing the H_2 norm of $T_{zw} = \tilde{C}(sI - \tilde{A})^{-1}\tilde{B}$ utilizes the same Lagrangian as given in equation (27), but now L is only a function of three parameter matrices, i.e., $L(Q,L,G)$. Thus, the resulting first order necessary conditions are

$$\frac{\partial L}{\partial Q} = \tilde{A}L + L\tilde{A}^T + \tilde{B}\tilde{B}^T = 0 \tag{39}$$

15

$$\frac{\partial L}{\partial L} = \tilde{A}^T Q + Q\tilde{A} + \tilde{C}^T \tilde{C} = 0 \tag{40}$$

$$\frac{\partial L}{\partial G} = 2\left(\overline{D}_{12}^T \overline{D}_{12} G\overline{C}_2 - \overline{D}_{12}^T \overline{C}_1 - \overline{B}_2^T Q\right) L\overline{C}_2^T = 0. \tag{41}$$

Controller canonical forms can also be used to solve the H_∞ problem. The objective is now to minimize the norm of the transfer function from disturbance inputs w to performance outputs z given by

$$\|T_{zw}\|_\infty = \sup_{w \in L_2} \frac{\|T_{zw}\|_2}{\|w\|_2} = \sup_{\|w\|_2 \leq 1} \|T_{zw}\|_2 . \tag{42}$$

From reference 14, the optimization problem is to find

$$\inf\left\{\|T_{zw}(G)\|_\infty : G \in \mathbf{G}\right\} \equiv \gamma^*, \tag{43}$$

where $\mathbf{G} = \left\{G \in \Re^{(nu+ny)\times nc} : \tilde{A} \text{ is stable}\right\}$. A more practical design objective is to find a G that ensures $\|T_{zw}\|_\infty \leq \gamma$ for some $\gamma > \gamma^*$. This optimization problem may be formulated as a min-max problem using the cost functional

$$J_\gamma(w,G) = E\left\{\int_0^\infty \left(z^T z - \gamma^2 w^T w\right) dt\right\} . \tag{44}$$

where the expectation operator, $E\{*\}$, is taken over a distribution of initial conditions with zero mean and variance $\tilde{B}\tilde{B}^T$. In the min-max problem, the minimizing player acts first, so the loop is closed around G and the disturbance w^* which maximizes J_γ is determined. Then the control G which minimizes $J_\gamma(w^*,G)$ is determined, resulting in the upper value

$$J_\gamma^* = \min_{G \in \mathbf{G}_\gamma} \max_{w \in L_2}\left\{J_\gamma(w,G)\right\} . \tag{45}$$

G is restricted to the set of admissible controllers defined by $\mathbf{G}_\gamma = \{G \in \Re^{(nu+ny)\times nc} : \tilde{A} \text{ is stable and } \|T_{zw}\|_\infty < \gamma\}$.

For any $G \in \mathbf{G}_\gamma$, a unique worst-case disturbance exists and is a feedback of states given by

$$w = \gamma^{-2}\tilde{B}^T Q_\infty x , \tag{46}$$

16

where Q_∞ is the positive semidefinite solution of the Riccati equation

$$\tilde{A}^T Q_\infty + Q_\infty \tilde{A} + \tilde{C}^T \tilde{C} + \gamma^{-2} Q_\infty \tilde{B} \tilde{B}^T Q_\infty = 0 \ . \tag{47}$$

Substituting the worst-case disturbance from equation (46) into equation (44), the performance index becomes

$$J_\gamma(G) = E\left\{ \int_0^\infty \bar{x}^T \left(\tilde{C}^T \tilde{C} - \gamma^{-2} Q_\infty \tilde{B} \tilde{B}^T Q_\infty \right) \bar{x} dt \right\} \ . \tag{48}$$

The objective of minimizing $\|T_{zw}\|_\infty$ using a fixed-order controller can be formulated

$$\min_{G \in G_\gamma} \left\{ J_\gamma(G) = \mathrm{tr}\left\{ Q_\infty \tilde{B} \tilde{B}^T \right\} \right\} \ , \tag{49}$$

subject to equation (47). Using the Lagrange multiplier matrix L, the Lagrangian is

$$L(Q_\infty, L, G) = \mathrm{tr}\left\{ Q_\infty \tilde{B} \tilde{B}^T + \left(\tilde{A}^T Q_\infty + Q_\infty \tilde{A} + \tilde{C}^T \tilde{C} + \gamma^{-2} Q_\infty \tilde{B} \tilde{B}^T Q_\infty \right) L \right\} \ . \tag{50}$$

Matrix gradients are taken to determine the first order necessary conditions for an H_∞ suboptimal fixed-order compensator gain G:

$$\frac{\partial L}{\partial Q_\infty} = \left(\tilde{A} + \gamma^{-2} \tilde{B} \tilde{B}^T Q_\infty \right) L + L\left(\tilde{A} + \gamma^{-2} \tilde{B} \tilde{B}^T Q_\infty \right)^T + \tilde{B} \tilde{B}^T = 0 \tag{51}$$

$$\frac{\partial L}{\partial L} = \tilde{A}^T Q_\infty + Q_\infty \tilde{A} + \tilde{C}^T \tilde{C} + \gamma^{-2} Q_\infty \tilde{B} \tilde{B}^T Q_\infty = 0 \tag{52}$$

$$\frac{\partial L}{\partial G} = 2\left(\overline{D}_{12}^T \overline{D}_{12} G \overline{C}_2 - \overline{D}_{12}^T \overline{C}_1 - \overline{B}_2^T Q_\infty \right) L \overline{C}_2^T = 0 \ . \tag{53}$$

As in the H_2 problem, three coupled equations have to be solved to obtain a fixed-order compensator which satisfies the constraint $\|T_{zw}\|_\infty < \gamma$.

This formulation minimizes an upper bound on the H_2 cost which corresponds to an entropy controller.[44] Although this controller guarantees an H_∞ norm constraint, as written it is not a pure H_∞ controller in the sense of reference 33, but can be specialized to the pure H_∞ controller.[10]

Fixed-order H_∞ design has also been extended to fixed-order μ-synthesis.[36-38, 45-47] The approach taken in reference 36 differs from that of references 45–47 by using optimized fixed-structure multipliers instead of multiplier-controller iteration and is based on the earlier developments in references 37 and 38. Because H_∞ controller design is a subproblem when designing for robust performance with structured uncertainty, the fixed-order technique just introduced has the potential to constrain the order of the controller which is normally subject to significant increases in the μ-synthesis procedure.

The mixed H_2 / H_∞ problem can be approached in a similar fashion.[14] In this case, the generalized plant has additional inputs and outputs with dynamics given by

$$\dot{x} = Ax + B_p w_p + B_1 w + B_2 u \tag{54}$$

$$z_p = C_p x + D_{1p} u \tag{55}$$

$$z = C_1 x + D_{12} u \tag{56}$$

$$y = C_2 x + D_{2p} w_p + D_{21} w + D_{22} u \ , \tag{57}$$

where $w_p \in R^{n_{w_p}}$ and $z_p \in R^{n_{z_p}}$ are the inputs and outputs defining the H_2 subproblem, and $w \in R^{n_w}$ and $z \in R^{n_z}$ are the inputs and outputs defining the H_∞ subproblem. It is assumed that (A, B_2, C_2) is stabilizable and detectable. Using the controller canonical form for the compensator, the augmented system for the mixed problem is

$$\dot{\bar{x}} = \bar{A}\bar{x} + \bar{B}_1 w + \bar{B}_p w_p + \bar{B}_2 \bar{u} \tag{58}$$

$$z_p = \bar{C}_p \bar{x} + \bar{D}_{1p} \bar{u} \tag{59}$$

$$z = \bar{C}_1 \bar{x} + \bar{D}_{12} \bar{u} \tag{60}$$

$$\bar{y} = \bar{C}_2 \bar{x} \tag{61}$$

$$\bar{u} = -G\bar{y} \ , \tag{62}$$

where

$$\bar{B}_p = \begin{bmatrix} B_p \\ -N^0 D_{2p} \end{bmatrix}, \quad \bar{C}_p = \begin{bmatrix} C_p & 0 \end{bmatrix}, \quad \bar{D}_{1p} = \begin{bmatrix} D_{1p} & 0 \end{bmatrix} . \tag{63}$$

18

The other expressions are the same as in equations (32)–(35). Consequently, the closed-loop system is given by

$$\dot{x} = \left(\overline{A} - \overline{B}_2 G \overline{C}_2\right)\overline{x} + \overline{B}_p w_p + \overline{B}_1 w$$

$$= \tilde{A}\overline{x} + \tilde{B}_p w_p + \tilde{B}w \tag{64}$$

$$z_p = \left(\overline{C}_p - \overline{D}_{1p} G \overline{C}_2\right)\overline{x} = \tilde{C}_p \overline{x} \tag{65}$$

$$z = \left(\overline{C}_1 - \overline{D}_{12} G \overline{C}_2\right)\overline{x} = \tilde{C}\overline{x} \quad . \tag{66}$$

In order to formulate the performance index of the mixed problem, the Lagrangian for the H_2 problem is adjoined to the Lagrangian for the H_∞ problem in equation (50) by a scalar weight, λ:

$$L = \mathrm{tr}\left\{Q_\infty \tilde{B}\tilde{B}^T + \lambda X \tilde{C}_p^T \tilde{C}_p + \left(\tilde{A}^T Q_\infty + Q_\infty \tilde{A} + \tilde{C}^T \tilde{C}\right.\right.$$

$$\left.\left. + \gamma^{-2} Q_\infty \tilde{B}\tilde{B}^T Q_\infty\right)L + \left(\tilde{A}X + X\tilde{A}^T + \tilde{B}_p \tilde{B}_p^T\right)L_p\right\} \quad . \tag{67}$$

Note that the H_2 portion of the mixed-norm Lagrangian uses the dual form of the cost and constraint in equations (15) and (16). This problem was first formulated in reference 10. The weight, λ, on the H_2 norm allows a tradeoff between performance (H_2 norm) and robustness (H_∞ norm). The first order necessary conditions are

$$\frac{\partial L}{\partial Q_\infty} = \left(\tilde{A} + \gamma^{-2}\tilde{B}\tilde{B}^T Q_\infty\right)L + L\left(\tilde{A} + \gamma^{-2}\tilde{B}\tilde{B}^T Q_\infty\right)^T + \tilde{B}\tilde{B}^T = 0 \tag{68}$$

$$\frac{\partial L}{\partial L} = \tilde{A}^T Q_\infty + Q_\infty \tilde{A} + \tilde{C}^T \tilde{C} + \gamma^{-2} Q_\infty \tilde{B}\tilde{B}^T Q_\infty = 0 \tag{69}$$

$$\frac{\partial L}{\partial X} = \tilde{A}^T L_p + L_p \tilde{A} + \lambda \tilde{C}_p^T \tilde{C}_p = 0 \tag{70}$$

$$\frac{\partial L}{\partial L_p} = \tilde{A}X + X\tilde{A}^T + \tilde{B}_p \tilde{B}_p^T = 0 \tag{71}$$

$$\frac{\partial L}{\partial G} = 2\left[\left(\overline{D}_{12}^T \overline{D}_{12} G \overline{C}_2 - \overline{D}_{12}^T \overline{C}_1 - \overline{B}_2^T Q_\infty\right)L\right.$$

$$\left. + \left(\lambda \overline{D}_{1p}^T \overline{D}_{1p} G \overline{C}_2 - \lambda \overline{D}_{1p}^T \overline{C}_p - \overline{B}_2^T L_p\right)X\right]\overline{C}_2^T = 0 \quad . \tag{72}$$

In section 4, a homotopy method is presented to synthesize fixed-order H_2, H_∞, and mixed H_2 / H_∞ controllers.

4. HOMOTOPY ALGORITHM FOR MIXED H_2/H_∞ CONTROL DESIGN

Using the formulation and necessary conditions of the fixed-order mixed H_2/H_∞ control design problem in section 3, this section presents a homotopy algorithm for synthesis of fixed-order mixed H_2/H_∞ controllers. Fixed-order H_2 and H_∞ controllers are obtained in the same manner, but for the sake of brevity only the mixed-norm algorithm is presented here. A complete development of the H_2 and H_∞ algorithms is given in reference 48. The approach and algorithms developed here are patterned after references 49 and 50. Before embarking on the homotopy algorithm for mixed-norm design, an introduction to homotopy methods is presented.

4.1 Homotopy Methods

Homotopy methods offer an attractive alternative to more standard approaches of optimal controller synthesis such as sequential and conjugate gradient methods. The basic philosophy of homotopy methods is to deform a problem which is relatively easily solved into the problem for which a solution is desired.

Homotopy (or continuation) methods, arising from algebraic and differential topology, embed a given problem in a parameterized family of problems. More specifically, consider sets Θ and $Y \in \Re^n$ and a mapping $F : \Theta \to Y$, where solutions of the problem,

$$F(\theta) = 0 , \tag{73}$$

are desired with $\theta \in \Theta$ and $F(\theta) \in Y$. The homotopy function is defined by the mapping $H : \Theta \times [0,1] \to \Re^n$ such that

$$H(\theta_1,1) = F(\theta) , \tag{74}$$

and there exists a known (or easily calculated) solution, θ_0, such that

$$H(\theta_0,0) = 0 . \tag{75}$$

The homotopy function is a continuously differentiable function given by

$$H(\theta(\alpha),\alpha) = 0, \quad \alpha \in [0,1] . \tag{76}$$

The existence of a continously differentiable homotopy function is assumed, although in many cases such as output feedback optimal control design, a continuously differentiable homotopy function

may in fact not exist. Also, to be precise, the approach used herein is a continuation algorithm, which differs from homotopy algorithms in that the zero curve of a homotopy algorithm is parameterized by the arc length.

Thus the homotopy begins with a simple problem with a known solution, equation (75), which is deformed by continuously varying the parameter until the solution of the original problem, equation (73), is obtained.[51] The power of homotopy methods is that minimization is not strongly dependent on starting solution, but depends on local, small variations in the solution. Theoretically, these methods are globally convergent for a wide range of complex optimization problems, but in actuality, finite wordlength computation often introduces numerical ill-conditioning, resulting in difficulties with convergence. In light of these numerical limitations, a judicious choice of the initial problem and the associated initial stabilizing compensator is necessary for convergence and efficient computation. However, the ability to select an initial problem with a simple solution renders homotopy methods more widely applicable than sequential or gradient-based methods, which have a stringent requirement for an initial stabilizing solution. A new procedure for numerical optimization when the Hessian is ill-conditioned or indefinite is presented in appendix A.

Both discrete and continuous methods are used to solve the homotopy. Discrete methods simply partition the interval [0,1] to obtain a finite chain of problems:

$$H(\theta, \alpha_n) = 0, \quad 0 = \alpha_0 < \alpha_1 < L < \alpha_N = 1 \ . \tag{77}$$

Starting with a known solution at α_n, the solution for $H(\theta, \alpha_{n+1})$ is computed by a local iteration scheme. Continuous methods involve integration of Davidenko's differential equation, which is obtained by differentiating equation (76) with respect to α, yielding

$$\frac{d\theta}{d\alpha} = -\left(\frac{\partial H}{\partial \theta}\right)^{-1} \frac{\partial H}{\partial \alpha} \ . \tag{78}$$

Given $\theta(0) = \theta_0$, this initial value problem may be numerically integrated to obtain the solution at $\alpha = 1$ if the solution exists and is uniquely defined.

In the next section, a continuous homotopy algorithm is presented for fixed-order mixed H_2 / H_∞ compensator design. The set of homotopy algorithms for synthesizing fixed-order H_2, H_∞, and mixed H_2 / H_∞ compensators has been organized into a MATLAB™ toolbox called Fixed-Order Compensation of Uncertain Systems (FOCUS).

4.2 Homotopy Algorithm

This section describes the continuous homotopy algorithm for mixed H_2 / H_∞ control design. In essence, a mixed discrete and continuous approach is employed where Davidenko's differential

equation, equation (78), is integrated along the homotopy path and at discrete points along the trajectory, a local optimization is used to remove integration error. The optimization scheme is a partitioned Newton search method developed for this application and presented in appendix A. Local optimization at discrete points along the homotopy trajectory allows a crude integration procedure with large step sizes to be employed for efficiently tracking the solution curve. This approach is implemented in the following algorithm:

1. Find initial solution ($\alpha = 0$).

2. Advance α :

$$\alpha_{1,k} = \alpha_0 + \Delta\alpha_{0,k} \quad .$$

3. Predict θ :

$$\theta(\alpha_{1,k}) = \theta(\alpha_0) + \Delta\alpha_{0,k}\theta'(\alpha_0) \quad ,$$

where

$$\theta'(\alpha) = \frac{d\theta}{d\alpha} = -\left(\frac{\partial H}{\partial \theta}\right)^{-1}\frac{\partial H}{\partial \alpha} \quad .$$

4. Check prediction error:

$$e_k(\theta,\alpha) = \left\|J_\theta\left(\theta(\alpha_{1,k})\right)\right\| < \epsilon$$

   a. If error less than tolerance, continue.
   b. If not, $0.5\Delta\alpha_{0,k} \to \Delta\alpha_{0,k+1}$.
   c. Increment k and repeat steps 2–4.

5. Correct with partitioned Newton method to compute local minimum.

6. If $\alpha = 1$, stop. Otherwise, go to step 2.

Various approaches may be taken when selecting the deformation, but the general procedure applied in this effort is outlined as follows:

- Synthesize a low authority H_2 (full order) compensator
- Reduce the compensator to desired order and transform to canonical form[42]
- Set γ large enough so that the H_2 and H_∞ compensators are approximately equivalent
- Use homotopy to deform the initial low authority, reduced-order H_2 compensator into a full authority reduced-order H_2 compensator (H_2 homotopy)
- Deform the full authority H_2 compensator into a nearly optimal H_∞ compensator with γ approaching its infimum (H_∞ homotopy)
- At discrete values of λ, fix γ and deform the compensator into the mixed H_2/H_∞ compensator by varying λ (mixed H_2/H_∞ homotopy).

22

This procedure was chosen because it has been observed numerically that order reduction techniques tend to work best for low authority LQG controllers.[49, 52] A canonical form is imposed on the compensator structure to minimize the number of free parameters, which in some cases can also lead to numerical ill-conditioning. A balancing transformation which does not affect the controller characteristics relaxes the strict structure in the P^0 and N^0 matrices in equation (29) and improves the conditioning of the problem.

The procedure outlined above separates the compensator synthesis into distinct phases. The initial reduced-order full authority compensator is synthesized using the H_2 homotopy, which is then deformed into the reduced-order H_∞ compensator. During the H_∞ phase, the scalar H_2 norm weight λ is fixed (as are the plant matrices) and only the H_∞ norm overbound γ is varied. At discrete values, γ is fixed and λ is varied to perform the H_2 norm minimization. Thus, the procedure alternates between the H_∞ and H_2 norm minimization. A similar approach was introduced in reference 15.

During the homotopy, both the predicted and corrected gains are checked to ensure closed-loop stability. After each correction step, the cost gradient is checked to verify descent. During the H_∞ homotopy, the solvability of the Riccati equation using predicted or corrected gains must also be checked. If any of these conditions are violated, the prediction step size is decreased and the prediction phase is repeated. This process continues until the homotopy is completed or until the prediction step size is decreased below a prespecified tolerance.

The following section details the derivations employed in the homotopy algorithm for mixed H_2 / H_∞ design.

4.3 Mixed H_2/H_∞ Development

The homotopy function as well as the gradient and Hessian matrices are determined from the first order necessary conditions for an optimal mixed H_2 / H_∞ compensator given by equations (68)–(72). Define θ be a vector comprised of the free compensator parameters

$$\theta = vec(G) , \tag{79}$$

where G is the output feedback gain matrix defined in equation (35). The gradient of the cost is

$$f(\theta) = \frac{\partial L}{\partial \theta} = vec\left(\frac{\partial L}{\partial G}\right) = 0 , \tag{80}$$

where $\partial L / \partial G$ is given by equation (72).

The homotopy function is defined as

$$H(\theta,\alpha) = \frac{\partial L(\theta,\alpha)}{\partial \theta} = vec\left(\frac{\partial L(\theta,\alpha)}{\partial G}\right) = 0 \quad . \tag{81}$$

Note that L is now a function of the homotopy parameter α since the system matrices are now functions of α. The gradient of the homotopy function is

$$\nabla\left[H^T(\theta,\alpha)\right] = \left[\nabla_\theta H^T \quad \nabla_\alpha H^T\right] \quad . \tag{82}$$

4.3.1 Computation of Hessian

The derivative of the $N \times 1$ vector valued homotopy function, $H^T(\theta) = \left[h_1(\theta), h_2(\theta), L, h_N(\theta)\right]$, with respect to the N free parameter vector θ is the $N \times N$ Hessian matrix given by

$$\nabla_\theta H = \left[\frac{\partial H}{\partial \theta_1} \quad \frac{\partial H}{\partial \theta_2} L \quad \frac{\partial H}{\partial \theta_N}\right] \quad . \tag{83}$$

where

$$\frac{\partial H}{\partial \theta_j} = vec\left[\frac{\partial\left(\frac{\partial L}{\partial G}\right)}{\partial \theta_j}\right] \quad . \tag{84}$$

and using equation (72),

$$\frac{\partial H}{\partial \theta_j} = vec\left(\frac{\partial}{\partial \theta_j}\left\{2\left[\left(\overline{D}_{12}^T\overline{D}_{12}G\overline{C}_2 - \overline{D}_{12}^T\overline{C}_1 - \overline{B}_2^T Q_\infty\right)L\overline{C}_2^T\right.\right.\right.$$

$$\left.\left.\left. + \left(\lambda\overline{D}_{1p}^T\overline{D}_{1p}G\overline{C}_2 - \lambda\overline{D}_{1p}^T\overline{C}_p - \overline{B}_2^T L_p\right)X\overline{C}_2^T\right]\right\}\right) \tag{85}$$

$$= vec\left\{2\left[\left(\overline{D}_{12}^T\overline{D}_{12}G^{(j)}\overline{C}_2 - \overline{B}_2^T Q_\infty^{(j)}\right)L\overline{C}_2^T\right.\right.$$

$$+ \left(\overline{D}_{12}^T\overline{D}_{12}G\overline{C}_2 - \overline{D}_{12}^T\overline{C}_1 - \overline{B}_2^T Q_\infty\right)L^{(j)}\overline{C}_2^T$$

$$+ \left(\lambda\overline{D}_{1p}^T\overline{D}_{1p}G^{(j)}\overline{C}_2 - \overline{B}_2^T L_p^{(j)}\right)X\overline{C}_2^T$$

$$\left.\left. + \left(\lambda\overline{D}_{1p}^T\overline{D}_{1p}G\overline{C}_2 - \lambda\overline{D}_{1p}^T\overline{C}_p - \overline{B}_2^T L_p\right)X^{(j)}\overline{C}_2^T\right]\right\} \quad . \tag{86}$$

24

The derivatives with respect to θ are denoted

$$(*)^{(j)} = \frac{\partial(*)}{\partial \theta_j} \quad . \tag{87}$$

For $\theta_j = g_{ik}$,

$$G^{(j)} = \frac{\partial G}{\partial \theta_j} = E_{ik} \quad , \tag{88}$$

which is a matrix of zeros except for a one in the (i, k) element.

To obtain expressions for $L^{(j)}, Q_\infty^{(j)}, L_p^{(j)}$, and $X^{(j)}$, differentiate equations (68)–(71) with respect to θ_j to obtain

$$0 = \left(\tilde{A} + \gamma^{-2} \tilde{B} \tilde{B}^T Q_\infty \right) L^{(j)} + L^{(j)} \left(\tilde{A} + \gamma^{-2} \tilde{B} \tilde{B}^T Q_\infty \right)^T$$

$$+ \left[\left(\tilde{A}^{(j)} + \gamma^{-2} \tilde{B} \tilde{B}^T Q_\infty^{(j)} \right) L + L \left(\tilde{A}^{(j)} + \gamma^{-2} \tilde{B} \tilde{B}^T Q_\infty^{(j)} \right)^T \right] \tag{89}$$

$$0 = \left(\tilde{A} + \gamma^{-2} \tilde{B} \tilde{B}^T Q_\infty \right)^T Q_\infty^{(j)} + Q_\infty^{(j)} \left(\tilde{A} + \gamma^{-2} \tilde{B} \tilde{B}^T Q_\infty \right)$$

$$+ \left(\tilde{A}^{(j)T} Q_\infty + Q_\infty \tilde{A}^{(j)} + \left(\tilde{C}^T \tilde{C} \right)^{(j)} \right) \tag{90}$$

$$0 = \tilde{A}^T L_p^{(j)} + L_p^{(j)} \tilde{A} + \left[\tilde{A}^{(j)T} L_p + L_p \tilde{A}^{(j)} + \lambda \left(\tilde{C}_p^T \tilde{C}_p \right)^{(j)} \right] \tag{91}$$

$$0 = \tilde{A} X^{(j)} + X^{(j)} \tilde{A}^T + \left[\tilde{A}^{(j)} X + X \tilde{A}^{(j)T} + \left(\tilde{B}_p \tilde{B}_p^T \right)^{(j)} \right] \quad . \tag{92}$$

Derivatives of the closed-loop matrices are obtained from equations (64)–(66) and are given by

$$\tilde{A}^{(j)} = -\overline{B}_2 G^{(j)} \overline{C}_2 \tag{93}$$

$$\left(\tilde{B} \tilde{B}^T \right)^{(j)} = 0, \ \left(\tilde{B}_p \tilde{B}_p^T \right)^{(j)} = 0 \tag{94}$$

25

$$\left(\tilde{C}^T\tilde{C}\right)^{(j)} = \left(\overline{C}_2^T G^{(j)T}\overline{D}_{12}^T\overline{D}_{12}G\overline{C}_2\right) + \left(\overline{C}_2^T G^{(j)T}\overline{D}_{12}^T\overline{D}_{12}G\overline{C}_2\right)^T$$

$$-\left(\overline{C}_1^T\overline{D}_{12}G^{(j)}\overline{C}_2\right) - \left(\overline{C}_1^T\overline{D}_{12}G^{(j)}\overline{C}_2\right)^T \tag{95}$$

$$\left(\tilde{C}_p^T\tilde{C}_p\right)^{(j)} = \left(-\overline{D}_{1p}G^{(j)}\overline{C}_2\right)^T\left(\overline{C}_p - \overline{D}_{1p}G\overline{C}_2\right) + \left(\overline{C}_p - \overline{D}_{1p}G\overline{C}_2\right)^T\left(-\overline{D}_{1p}G^{(j)}\overline{C}_2\right) . \tag{96}$$

4.3.2 Computation of H_a

Similarly, the derivative of the homotopy function with respect to the homotopy parameter, α, is the $N \times 1$ vector

$$\nabla_\alpha H^T = \frac{\partial H^T}{\partial \alpha} \tag{97}$$

and

$$\frac{\partial H}{\partial \alpha} = vec\left[\frac{\partial\left(\frac{\partial L}{\partial G}\right)}{\partial \alpha}\right] \tag{98}$$

$$= vec\left(\frac{\partial}{\partial \alpha}\left\{2\left[\left(\overline{D}_{12}^T\overline{D}_{12}G\overline{C}_2 - \overline{D}_{12}^T\overline{C}_1 - \overline{B}_2^T Q_\infty\right)L\overline{C}_2^T\right.\right.\right.$$

$$\left.\left.\left.+\left(\lambda\overline{D}_{1p}^T\overline{D}_{1p}G\overline{C}_2 - \lambda\overline{D}_{1p}^T\overline{C}_p - \overline{B}_2^T L_p\right)X\overline{C}_2^T\right]\right\}\right) \tag{99}$$

$$= vec\left\{2\left[\left(\dot{\overline{D}}_{12}^T\overline{D}_{12}G\overline{C}_2 + \overline{D}_{12}^T\dot{\overline{D}}_{12}G\overline{C}_2 - \dot{\overline{D}}_{12}^T\overline{C}_1 - \overline{B}_2^T\dot{Q}_\infty\right)L\overline{C}_2^T\right.\right.$$

$$+\left(\overline{D}_{12}^T\overline{D}_{12}G\overline{C}_2 - \overline{D}_{12}^T\overline{C}_1 - \overline{B}_2^T Q_\infty\right)\dot{L}\overline{C}_2^T$$

$$+\left(\lambda\overline{D}_{1p}^T\overline{D}_{1p}G\overline{C}_2 - \lambda\overline{D}_{1p}^T\overline{C}_p - \overline{B}_2^T L_p\right.$$

$$\left.\left.\left.+\lambda\left(\dot{\overline{D}}_{1p}^T\overline{D}_{1p}G\overline{C}_2 + \overline{D}_{1p}^T\dot{\overline{D}}_{1p}G\overline{C}_2 - \dot{\overline{D}}_{1p}^T\overline{C}_p\right)\right)X\overline{C}_2^T\right]\right\} , \tag{100}$$

26

where

$$\dot{(*)} = \frac{\partial(*)}{\partial\alpha} \quad .$$
(101)

Implicit in these equations is the assumption that only the system matrices $\overline{D}_{12}$ and $\overline{D}_{1p}$ and the parameters λ and γ are functions of α. In general, the homotopy can be performed with any/all system matrices deformed.

The derivative terms in equation (100) depend on the deformation undertaken in the specified problem, i.e., the initial and final problem. Suppose that the deformation of the matrix $\overline{D}_{12}$ is prescibed to be

$$\overline{D}_{12}(\alpha) = \overline{D}_{12,0}(\alpha) + \alpha\left(\overline{D}_{12,f}(\alpha) - \overline{D}_{12,0}(\alpha)\right) \quad ,$$
(102)

where the 0 and f subscripts indicate the initial and final system matrices, respectively. It follows that

$$\dot{\overline{D}}_{12} = \overline{D}_{12,f} - \overline{D}_{12,0} \quad .$$
(103)

The derivatives of other plant matrices and the parameters λ and γ are determined accordingly. To obtain expressions for the derivatives of L, Q_∞, L_p, and X with respect to α, equations (68)–(71) are differentiated, resulting in the following:

$$0 = \left(\tilde{A} + \gamma^{-2}\tilde{B}\tilde{B}^T Q_\infty\right)\dot{L} + \dot{L}\left(\tilde{A} + \gamma^{-2}\tilde{B}\tilde{B}^T Q_\infty\right)^T + \left(\Gamma L + L\Gamma^T\right)$$
(104)

$$0 = \left(\tilde{A} + \gamma^{-2}\tilde{B}\tilde{B}^T Q_\infty\right)^T \dot{Q}_\infty + \dot{Q}_\infty\left(\tilde{A} + \gamma^{-2}\tilde{B}\tilde{B}^T Q_\infty\right) - \left(2\gamma^{-3}\dot{\gamma} Q_\infty \tilde{B}\tilde{B}^T Q_\infty\right)$$
(105)

$$0 = \tilde{A}^T \dot{L}_p + \dot{L}_p \tilde{A} + \left(\dot{\tilde{A}}^T L_p + L_p \dot{\tilde{A}} + \lambda \dot{\tilde{C}}_p^T \tilde{C}_p + \lambda \tilde{C}_p^T \dot{\tilde{C}}_p + \dot{\lambda}\tilde{C}_p^T \tilde{C}_p\right)$$
(106)

$$0 = \tilde{A}\dot{X} + \dot{X}\tilde{A}^T + \left(\dot{\tilde{A}}X + X\dot{\tilde{A}}^T + \dot{\tilde{B}}_p\tilde{B}_p^T + \tilde{B}_p\dot{\tilde{B}}_p^T\right) \quad ,$$
(107)

where

$$\Gamma = \dot{\tilde{A}} - 2\gamma^{-3}\dot{\gamma}\,\tilde{B}\tilde{B}^T Q_\infty + \gamma^{-2}\left(\dot{\tilde{B}}\tilde{B}^T Q_\infty + \tilde{B}\dot{\tilde{B}}^T Q_\infty + \tilde{B}\tilde{B}^T \dot{Q}_\infty\right) \quad ,$$
(108)

and from equations (64)–(66)

$$\dot{\overline{A}} = \dot{\overline{A}} - \dot{\overline{B}}_2 G \overline{C}_2 - \overline{B}_2 G \dot{\overline{C}}_2 \tag{109}$$

$$\dot{\overline{B}}_p = \dot{\overline{B}}_p \tag{110}$$

$$\dot{\overline{B}} = \dot{\overline{B}}_1 \tag{111}$$

$$\dot{\overline{C}}_p = \dot{\overline{C}}_p - \dot{\overline{D}}_{1p} G \overline{C}_2 - \overline{D}_{1p} G \dot{\overline{C}}_2 \tag{112}$$

$$\dot{\overline{C}} = \dot{\overline{C}}_1 - \dot{\overline{D}}_{12} G \overline{C}_2 - \overline{D}_{12} G \dot{\overline{C}}_2 \quad , \tag{113}$$

where from equations (58)–(61), the augmented matrix derivatives reduce to

$$\dot{\overline{A}} = \begin{bmatrix} A_f - A_0 & 0 \\ -N^0 \left(C_{2,f} - C_{2,0} \right) & 0 \end{bmatrix} \tag{114}$$

$$\dot{\overline{B}}_p = \begin{bmatrix} B_{p,f} - B_{p,0} \\ -N^0 \left(D_{2p,f} - D_{2p,0} \right) \end{bmatrix} \tag{115}$$

$$\dot{\overline{B}}_1 = \begin{bmatrix} B_{1,f} - B_{1,0} \\ -N^0 \left(D_{21,f} - D_{21,0} \right) \end{bmatrix} \tag{116}$$

$$\dot{\overline{B}}_2 = \begin{bmatrix} B_{2,f} - B_{2,0} & 0 \\ -N^0 \left(D_{22,f} - D_{22,0} \right) & 0 \end{bmatrix} \tag{117}$$

$$\dot{\overline{C}}_p = \begin{bmatrix} C_{p,f} - C_{p,0} & 0 \end{bmatrix} \tag{118}$$

$$\dot{\overline{C}}_1 = \begin{bmatrix} C_{1,f} - C_{1,0} & 0 \end{bmatrix} \tag{119}$$

$$\dot{\overline{C}}_2 = \begin{bmatrix} 0 & 0 \end{bmatrix} \tag{120}$$

$$\dot{\overline{D}}_{1p} = \begin{bmatrix} D_{1p,f} - D_{1p,0} & 0 \end{bmatrix} \tag{121}$$

28

$$\dot{\bar{D}}_{12} = \begin{bmatrix} D_{12,f} - D_{12,0} & 0 \end{bmatrix} . \tag{122}$$

The presence of the zero subblocks significantly enhances the computational efficiency of this approach. When implementing the procedure described at the beginning of this section, the above equations may be further specialized. In the initial H_2 homotopy procedure, the initial and final plant matrices are the same and the homotopy is performed only on the measurement and process noise intensities, D_{12} and D_{21}. Hence $\dot{\bar{A}}$, $\dot{\bar{B}}_2$, $\dot{\bar{C}}_1$, and $\dot{\bar{C}}_2$ are identically zero. For the mixed H_2 / H_∞ homotopy, the H_∞ and H_2 homotopies are performed distinctly, which simplifies the computations significantly since the plant matrices remain fixed and only γ or λ are varied at one time.

5. DESIGN EXAMPLES

5.1 Example 1: Flexible Four-Disk Example

To demonstrate the homotopy algorithm applied to optimal controller synthesis, the four-disk example originally described in reference 53 and more recently by numerous others[49] will be used. The four-disk model used in the example problem was derived from a laboratory experiment and represents an apparatus developed for testing of pointing control systems for FSS's with noncolocated sensors and actuators. Four disks are rigidly attached to a flexible axial shaft with control torque applied to selected disks and the angular displacement of selected disks measured. The plant parameters are taken from reference 1.

The seminal paper dealing with mixed H_2 / H_∞ design addressed the case where $w = w_p$ in equation (58) with results from the four-disk problem given for the full order case.[1] In this section, the one input, two output case will be repeated with the FOCUS algorithm as well as a two input, two output case with full- and fixed-order compensators to demonstrate the capabilities of the homotopy algorithm.

Table 1 presents a comparison of the results from the FOCUS algorithm and the results published in reference 1. In table 1, the "BH" subscript indicates results from reference 1 and the "F" subscript indicates results from FOCUS. Gaps in the columns of table 1 denoted "BH" correspond to values of γ for which results were not published. The absence of data generated by FOCUS for $\gamma = 2$ and 1.5 is due to the fact that γ is larger than the maximum ∞ norm as described in the next section. A key distinction between the formulations of the mixed H_2 / H_∞ optimization problem used herein and that of reference 1 is that while their formulation minimizes an overbound on the H_2 norm, the formulation utilized in FOCUS minimizes the actual H_2 norm. Consequently, as shown in figure 4, the FOCUS algorithm results in smaller H_2 norms for a given γ with the gap in the H_∞ norm overbound smaller than the reference 1 results in the meaningful region for γ, as described in the next section. Whereas $\gamma = 0.52$ was the smallest γ value reported in reference 1, γ values of 0.5, 0.4, and 0.3 are utilized with FOCUS, as indicated in table 1. A quasi-Newton technique based on the Broyden-Fletcher-Goldfarb-Shanno (BFGS) variable metric algorithm was used to extend these results for a full-order mixed H_2 / H_∞ controller, achieving $\gamma = 0.29$, corresponding to an actual H_∞ norm of 0.28.[54]

This example also demonstrates the synthesis of fixed-order mixed controllers with singular H_∞ constraints. In practice, compensators representing the extreme values of γ or λ will not typically be used since either performance or robustness would be severely diminished. A compromise value in the "elbow" of figure 4 would typically be chosen. While the FOCUS results in table 1 are not significantly better than the results of reference 1, the example demonstrates that the FOCUS code performs satisfactorily and lessens the gap between the overbound and the H_∞ norm.

30

Table 1. Comparison of FOCUS and reference 1 results.

γ	$\left\|T_{zw}\right\|_{\infty,BH}$	$\left\|T_{zw}\right\|_{\infty,F}$	$\left\|T_{zpwp}\right\|_{2,BH}$	$\left\|T_{zpwp}\right\|_{2,F}$
2.0	1.18		0.382	
1.5	1.06		0.389	
1.0	0.855	0.947	0.410	0.398
0.9	0.797	0.889	0.420	0.403
0.8	0.732	0.776	0.432	0.421
0.7	0.661	0.668	0.451	0.438
0.6		0.589		0.460
0.52	0.511	0.520	0.512	0.508
0.5		0.5		0.518
0.4		0.398		0.572
0.3		0.300		0.799
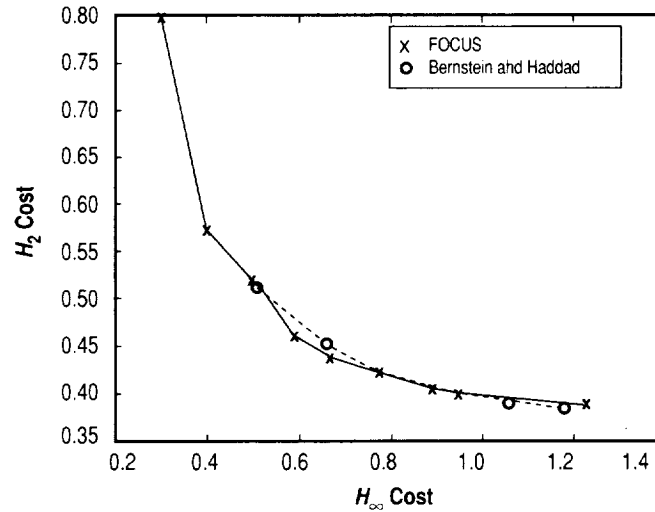
Figure 4. H_∞ versus H_2 cost for four-disk example.

This example serves to illustrate some interesting features of the mixed H_2 / H_∞ formulation implemented in FOCUS as well as distinctions from other formulations. The formulation implemented in FOCUS is a method for generating suboptimal H_∞ controllers of fixed order that are subject to an H_2 constraint. The cost functional for the mixed H_2 / H_∞ problem can be written as

$$J_{mix} = J_\infty + \lambda J_2 \,, \tag{123}$$

where

$$J_\infty = \mathrm{trace}\left\{Q_\infty \tilde{B}\tilde{B}^T\right\} \tag{124}$$

$$J_2 = \mathrm{trace}\left\{X\tilde{C}_p^T\tilde{C}_p\right\}, \tag{125}$$

subject to the corresponding Riccati and Lyapunov equations. The resulting lagrangian is given by equation (67).

Minimization of J_∞ results in an H_∞ controller with an upper bound on the ∞ norm given by the ∞ norm of the H_2 controller (as $\gamma \to \infty$, the H_2 compensator for T_{zw} is recovered by minimizing J_∞). By successively lowering gamma, the minimum H_∞ norm controller for T_{zw} is obtained. Minimization of J_2 results in the optimal H_2 compensator for T_{zpwp}. So when nonzero λ is used in J_{mix}, the H_∞ cost functional imposes an additional constraint on the H_∞ norm of T_{zw}, and for large γ, the necessary conditions for the mixed problem yield the simultaneous solution of two H_2 problems. By increasing the H_2 weight, λ, for a fixed γ, $\left\|T_{zpwp}\right\|_2$ is reduced while $\left\|T_{zw}\right\|_\infty$ approaches the gamma overbound. At that point, the minimum H_2 controller for T_{zpwp} such that $\left\|T_{zw}\right\|_\infty \leq \gamma$ is obtained.

For this example problem, the optimal H_2 controller for T_{zpwp} results in $\left\|T_{zw}\right\|_\infty = 1.392$ and $\left\|T_{zw}\right\|_2 = 0.3786$. γ values larger than 1.392 are not meaningful for our formulation because the optimal H_2 compensator for T_{zpwp} satisfies the γ constraint on $\left\|T_{zw}\right\|_\infty$. In that case, the H_∞ norm constraint is inactive in the mixed-norm optimization. However, since the reference 1 formulation seeks to minimize the H_2 norm overbound, it is possible for their formulation to generate meaningful solutions for $\gamma > 1.392$. When using FOCUS, the first step should be to establish an upper bound on γ by computing $\left\|T_{zw}\right\|_\infty$ resulting from the optimal H_2 compensator for T_{zpwp}.

5.2 Example 2: Building Control Example

An interesting example problem is that of controlling the vibration of a building subject to an earthquake excitation. The problem from a controls point of view is the need to develop a controller that can reliably accommodate the uncertainty in excitation that is characteristic of earthquakes, while at the same time handle the presence of uncertainties caused by inelastic structural response. This example examines design approaches which achieve nominal performance only (H_2), robust performance (μ-synthesis), and nominal performance/robust stability (mixed H_2 / μ), applied to the problem of building structural control. The challenge is to achieve the highest attainable level of RMS performance for a specified bounded set of uncertainties. A comparison of these controller design techniques is given based on an experimental model of a three-story tendon controlled structure at the National Center for Earthquake Engineering Research.[55] The laboratory structure is depicted in figure 5.
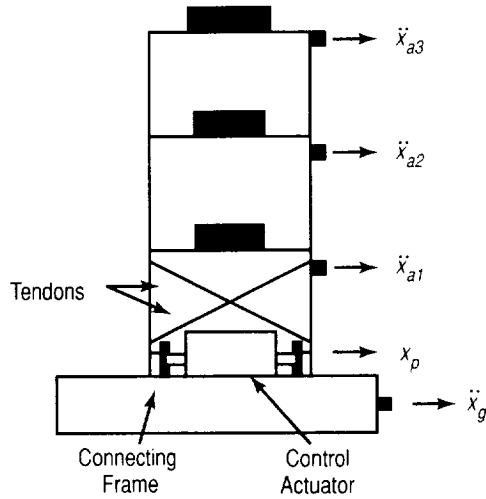
32

Figure 5. Structural control experiment.

5.2.1 Control Design Model

The evaluation model for performance assessment is a 20-state model from reference 55, obtained by system identification experiments on the laboratory structure. A 6-state nominal design model was obtained by balancing and residualizing the 20-state evaluation model, retaining modes at 2.268, 7.332, and 12.240 Hz. Inputs to the model consist of the ground acceleration disturbance, $\ddot{x}_g$, sensor noise, and the tendon control input, u. Performance outputs include the weighted displacement of the three floors relative to the ground, zp, and the weighted control force, zu. The measurement output, y, is the absolute acceleration of each of the three floors. All units are in volts. Figures 6 and 7 illustrate the fidelity of the reduced-order design model by comparing the frequency response of the design model and evaluation model and are typical of the other input-output pairs. Figure 6 presents the transfer function from the control input to the relative displacement of the third floor. The frequencies of the first three dominant modes are matched well, although some error exists with the modal gains. Figure 7 shows excellent matching with the transfer function from the disturbance input to the relative displacement of the third floor.

To provide robustness to model errors, the design model is extended to include parametric uncertainty within the control bandwidth in the form of errors in the modal damping and frequency squared terms as introduced in reference 17. Uncertainty will only be used for the natural frequency squared terms in this design, but for completeness, the formulation for uncertain modal damping will also be presented. Although the uncertain natural frequency square terms are real parameters, using a complex uncertainty also accounts for variations in modal damping if a hysteretic damping model is assumed.

In modal form, the nominal A matrix for a second order system is written

$$A_o = \begin{bmatrix} 0 & 1 \\ -\omega^2 & -2\zeta\omega \end{bmatrix}.$$

(126)
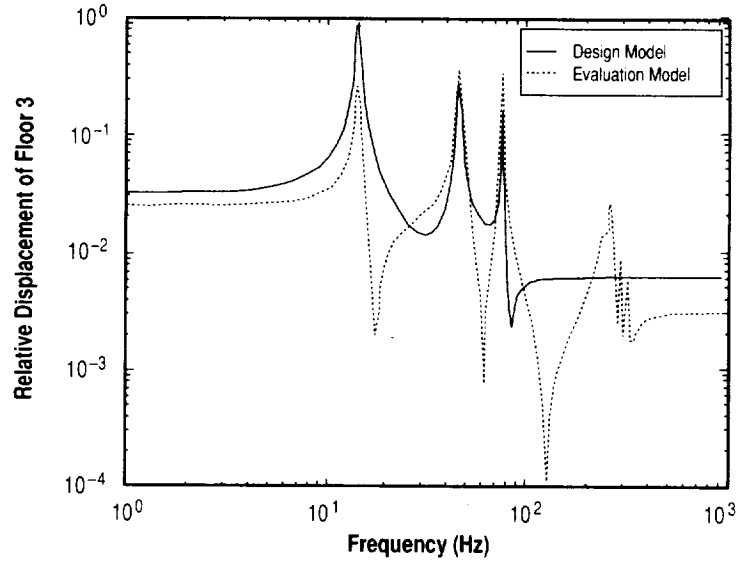
Figure 6. Comparison of design and evaluation models for relative
displacement of floor 3 to control input.

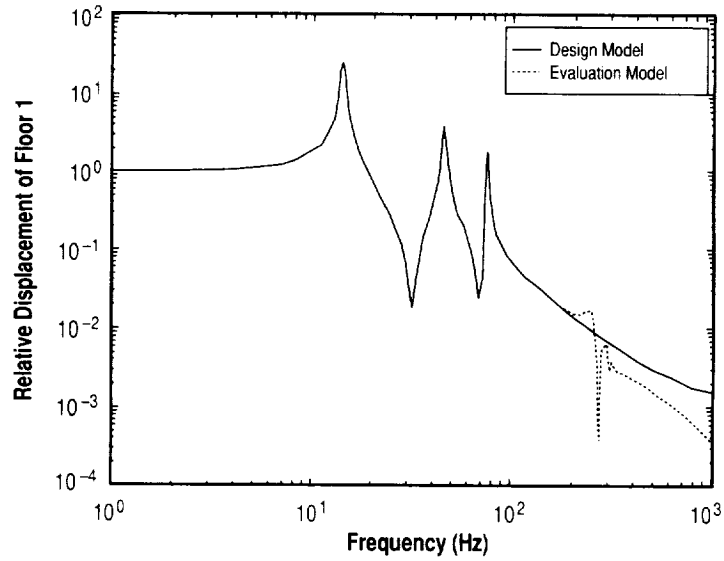Figure 7. Comparison of design and evaluation models for relative
displacement of floor 1 to disturbance input.

Introducing multiplicative uncertainty in the modal frequency square and modal damping terms
results in

$$A = \begin{bmatrix} 0 & 1 \\ -\omega^2(1 + \delta_1) & -2\zeta\omega(1 + \delta_2) \end{bmatrix} \tag{127}$$

$$= A_0 + \Delta A \quad, \tag{128}$$

where

$$\Delta A = \begin{bmatrix} 0 & 0 \\ -\omega^2 \delta_1 & -2\zeta\omega\delta_2 \end{bmatrix} \tag{129}$$

$$= \delta_1 \begin{bmatrix} 0 \\ 1 \end{bmatrix} \begin{bmatrix} -\omega^2 & 0 \end{bmatrix} + \delta_2 \begin{bmatrix} 0 \\ 1 \end{bmatrix} \begin{bmatrix} 0 & -2\zeta\omega \end{bmatrix} . \tag{130}$$

For a system with n total modes and m uncertain modes, $A = A_0 + \sum_{i=1}^{m} \Delta A_i$, and

$$\Delta A_i = (e_{2i})\delta_{1i}(-\omega_i^2)(e_{2i-1})^T + (e_{2i})\delta_{2i}(-2\zeta_i\omega_i)(e_{2i})^T , \tag{131}$$

where (e_j) is the jth standard basis vector for $\Re^{2n}$. Defining k to be the set of indices of uncertain modes allows the plant with uncertain natural frequency square and damping terms to be as shown in figure 8 with the following definitions:

$$\Delta A_{LW} = \Delta A_{LD} = E_{2k}, \quad \Delta A_{RW} = -\Omega^2 E_{2k-1}^T, \quad \Delta A_{RD} = -D\Omega E_{2k}^T , \tag{132}$$

$$\Omega = \text{diag}[\omega_{k(i)}], \quad D = \text{diag}[2\zeta_{k(i)}], \quad \forall i = 1,2,\text{K} , m , \tag{133}$$

$$E_{2k} = \begin{bmatrix} e_{2k(1)} & e_{2k(2)} & \text{K} & e_{2k(m)} \end{bmatrix} . \tag{134}$$
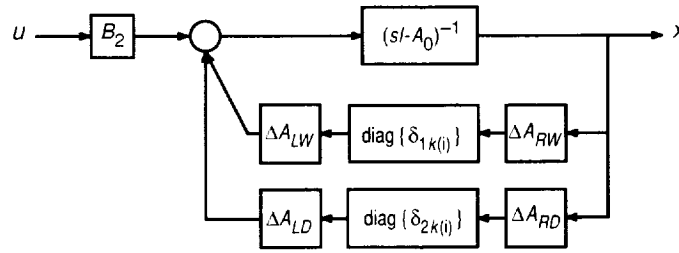
Figure 8. Plant with uncertain modal damping and frequency square terms.

In addition to the uncertainty in the modal frequency square terms, an additive uncertainty is included to represent model error outside the control bandwidth. This type uncertainty model forces the controller to gain stabilize the high-frequency modes that were truncated from the evaluation model. For robust control design, the baseline uncertainty model included 5-percent uncertainty for the natural frequency square error $(Wm = \sqrt{0.05})$ and an additive uncertainty weighting function given by

$$W_{additive} = 6.4 \frac{(s+5)^3}{(s+200)^3} = K_{add} * W_{add} . \tag{135}$$

Figure 9 presents the transfer function from control input to the acceleration of floor 1 and the corresponding additive uncertainty weight. In order to balance the plant for improved numerical results, the additive uncertainty model is realized as the frequency-dependent term, W_{add}, and the constant gain term, K_{add}.

Figure 9. Additive uncertainty weighting function.

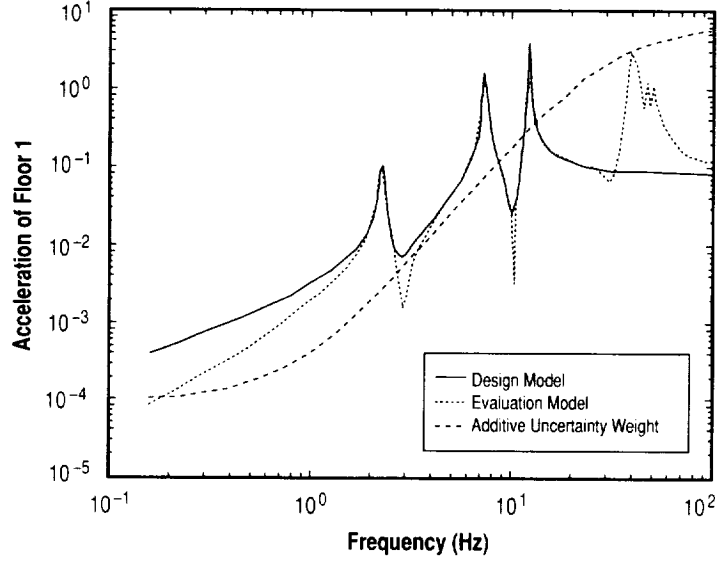Additional inputs for the robust control design generalized plant include inputs associated with the additive uncertainty, w_a, and the modal frequency uncertainty, w_m. Additional outputs include those associated with the additive uncertainty, z_a, and the modal frequency uncertainty, z_m. The uncertainty block has the structure

$$
\Delta = \begin{bmatrix} \delta_1 & & & & \\ & \delta_2 & & 0 & \\ & & \delta_3 & & \\ & 0 & & \Delta_4 & \\ & & & & \Delta_p \end{bmatrix},
\tag{136}
$$

with $\Delta_4 \in C^{3x1}$ and $\Delta_p \in C^{4x4}$. Figure 10 illustrates the generalized plant for robust control design.

5.2.2 Control Design Results

This section presents results of the design approaches for nominal performance (H_2), robust performance (μ-synthesis), and nominal performance/robust stability (mixed H_2 / μ) for the building structural control problem. For evaluating the nominal performance of these designs, performance is defined by Vz, the trace of the output covariance where the outputs are the three relative floor displacements, and Vu, the trace of the control input covariance.
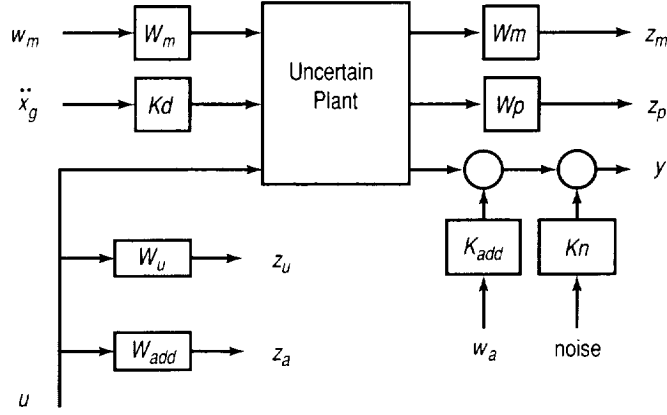
Figure 10. Generalized plant for robust control design: Building control example.

For the H_2 nominal performance design, the disturbance input and performance output vectors are

$$w = \begin{bmatrix} \text{noise} \\ \ddot{x}_g \end{bmatrix} \quad z = \begin{bmatrix} z_p \\ z_u \end{bmatrix}, \tag{137}$$

with the control weight, $Wu = \sqrt{\rho}$, the weight on the relative displacement of each floor, $Wp = 25$, the sensor noise intensity, $Kn = 0.001$, and the intensity of the ground disturbance, $Kd = 0.0017$. Kd was chosen to match the dc intensity of a reference earthquake excitation known as the Kanai-Tajimi (K-T) spectrum.[55] Control authority was varied in the design process using the scalar ρ.

For the μ-synthesis design, the corresponding disturbance and performance vectors are

$$w = \begin{bmatrix} w_m \\ w_a \\ \text{noise} \\ \ddot{x}_g \end{bmatrix} \quad z = \begin{bmatrix} z_m \\ z_a \\ z_u \\ z_p \end{bmatrix}. \tag{138}$$

A set of μ controllers of varying control authority was designed by fixing Wp and varying ρ. At each level of control authority, the relative weighting between z_p and z_u was determined by ρ and with the uncertainty weights fixed, $z = \begin{bmatrix} z_p^T, & z_u^T \end{bmatrix}^T$ was scaled (corresponding to the performance block for the μ design) to achieve a μ measure of one. By scaling the performance variables in this manner, at each level of control authority the controller was designed to maximize performance while providing a fixed level of robustness. Hence, a consistent comparison of control approaches was made from a robustness perspective. First order D-scales were used for each μ controller design, resulting in μ controllers with 19 states computed using the MATLAB™ μ-Analysis and Synthesis toolbox.[56]

37

Finally, a set of mixed H_2 / μ controllers were designed with fixed controller dimension of sixth order using the homotopy algorithm presented in section 4. In order to trade between nominal performance and robust stability, the H_2 subproblem is defined for nominal performance as above and the μ subproblem accounts for the additive and parametric uncertainty models. This paradigm is an effective means of exploiting the inherent trade between robustness and performance in mixed-norm design to separate the two competing design objectives. The H_2 subproblem is defined by the performance variables and the μ subproblem is defined by the variables associated with the uncertainty structure. The subproblems are defined by the inputs and outputs

$$
w_1 = \begin{bmatrix} w_m \\ w_a \end{bmatrix} \quad z_1 = \begin{bmatrix} z_m \\ z_a \end{bmatrix} \quad w_2 = \begin{bmatrix} \text{noise} \\ x_g \end{bmatrix} \quad z_2 = \begin{bmatrix} z_p \\ z_u \end{bmatrix} ,
\tag{139}
$$

and the D-scales for the μ subproblem are obtained from D–K iterations for $T_{z_1 w_1}$.

Figure 11 presents the mean-square (MS) nominal performance curves for each control design method. The robust control designs are for the baseline uncertainty model (which has 5-percent uncertainty in the natural frequency square parameters and the additive uncertainty). The costs are computed for the closed-loop with input noise filtered through the K–T spectrum. H_2 design costs are computed for both the design and evaluation models to illustrate the limitation on achievable performance due to model error. Although the cost curve evaluated with the design model extends to high control authority levels, the maximum performance with the evaluation model is obtained at $\rho = 15.63$ (indicated by "o" in fig. 11). The loop closed with the H_2 controllers and the evaluation model are unstable for smaller values of ρ. This cost comparison also indicates that for control authority levels lower than the instability level, the actual performance is almost identical to the design model performance.

Figure 11 also indicates the loss of MS performance that is incurred in exchange for robust performance. As a basis for comparison, the set of μ designs is evaluated in terms of MS performance. A substantial gap in performance exists between the H_2 and μ designs since the μ designs achieve a given level of output performance at a higher control cost than the H_2 designs. However, the mixed H_2 / μ designs effectively recover the MS performance of the H_2 designs while providing the same level of robust stability as the μ designs. The mixed H_2 / μ design procedure provides performance comparable to H_2 design while overcoming the major shortcoming of H_2 design, namely a lack of stability robustness.

The impact of uncertainty on performance in the mixed-norm design setting is evident in figure 12 where a set of mixed-norm designs for 10- and 20-percent parametric uncertainty are evaluated in addition to the baseline 5-percent parametric uncertainty mixed-norm designs. As the level of robustness increases, performance is sacrificed as indicated by the upward shift in the performance curve. A cursory comparison of figures 11 and 12 indicates that the mixed-norm controllers designed for 10- and 20-percent parametric uncertainty yield comparable performance to the μ controllers designed for 5-percent uncertainty. Hence, the mixed-norm designs provide more robust stability for a given level of performance than the μ controllers. Note that these comparisons are for nominal performance and

may not hold for robust performance. In these analyses, the additive uncertainty is held fixed since it is defined with respect to the model and serves only to force the controller to roll off and gain-stabilize the high-frequency unmodeled dynamics.
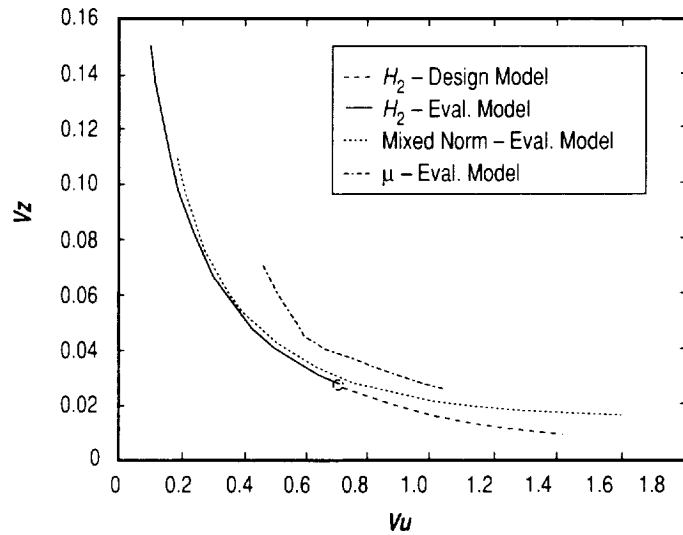

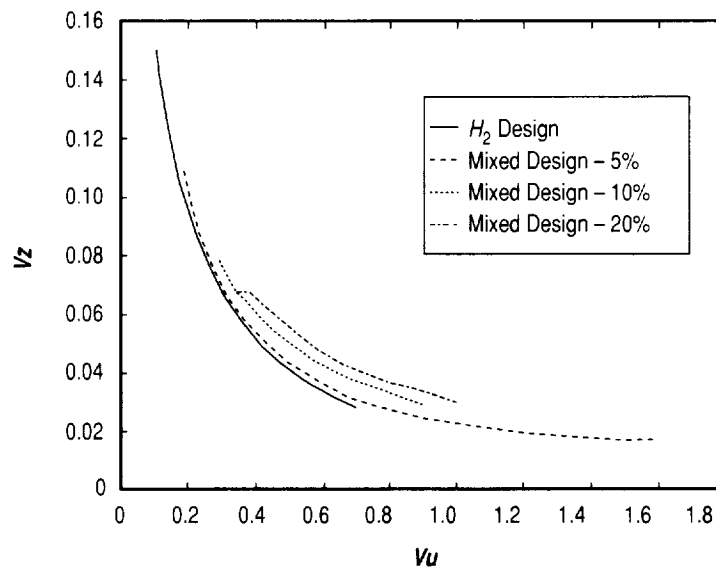Figure 11. Mean-square performance comparisons.

Figure 12. Impact of uncertainty level on mean-square performance.

Robust stability of each design is evaluated using mixed μ analysis where the parametric uncertainty is considered real and the additive uncertainty complex. As a result, the mixed μ measure is a less conservative measure of robust stability. Figure 13 plots the μ measure for the set of H_2 controllers for varying authority levels as a function of parametric uncertainty level. This plot should be interpreted as indicating the magnitude of perturbation required to destabilize the closed-loop. From equation (19), a μ measure < 1 indicates robust stability is guaranteed for all plants in the uncertain set. For a controller associated with a μ measure of β, the system will be unstable for $\|\Delta\|_\infty \geq \frac{1}{\beta}$. The H_2 designs are robust with respect to the uncertainty model only for very low authority controllers. Figure 13 illustrates the well known property of H_2 controllers that as control authority increases, the sensitivity (in terms of stability) to model error increases. This figure also indicates that the μ measure is relatively insensitive to different levels of parametric uncertainty at high control authority levels which indicates that the additive uncertainty dominates the stability analysis. Only at low authority levels are the H_2 designs sensitive to parametric uncertainty. Since control bandwidth is proportional to the authority level for these H_2 designs, the higher authority controllers interact with and destabilize the unmodeled modes.
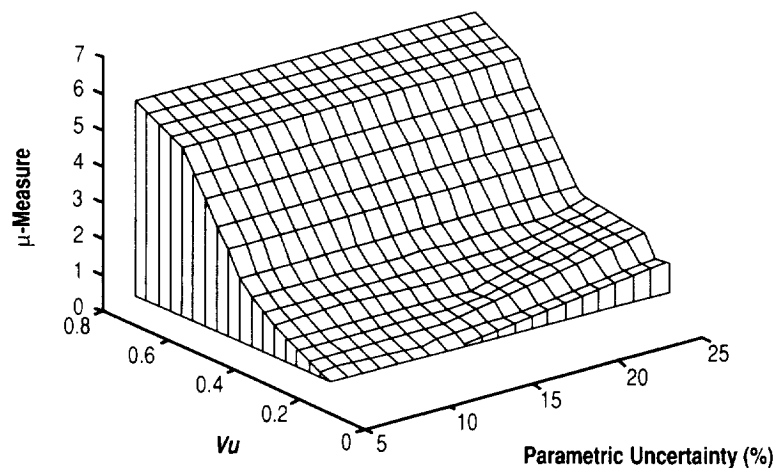

Figure 13. Robust stability analysis of H_2 controllers.

Robust stability analyses of the mixed-norm designs for 5-percent, 10-percent, and 20-percent parametric uncertainty are shown in figures 14–16. For the 5-percent uncertainty design, an H_∞ overbound of one was achieved. Although robust stability is not guaranteed for levels of uncertainty above 5 percent, the μ measure for 20-percent parametric uncertainty is <2, which is roughly 3 times better than the H_2 designs. It is also interesting to note that the μ measure for the mixed-norm design is sensitive to differences in parametric uncertainty and is relatively insensitive to the control authority, which is opposite the characteristic of the H_2 designs. As a matter of fact, the μ measure decreases slightly with control authority for the mixed-norm designs. Somewhat different behavior is observed with the mixed-norm designs for 10- and 20-percent parametric uncertainty. The mixed-norm design set for 10-percent parametric uncertainty used an H_∞ overbound of 1.3, so robust stability is not fully guaranteed for 10-percent variations in the uncertain natural frequency. The peak μ measure in figure 15 is 1.26. Similarly for the mixed-norm design with 20-percent parametric uncertainty, an H_∞ overbound of 2.1 was used and the peak μ measure is 1.75. These two designs have a characteristic behavior more similar to the H_2 designs in that the μ measure is more sensitive to control authority than parametric uncertainty level. However, the variation with control authority is significantly less than the H_2 designs.
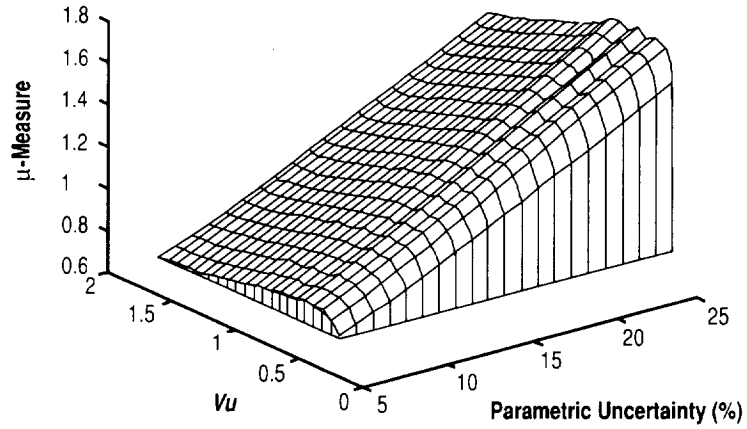
40

Figure 14. Robust stability analysis of mixed-norm designs performed for 5-percent uncertainty.
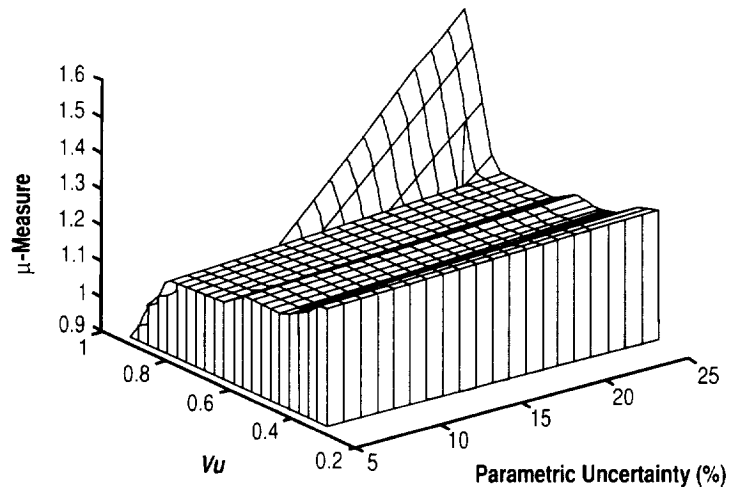

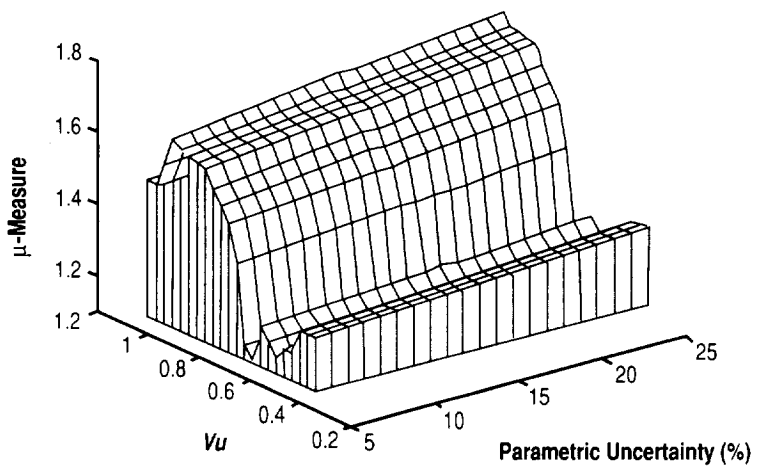Figure 15. Robust stability analysis of mixed-norm designs performed for 10-percent uncertainty.

Figure 16. Robust stability analysis of mixed-norm designs performed for 20-percent uncertainty.

41

For a second-order system with an uncertain natural frequency square parameter (equation (127)) with $\delta_2 = 0$), if δ_1 is considered a real parameter, the uncertain system will be stable when $\delta_1 > -1$. However, if δ_1 is a complex variation, the system is stable only when $|\delta_1| < 2\zeta$.[57] Thus representing the real parameter uncertainty as a complex variation introduces significant conservatism in the control design. The impact of this is evident in the mixed-norm design with 10- and 20-percent parametric uncertainty. The homotopy began with a fixed-order μ design for $T_{z_1 w_1}$ which exists because of the artificial destabilizing effect of the complex parametric uncertainty. For the 10-percent uncertainty level, the fixed-order H_∞ design with the D-scales from the full-order μ design resulted in a minimum H_∞ norm of 1.2539. For 20-percent uncertainty, the minimum H_∞ norm is 2.0463. Since these designs are for the H_∞ subproblem only, they represent a lower limit on the H_∞ norm for the mixed H_2 / μ designs and are used as the initial points for the λ homotopies in the mixed-norm designs.

The complex μ measure of each mixed-norm boundary controller is only very slightly less than the H_∞ norm overbound, indicating that the D-scales obtained from the full order D-K iteration for $T_{z_1 w_1}$ for each uncertainty level are nearly optimal for the sixth order mixed-norm controllers. Had this not been the case, the D-scales could have been optimized for a mixed-norm boundary controller, followed by another fixed order controller optimization step.

This design example also serves to illustrate the characteristics of the homotopy algorithm along the solution path. The mixed H_2 / μ design begins with a full-order μ design for $T_{z_1 w_1}$ followed by order reduction and a γ homotopy to obtain the minimum fixed-order μ design for $T_{z_1 w_1}$. This corresponds to a mixed H_2 / μ design for $\lambda = 0$, from which the λ homotopy begins by fixing the γ overbound slightly higher than the minimum γ and incrementally increasing λ. λ is increased until the H_2 norm of $T_{z_2 w_2}$ reaches a minimum and the H_∞ norm of $T_{z_1 w_1}$ is approximately equal to the γ overbound. At that point, one boundary design is obtained for a given value of ρ. The set of boundary designs are computed by varying ρ from this point.

As the λ homotopy progresses, the H_2 norm decreases from the minimum fixed-order μ controller value to the minimum H_2 norm subject to the H_∞ norm overbound. The variation of the H_2 norm during the λ homotopy for the 5-percent uncertainty level is shown in figure 17 along with the H_2 norms obtained with the fixed-order μ design and the full-order H_2 design. The mixed-norm design reduces the H_2 norm of the fixed order μ design by 50 percent while providing the same level of robust stability. Conversely, the mixed-norm design only increases the H_2 norm by 10 percent over the full-order H_2 design in exchange for robust stability. Note also that the most significant H_2 cost reduction occurs in the first few iterations which indicates that the entire λ homotopy does not have to be performed to make substantial improvements in H_2 cost. Figure 18 shows the constraint on the H_∞ norm is satisfied as the H_2 norm decreases to the minimum.
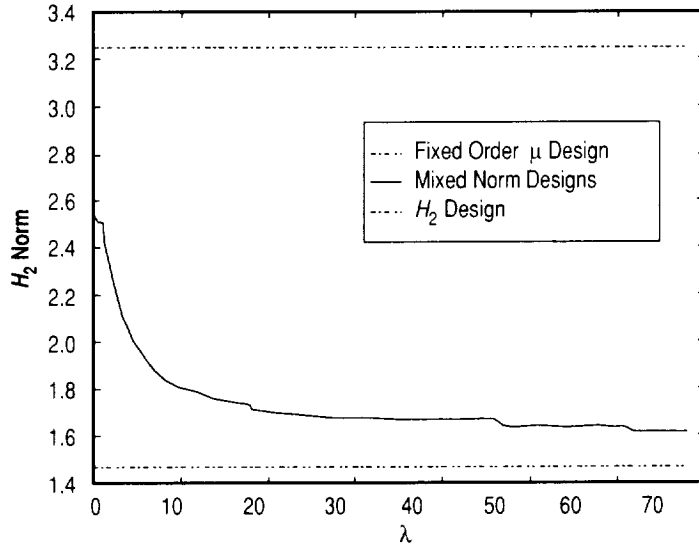
42

Figure 17. H_2 norm variation for λ homotopy with 5-percent uncertainty.
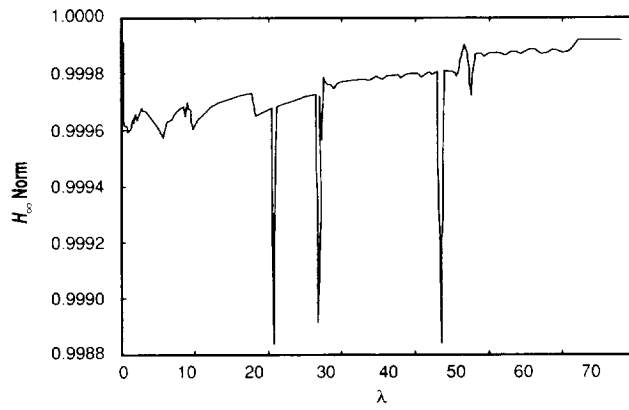
Figure 18. H_∞ norm variation for λ homotopy with 5-percent uncertainty.

The spikes in figure 18 are artifacts of the numerical optimization algorithm and are indicative of the numerical sensitivity of the homotopy algorithm. The controller canonical form tends to be poorer conditioned than a nonminimal realization which makes optimization of the fixed-order controller parameters difficult. After order reduction and transformation of the controller to canonical form, the initial gains are typically not optimum and the Hessian is often ill-conditioned and indefinite. Standard Newton optimization methods fail when the Hessian is ill-conditioned and indefinite. When using a standard Newton optimization method, the homotopy would terminate prematurely due to the ill-conditioned and indefinite Hessian. This numerical sensitivity motivated the development of a numerical optimization method that accounts for ill-conditioned and indefinite Hessians. Implementation of this optimization algorithm, described in appendix A, resulted in a numerically robust algorithm which converged along the homotopy path.

As for the homotopy along the boundary for variation in p, a typical gain trajectory is shown in figure 19 which is the second element of the parameter vector corresponding to the (1,2) element of the gain matrix G. Note that the gain variation is not monotonic. The trajectory of control gains in essence provides the mechanism by which the gains of a multivariable controller may be "dialed in," much the same manner as the dc gain of a classical controller. This enables an incremental implementation which may be monitored to determine the onset of instability and the maximum achievable nominal performance for a given design model. Hence, this example illustrates how the mixed-norm design procedure may effectively be used as a means of tuning multivariable controllers in orbit to achieve maximum performance.

Figure 19. Gain variation along boundary homotopy with 5-percent uncertainty.

5.3 Example 3: Flexible Space Structure Experimental Example
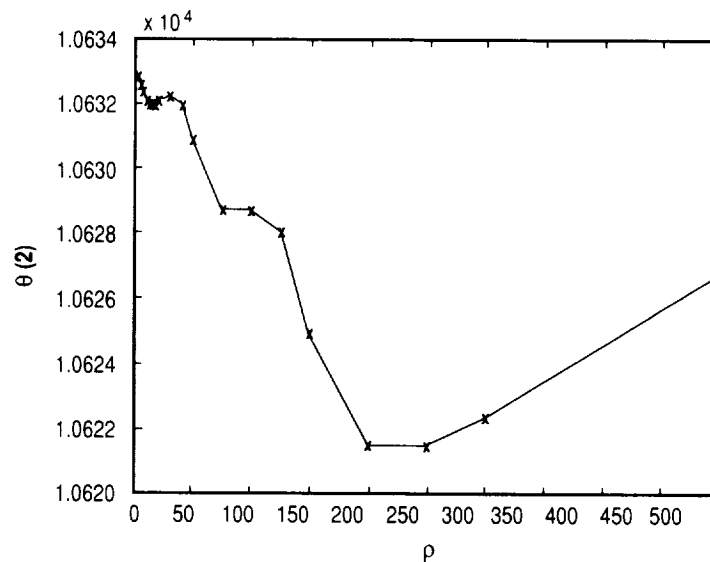
5.3.1 Facility Description

The Controls/Structure Interaction Ground Test Facility (CSI GTF) at the NASA Marshall Space Flight Center (MSFC) has been developed for experimental investigation into the control, system identification, and dynamics of an FSS. Characteristics of FSS's which make modeling, simulation, and control design challenging are embodied in the facility. The experiment is a large, flexible structure which has numerous low-frequency, coupled, tightly spaced, lightly damped modes. The present configuration includes a flexible, deployable boom which once flew on the Shuttle for the Solar Array Flight Experiment (SAFE). Initially, the facility was designed as a GTF for the Control, Astrophysics, and Structures Experiment in Space (CASES) flight experiment.

As shown in figure 20, the test article is inverted and vertically suspended from a platform 132 ft above ground level. A disturbance system provides two translational degrees of freedom to the base of the structure (the base refers to the portion of the experiment at the top platform). A simulated mission peculiar equipment support structure (MPESS) interfaces the disturbance system with the test article to simulate a flight experiment interface between the Shuttle, MPESS, and the payload. The test article consists of a 105-ft boom which supports a simulated occulting plate at the boom tip. The control objective of the flight experiment is to maintain alignment of the tip plate with a detector at the base of the boom on the Shuttle; this would allow the occulting plate to point towards a star to perform an x-ray experiment. Similarly, the ground experiment strives to maintain alignment of the tip plate with the simulated detector at the MPESS.

Control authority is provided by angular momentum exchange devices (AMED's) and bi-directional linear thrusters (BLT's). Each AMED package consists of two motors attached to reaction wheels, two two-axis gyros, and associated electronics. One AMED package is located at midboom and a second AMED which is augmented with a third reaction wheel is located at the tip. Each AMED motor has a peak rated torque of 290 oz-in. Two single-axis bidirectional linear thrusters are located at the boom tip which have a force capability of ± 2 lb up to 10 Hz. The shakers are considered actuators for disturbance generation and not for control. The measurement system includes sensors available for feedback control, disturbance, and safety monitoring. Control sensors include three single-axis accelerometers at the base (MPESS), two dual-axis gyroscopes (one redundant axis) in the midlength and tip AMED packages, three single-axis tip accelerometers, and a three-degree-of-freedom tip displacement sensor (TDS). Hence there are seven control actuators, 15 control sensors, and two programmable disturbance inputs. The CSI GTF computer system consists of a Sun host and a separate real-time system. Real-time control is provided with the capability of 64 sensor measurements, 64 actuator commands, and up to a 100th order controller at a rate of 250 Hz.

5.3.2 System Identification

The CSI GTF exhibits the pathologies that make control of FSS's challenging. System identification and control design for this structure is difficult due to the modal density and light damping at low
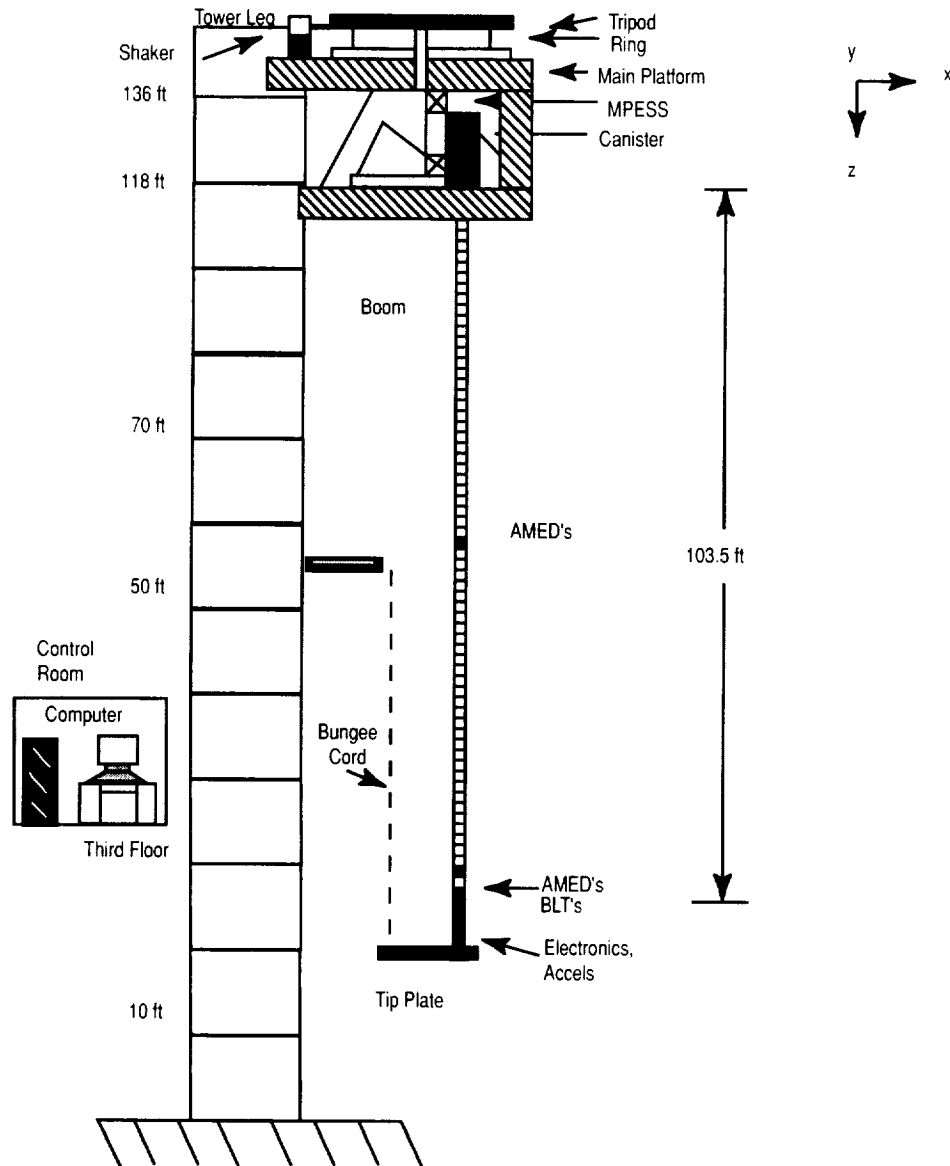
Figure 20. CSI ground test facility.

frequencies. Since the tip displacement is dominated by the low frequency bending modes, the model fidelity must be high in this regime. Modal density at low frequency also leads to high-order design plants.

The Eigensystem Realization Algorithm with Data Correlation (ERA/DC)[58] was used to obtain control design models for the CSI GTF. Time response data are used by ERA/DC to generate a discrete-time state space realization of the system. Inputs for system identification were the two disturbance shakers, the two tip thrusters, and the tip z-axis reaction wheel. In the initial iteration of system identification, each actuator was individually excited with an 80-sec burst of uncorrelated random noise with impulses interspersed every 20 sec. Comparison of the resulting models with frequency responses of the actual data indicated that several significant modes below 1 Hz were not accurately identified. Impulsive

46

inputs primarily excited the dominant first bending modes. To provide more energy at the frequencies where the unidentified modes were expected (from modal testing), a set of inputs were formed by summing sine waves at the 10 discrete target frequencies with a random phase. An uncorrelated noise sequence filtered with two poles at 25 Hz was added to each input in an effort to better facilitate identification of zeros. For one experiment, each actuator was excited simultaneously for 200 sec and the response was measured at the feedback control sensors. This procedure was repeated four times. The 200-sec response time histories were sampled at 250 Hz and postprocessed by removing the mean, low-pass filtering with four poles at 5 Hz and decimating to a 10-Hz sample rate.

To generate control design models from the time history data using ERA/DC, the System/Observer/Controller Identification Toolbox for MATLAB™ was used.[59] A 100-state model was obtained which identified the significant modes in the frequency range of interest for control design. This 100th-order model was reduced to a 40-state model by transforming to a balanced realization and truncating the states with low controllability/observability grammians. The modes above 3 Hz were then residualized resulting in a 26-state nominal model of the plant dynamics used for control design. Table 2 presents a comparison of the modes below 3 Hz from the 40-state system identification model with those generated by modal testing[60] and finite element modeling[61] and a description of each mode. Note that the modal test and system identification tests used different excitation and sensing.

As table 2 indicates, the structure exhibits a high degree of modal density with closely spaced, lightly damped modes, which taxes the system identification procedure. However, good results were obtained by ERA/DC and the resulting design model accurately describes the dynamics of the CSI GTF in the desired frequency range of <3 Hz. Due to the offset of the center of mass from the boom axis in the x direction (as well as coupling with the tip suspension system), bending in y couples strongly with torsional motion. Accurately representing this dynamic coupling in the identified model is critical for control design and is an indication of the fidelity of the ERA/DC identified model. The third and fourth x and y bending modes involve coupling with tip plate bending also.

Table 2. Comparison of experimental and analytical frequencies.

System ID		Modal Test	Finite Element	Mode
Frequency (Hz)	Damping (%)	Frequency (Hz)	Frequency (Hz)	Description
0.118	0.506	0.112	0.08	y 1st Bending
0.119	6.48	0.120	0.09	x 1st Bending
0.215	0.904	0.210	0.16	1st Torsion
0.325	57.3			
0.535	1.07	0.520	0.56	x 2nd Bending
0.554	0.604	0.530	0.58	y 2nd Bending
0.953	3.60			
1.214	38.8	1.391	1.23	x 3rd Bending
1.539	17.7			
1.771	3.15			
1.872	2.76	1.868	1.82	y 3rd Bending
2.061	13.2			
2.839	9.45	2.802	2.73	y 4th Bending
3.073	3.58	2.995	3.28	x 4th Bending

5.3.3 Control Design

The control objective for CSI GTF is to maintain alignment of the tip plate with respect to a sensor at the base of the boom when subjected to a disturbance force (DSy) applied at the base. To accomplish this objective, the measurements used for control are displacement sensed by the tip displacement sensors $(TDSx$ and $TDSy)$ and the three rotational rates sensed by tip rate gyroscopes $(TGx, TGy,$ and $TGz)$. Sensor noise is added to the plant output for control design. The BLT and the tip z axis reaction wheel (MC5) comprise the set of actuators used for feedback control. Due to the large generalized mass of the first x and y bending modes, the BLT's are the only actuators that have sufficient control authority to affect these modes.

The design results which follow are based on the mixed H_2 / H_∞ control methodology to achieve high nominal performance as measured by the MS alignment error of the tip plate while providing stability robustness in the presence of model errors. A compensator dimension of five was chosen for these design comparisons. Enforcing a constraint on the compensator order of five states is an extreme case chosen to highlight the effect of compensator dimension for fixed- and reduced-order designs. Five states result in a true canonical form for the compensator (the plant has five measured outputs) and also reduces computation. A major factor contributing to the computational burden of the mixed-norm homotopy algorithm is computing the Hessian. Since the Hessian is computed one row at a time and the number of rows is a multiple of the compensator dimension, keeping the compensator dimension small is important for computational efficiency.

A set of full-order H_2 designs provides a baseline for nominal performance evaluation with weighted control and weighted tip displacements as performance outputs and disturbance force and sensor noise as inputs. With reference to figure 21, the H_2 subproblem is defined by

$$ w_2 = \begin{bmatrix} \text{noise} \\ DSy \end{bmatrix} \quad z_2 = \begin{bmatrix} z_p \\ z_u \end{bmatrix} . \tag{140} $$

The baseline nominal performance design uses the weights $KDSy = 25$, $Wp = 100$, $Kn = 0.001$, and $W_u = \sqrt{\rho}$ where ρ is scaled to vary control authority. Figure 22 shows the performance of the full-order baseline H_2 designs and reduced fifth order H_2 compensators evaluated by comparing output and control cost with ρ varied from 1,000 to 100 (ρ is inversely proportional to control authority). The output and input costs plotted in figure 22 are the traces of the output and control covariances. Note that the solid line corresponding to the fifth order H_2 controllers obtained by balanced model reduction indicates that the order reduction process does not preserve closed-loop stability with the design model for higher levels of control authority (corresponding to ρ values <600).

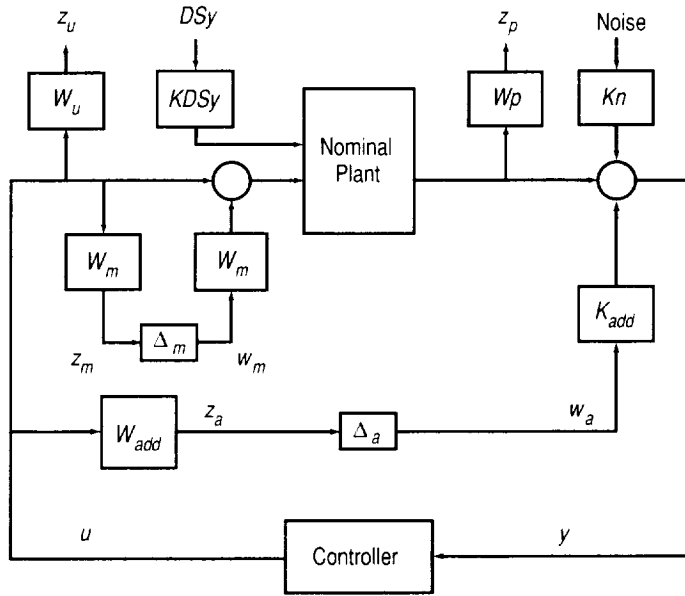Figure 21. Generalized plant of the CSI GTF for control design.
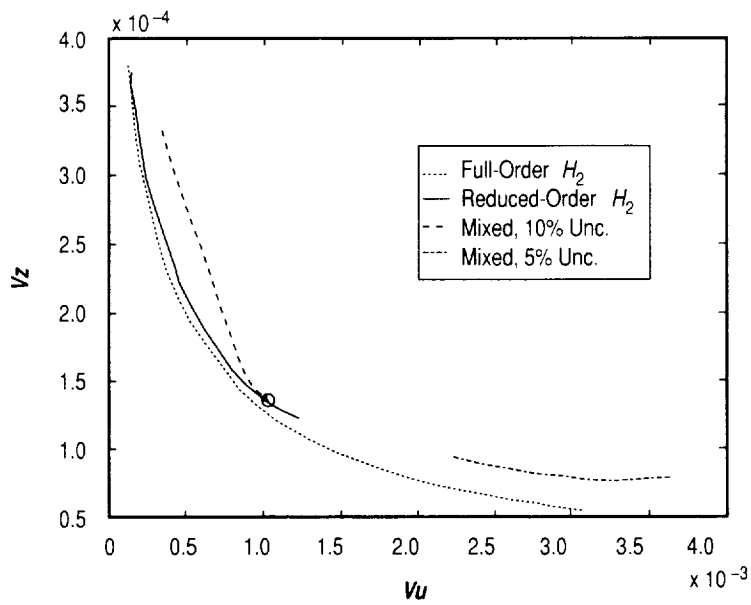

Figure 22. Mean-square cost trades for CSI GTF control design.

Phase I:

In the initial mixed-norm designs, the H_∞ subproblem employed a frequency-dependent additive uncertainty, $W_{additive}$, to constrain control bandwidth and a constant multiplicative uncertainty at the plant input, W_{mult}, to account for model error in the control bandwidth. A constant 5-percent multiplicative uncertainty is used. The additive uncertainty weight is a high-pass filter which is shaped to envelope the frequency response magnitude of each actuator to sensor transfer function above the control bandwidth. To control modes below 1 Hz and gain-stabilize the higher frequency unmodeled or poorly modeled modes, the additive uncertainty weight

$$W_{add} = 0.25 \frac{(s+5)^2}{(s+25)^2} \qquad (141)$$

is used, as indicated in figure 21. This weight effectively limits the control bandwidth to 1 Hz. The diagonal weighting matrix K_{add} provides a separate scaling for the additive uncertainty in each sensor channel and is given by $K_{add} = \text{diag}(1,1,0.5,25,0.75)$. The additive uncertainty output associated with the MC5 actuator was also scaled by a factor of 0.5. These scalings were determined to provide a tight covering for the additive uncertainty weight. The uncertainty structure for D-scaling is

$$\Delta = \begin{bmatrix} \Delta_{add} & 0 \\ 0 & \Delta_{mult} \end{bmatrix}, \qquad (142)$$

where Δ_{add} is a 5×3 unstructured block and

$$\Delta_{mult} = \begin{bmatrix} \delta_1 & 0 & 0 \\ 0 & \delta_2 & 0 \\ 0 & 0 & \delta_3 \end{bmatrix}. \qquad (143)$$

With reference to figure 21, the H_∞ subproblem is defined by

$$w_1 = \begin{bmatrix} w_a \\ w_m \end{bmatrix} \quad z_1 = \begin{bmatrix} z_a \\ z_m \end{bmatrix}. \qquad (144)$$

Although several options exist for defining the respective subproblems of the mixed H_2 / H_∞ formulation, this approach separates performance and robustness according to the most appropriate norms.

Using this uncertainty structure, D-scales were included in the generalized plant for fixed order mixed-norm control design. The generalized plant had 40 states including 26 for the nominal plant, 6 for the multiplicative uncertainty (a second-order weighting function for each of three plant input channels), and 4 each for the left and right frequency varying D-scales. A compensator dimension of five

50

was chosen to result in a true canonical form (the plant has five measured outputs) and reduce computation.

Varying ρ from 1 to 0.001 in the H_2 subproblem resulted in mixed-norm designs of such low authority that the performance was basically the same as open-loop. To allow a higher control bandwidth, the additive uncertainty weight was modified to envelope modes above 3 Hz, but no appreciable improvement in control authority was realized. The probable cause of this severely limited control authority is the excess conservatism associated with the full unstructured additive uncertainty block. Full unstructured uncertainty allows for cross-coupling between inputs and outputs which may not be realistic. This uncertainty model also neglects the inherent kinematic coupling of the displacements and rates.

In an attempt to mitigate this excess conservatism, the rate measurements were removed from the additive uncertainty, resulting in a 2×3 unstructured additive uncertainty block. However, using additive uncertainty weights for both 1- and 3-Hz control bandwidths again resulted in similar low authority controllers. Thus, with the compensator dimension constrained to five states, unstructured additive uncertainty appears to introduce excessive conservatism which severely limits nominal performance in the mixed norm design setting. The effect of uncertainty models with compensators having larger dimension remains to be assessed.

Phase II:

An alternative means of limiting control bandwidth and gain-stabilizing high-frequency modes is to use frequency-dependent multiplicative uncertainty in the H_∞ subproblem. In this second design phase, the additive uncertainty weight is removed and the multiplicative uncertainty at the plant input is given by

$$W_{mult} = W_m \frac{\left(\frac{s}{2\pi}+1\right)^2}{\left(\frac{s}{25}+1\right)^2} ,$$

(145)

where W_m represents a percentage uncertainty in magnitude of the frequency response at dc. The same uncertainty structure for Δ_{mult} given in equation (143) is used for this design phase.

When using the mixed norm design procedure, it is important to recognize that the mixed norm design is only merited when the underlying H_2 controller does not provide robust stability for a given uncertainty model and control authority level. Figures 23 and 24 present the robust stability of the full-order and reduced-order (5th) baseline H_2 designs, respectively, as a function of percent multiplicative uncertainty. For less than 10-percent multiplicative uncertainty, the full-order H_2 designs satisfy the robust stability constraints and the mixed norm design is not merited. However for 10 percent or larger

uncertainty, the full-order H_2 designs are only robustly stable in the low authority range. As expected, the shape of the surface in figure 23 indicates that the stability robustness is inversely proportional to control authority for a given level of uncertainty and is also inversely proportional to uncertainty at a fixed level of control authority. This is a well-known property of H_2 control design that in part motivates the development of robust control theory. The robust stability plot of the reduced-order H_2 designs indicates the same trend except that loss of stability due to order reduction precludes high authority controllers which violate robust stability to 10-percent uncertainty or larger. The point on figure 22 denoted 'o' is the highest authority reduced-order H_2 controller that satisfies robust stability for 10-percent multiplicative uncertainty.
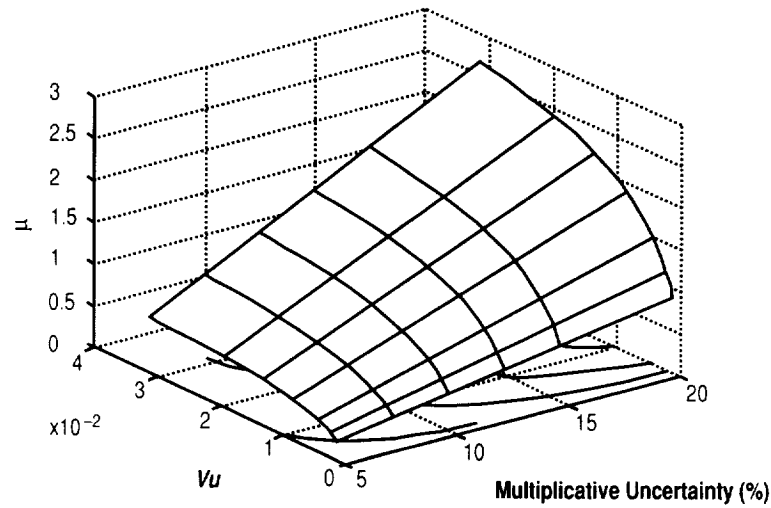

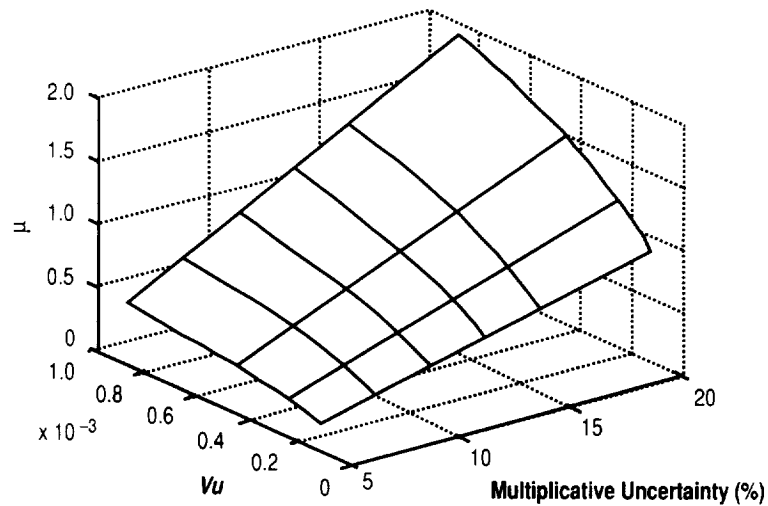Figure 23. Robust stability of full-order H_2 controllers.

Figure 24. Robust stability of reduced-order H_2 controllers.

52

Nominal performance of the fixed-order, mixed-norm designs with 5-, 10-, and 20-percent multiplicative (dc) uncertainty is shown in figure 22. Note that for each uncertainty level, a set of mixed-norm controllers results with nominal performance in different regions of the cost trade curve. Figure 22 indicates that the effect of uncertainty is to limit the control authority and, hence, limit the attainable performance. Although this is the same trend observed with the mixed-norm designs that included the additive uncertainty model (phase I), the limiting effect of the multiplicative uncertainty is not as severe and controllers with better nominal performance are obtained. The gaps between the full-order H_2 design curve and the fixed-order, mixed-norm design curves are indicative of the performance sacrificed to accommodate compensator order constraints. Performance of the mixed-norm designs is severely limited by constraining the compensator to five states. Although the fixed-order, mixed-norm procedure produces higher authority stabilizing controllers than does order reduction on the H_2 designs, the loss of closed-loop stability with H_2 order reduction could possibly be remedied with fixed-order H_2 design.

It should also be noted that although the mixed-norm controllers guarantee robust stability according to the uncertainty model for which they are designed, these mixed-norm controllers (except for the very low authority designs for 20-percent uncertainty) are not stable with the 40-state evaluation model. Thus, the multiplicative uncertainty model does not adequately capture the error introduced to the design model during the process of model reduction. Figure 25 presents the frequency response magnitude of the 26-state design model, the 40-state model, and the envelope of the uncertain design model with 10-percent multiplicative uncertainty. Evident from this figure is truncation of modes above 3 Hz in the design model as well as the mismatch between models at low frequency that results from model reduction. Other input/output frequency responses are similar.
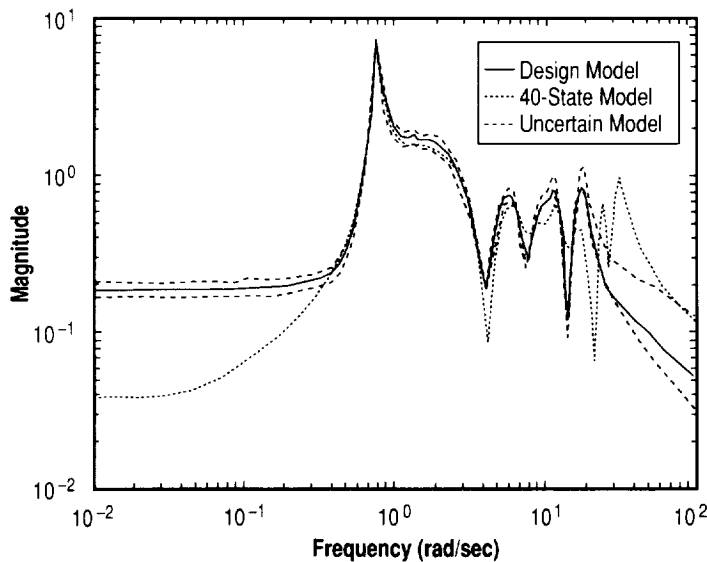

Figure 25. BLTx to TDSx transfer functions.

53

6. CLOSED-LOOP SYSTEM IDENTIFICATION FOR CONTROLLER REDESIGN

The traditional approach to control design is to obtain a nominal model of the plant, $\hat{P}$, which is the basis for control design. Since $\hat{P}$ is an approximation of the true plant, P, the model based compensator, $C_{\hat{P}}$, must provide a certain level of robust stability (i.e., $C_{\hat{P}}$ must internally stabilize $\hat{P}$ and P). In the system identification process, an attempt is made to bound the model error $\left\| P - \hat{P} \right\|$, which determines the amount of robustness required by the control design. It is also desirable that the controller provide some level of performance robustness; that is, the achievable performance should not differ significantly from the nominal design performance. High-performance control design for a flexible space structure is especially challenging since high-fidelity nominal plant models are difficult to obtain. The large error bounds that result typically require a very robust, low-performance control design which must be tuned on orbit to achieve the required performance.

An upper bound on achievable performance is[18, 29]

$$\left\| J\left(P,C_{\hat{P}}\right) \right\| \leq \left\| J\left(\hat{P},C_{\hat{P}}\right) \right\| + \left\| J\left(P,C_{\hat{P}}\right) - J\left(\hat{P},C_{\hat{P}}\right) \right\| , \tag{146}$$

where $\left\| J\left(P,C_{\hat{P}}\right) \right\|$ is the achieved performance, $\left\| J\left(\hat{P},C_{\hat{P}}\right) \right\|$ is the nominal performance, and $\left\| J\left(P,C_{\hat{P}}\right) - J\left(\hat{P},C_{\hat{P}}\right) \right\|$ is performance differential. The choice of a specific performance metric J and norm $\| * \|$ is determined by the control design methodology. To achieve high performance requires:

- High nominal performance $\left(\Leftrightarrow \left\| J\left(\hat{P},C_{\hat{P}}\right) \right\| \text{ small} \right)$

- Robust performance $\left(\Leftrightarrow \left\| J\left(P,C_{\hat{P}}\right) - J\left(\hat{P},C_{\hat{P}}\right) \right\| \ll \left\| J\left(\hat{P},C_{\hat{P}}\right) \right\| \right)$.

The second condition is actually a requirement on model fidelity and indicates that the nominal closed-loop system model must closely approximate the actual closed-loop system performance when the compensator $C_{\hat{P}}$ is used. Therefore, the "fitness" of the nominal model is a function of the compensator and must be judged from a closed-loop perspective. This fitness is not guaranteed by good open-loop model matching nor is it precluded by poor open-loop model matching.[3]

When the model error $\left\| P - \hat{P} \right\|$ is large, stability and performance robustness necessitates a low authority controller. Since a low authority controller is not as sensitive to model errors, the performance differential will be small compared to high authority controllers. However, the performance may not be satisfactory. To achieve high performance, the issues of modeling and control design must be treated

as a joint problem. The fitness of the design model, $\hat{P}$, is a function of $C_{\hat{P}}$, which is itself a function of the design plant. In some cases, high-performance control design requires an iterative closed-loop system identification and control design procedure.

A new closed-loop system identification method is presented in this section which is one step of an iterative closed-loop system identification and control design procedure. It is assumed that a moderately accurate dynamic model of the system to be controlled is available for the initial low authority controller design. However, this initial design model is not of sufficient fidelity to permit high authority control design. The objective of the closed-loop system identification procedure presented in this chapter is to refine the initial control design model based on closed-loop response data.

In the development of a closed-loop system identification method, consideration must be given to the nonuniqueness of the triple (A, B_2, C_2) in the identified realization. Although there is an infinite number of equivalent state space realizations for a system, a system with n states, nu inputs, and ny outputs can be uniquely expressed with a minimum of $n(nu + ny)$ parameters. Having as the objective of the closed-loop system identification process the ability to refine an existing design model, one approach which circumvents the nonuniqueness problem is to realize the open-loop system matrices in a unique, minimal form and directly identify the canonical parameters from closed-loop response data. Denery has developed a method of parameter estimation for multivariable state space systems from open-loop test data using canonical forms.[43] By utilizing the structure of the closed-loop system matrices, an extension of Denery's algorithm is developed to estimate the plant parameters based on closed-loop response data.

Proper selection of the objectives of system identification and control design further stresses the joint nature of the identification and control problem. Based on the prediction error method, the objective of the new closed-loop identification procedure developed in this section is to obtain a model $\hat{P}$ that minimizes the performance differential $\left\| T - \hat{T} \right\|_2$ where T is the actual closed-loop system and $\hat{T}$ is the identified closed-loop system. This system norm cannot be evaluated since T is not known. However, the actual and predicted closed-loop measurements are known and an equivalent objective is to minimize the prediction error of the closed-loop system, $\left\| y - \hat{y} \right\|_2$. The actual and predicted closed-loop system outputs, y and $\hat{y}$, respectively, are determined for the same set of inputs. The least-squares cost functional for control-dependent, closed-loop system identification then is

$$J = \frac{1}{2} \int_0^{t_f} (y - \hat{y})^T W(y - \hat{y}) dt \ , \tag{147}$$

where W is a constant matrix chosen to weight the relative importance of different measurement outputs. The control objective is matched with the identification objective by designing the controller to minimize the H_2 criterion $\left\| \hat{T} \right\|_2$.

The rest of the section is structured as follows. First, the algorithm developed by Denery for open-loop system identification procedure is presented in detail. Next, the extension of the canonical

system identification algorithm to closed-loop system identification is presented. Finally, an algorithm for iterative closed-loop system identification and control redesign is presented along with illustrative examples.

6.1 Denery's Open-Loop System Identification Algorithm

In reference 43, a two-step procedure is given which generates parameter estimates based on noisy measurement data. The algorithm begins with an equation error procedure, which is similar to a linear observer, to generate an initial estimate of the parameters. Noisy measurement data may cause the equation error estimates to be biased, but they are sufficiently accurate to initialize the second step, an iterative quasi-linearization output error procedure. Since the structure of the two procedures are identical with one exception that will be pointed out in the following, these two procedures are combined to form an iterative algorithm that is robust to initial parameter estimates and relatively insensitive to measurement noise. First, the details of the equation error procedure will be presented, followed by the output error procedure.

6.1.1 Equation Error Procedure

Consider a model of the state space system to be identified:

$$\dot{z} = F z + G u, \quad z(0) = z_0 \tag{148}$$

$$\hat{y} = H z . \tag{149}$$

The objective is to identify some F, G H, and z_0 which represents the dynamics of the unknown system based on knowledge of the inputs, $u(t)$, and noisy measurements, $y(t)$. An estimate of the unknown parameters may be obtained by minimizing the cost functional given in equation (147). Directly minimizing J results in a nonlinear optimization process, but in the absence of measurement noise, a linear formulation may be obtained. Recognizing that for a perfect model the output in equation (149) will exactly equal the measurements and $y - \hat{y} = 0$, this difference can be fed back to the model with arbitrary gains K and M according to

$$\dot{z} = F z + G u + K(y - Hz) \tag{150}$$

$$\hat{y} = H z + M(y - Hz) , \tag{151}$$

which can also be written

$$\dot{z} = F_N z + G_N u + \delta G u + K y \tag{152}$$

$$z(0) = z_{N0} + \delta z_0 \tag{153}$$

$$\hat{y} = H_N z + M y \tag{154}$$

56

by use of the definitions

$$F_N = F - KH \tag{155}$$

$$G_N = G - \delta G \tag{156}$$

$$H_N = (I - M)H \tag{157}$$

$$z_{N0} = z_0 - \delta z_0 \ . \tag{158}$$

The elements of $(F - KH)$ and $(I - MH)$ may be chosen independently of the unknown elements of F and H by using a maximum of $n * n_y$ parameters in K and M when the structure of the system is in a specific form. As a consequence, F_N, G_N, H_N, and z_{N0} are chosen and the unknown parameters are contained in K, M, δG, and δ_{z0}.

The structure of the system must be such that the unknown parameters in F are coefficients of measured states. To obtain this structure, Denery developed a canonical form for multivariable systems which is analogous to a canonical form in reference 62 for multi-input systems. Denery's canonical form is called the observer canonical form in reference 63, which is dual to the controller canonical form presented in section 3. It can be shown that if the plant dimension is an even multiple of the number of outputs and the first n rows of the observability matrix are linearly independent, then the realization is canonical and H will consist only of ones and zeros. Otherwise, some elements of H will be included as unknown parameters in the estimation procedure.

Equation (154) can now be rewritten as

$$\hat{y} = y_N + f(t)\gamma \ , \tag{159}$$

where y_N is the output of the linearized trajectory

$$z_N = F_N z_N + G_N u, \quad z_N(0) = z_{N0} \tag{160}$$

$$y_N = H_N z_N \ . \tag{161}$$

The sensitivity matrix, $f(t)$, is given by

$$f(t) = \frac{\partial \hat{y}}{\partial \gamma} \ , \tag{162}$$

where the vector of parameters to be estimated is

$$\gamma = \begin{bmatrix} vec(K) \\ vec(\delta G) \\ vec(M) \\ vec(\delta z_0) \end{bmatrix} .$$

(163)

Using the expression for $\hat{y}$ from equation (159) in the cost functional, equation (147), results in J becoming quadratic in the unknown parameters. By differentiating J with respect to the unknown parameters and equating the result to zero, the estimate of γ is given by

$$\hat{\gamma} = \left[\int_0^{t_f} f(t)^T W f(t) dt \right]^{-1} \left[\int_0^{t_f} f(t)^T W(y - \hat{y}) dt \right] ,$$

(164)

or for discrete measurements,

$$\hat{\gamma} = \left[\sum_{i=1}^N f(t_i)^T W f(t_i) \right]^{-1} \left[\sum_{i=1}^N f(t_i)^T W(y(t_i) - \hat{y}(t_i)) \right] .$$

(165)

The ith column of $f(t)$ is $\hat{y}_{\gamma_i}(t)$, which is the output of the ith sensitivity equation

$$\dot{z}_{\gamma_i} = F_N z_{\gamma_i} + \frac{\partial K}{\partial \gamma_i} y + \frac{\partial(\delta G)}{\partial \gamma_i} u$$

(166)

$$z_{\gamma_i}(0) = \frac{\partial(\delta z_0)}{\partial \gamma_i}$$

(167)

$$\hat{y}_{\gamma_i} = H_N z_{\gamma_i} + \frac{\partial M}{\partial \gamma_i} y .$$

(168)

From $\hat{\gamma}$, the system matrices are obtained by solving equations (155)–(158) for H, G F, and z_0. These values are used in F_N, G_N, H_N, and z_{N0} as the initial values for the next iteration.

6.1.2 Output Error Procedure

If the measurement data used in the equation error procedure are corrupted with unbiased measurement noise, a bias error will result in the parameter estimates. This can be circumvented by using

an output error procedure which yields unbiased parameter estimates based on unbiased noisy measurements, provided the initial estimates are sufficiently accurate. Typically, the biased estimates obtained from the equation error procedure are sufficiently accurate to initialize the output error procedure. Hence, the two procedures form a combined algorithm for unbiased parameter estimates based on unbiased noisy measurements.

The output error procedure implements the method of quasi-linearization, which is a well-known approach to minimize equation (147) subject to equations (148)–(149). The method of quasi-linearization approximates the response of the system model by a nominal trajectory y_N, based on the initial parameter estimates, plus a linearized correction about the nominal trajectory. By defining the initial estimates F, G, H, and z_0 to be F_N, G_N, H_N, and z_{N0}, respectively, $\hat{y}$ may be approximated by $\hat{y}_A$ from

$$\dot{\hat{z}}_A = F_N \hat{z}_A + \left[F - F_N\right]z_N + \left[G_N + \delta G\right]u, \quad \hat{z}_{A0} = z_{N0} + \delta z_0 \tag{169}$$

$$\hat{y}_A = H_N \hat{z}_A + \left[H - H_N\right]z_N . \tag{170}$$

where z_N is obtained from

$$\dot{z}_N = F_N z_N + G_N u, \quad z_N(0) = z_{N0}, \quad y_N = H_N z_N . \tag{171}$$

Using the definitions in equations (155)–(156), and recognizing that the initial estimates are sufficiently accurate, implies

$$KH = K\left[H_N + MH\right] \approx KH_N \tag{172}$$

$$MH = M\left[H_N + MH\right] \approx MH_N . \tag{173}$$

Substituting these expressions in equations (169)–(170) yields

$$\dot{\hat{z}}_A = F_N \hat{z}_A + G_N u + \delta G u + K y_N, \quad z_{A0} = z_{N0} + \delta z_0 \tag{174}$$

$$\hat{y}_A = H_N \hat{z}_A + M y_n , \tag{175}$$

which is identical to equations (152)–(154) except y_N replaces y. Using $\hat{y}_A$ in equation (147) instead of $\hat{y}$ reduces the minimization problem to a form identical to the equation error procedure, except y_N is used in the place of y when computing f in the sensitivity equations, equations (166)–(168). In the absence of noise in the measurements, the equation error estimate is the same as the quasi-linearization estimate.

6.2 Closed-Loop System Identification Algorithm

Denery's algorithm is extended to closed-loop system identification by expressing the plant in observer canonical form and exploiting the structure of the closed-loop matrices. For the plant given by

$$\dot{x} = Ax + B_1 w + B_2 u \tag{176}$$

$$y = C_2 x \tag{177}$$

and a dynamic compensator

$$\dot{x}_c = A_c x_c + B_c y \tag{178}$$

$$u = -C_c x_c , \tag{179}$$

the resulting closed-loop dynamics are

$$\begin{bmatrix} \dot{x} \\ \dot{x}_c \end{bmatrix} = \begin{bmatrix} A & -B_2 C_c \\ B_c C_2 & A_c \end{bmatrix} \begin{bmatrix} x \\ x_c \end{bmatrix} + \begin{bmatrix} B_1 & B_2 \\ 0 & 0 \end{bmatrix} \begin{bmatrix} w \\ u \end{bmatrix} \tag{180}$$

$$y = \begin{bmatrix} C_2 & 0 \\ 0 & I \end{bmatrix} \begin{bmatrix} x \\ x_c \end{bmatrix} . \tag{181}$$

As with the open-loop algorithm, noisy measurements are accounted for by averaging over multiple data sets.

If the plant (A, B_2, C_2) matrices are expressed in observer form, then the C_2 matrix consists of ones and zeroes and the unknown parameters in A are coefficients of the measured transformed states. (As stated earlier, in some cases the transformation may not be canonical, resulting in the C_2 matrix having additional nonzero elements, but these parameters can be estimated as well.) It is assumed that the compensator state vector time history is recorded. Comparison of equations (148)–(149) with equations (180)–(181) indicates that

$$F = \begin{bmatrix} A & -B_2 C_c \\ B_c C_2 & A_c \end{bmatrix}, \quad G = \begin{bmatrix} B_1 & B_2 \\ 0 & 0 \end{bmatrix}, \quad \text{and} \quad H = \begin{bmatrix} C_2 & 0 \\ 0 & I \end{bmatrix} . \tag{182}$$

Since the only unknowns in F and G are the plant matrices A, B_1, and B_2, the unknown parameter matrices are defined as

$$K = \begin{bmatrix} K_{11} & -K_{12} C_c \\ 0 & 0 \end{bmatrix}, \quad \delta G = \begin{bmatrix} \delta G_1 & \delta G_2 \\ 0 & 0 \end{bmatrix} . \tag{183}$$

60

In the case of a true canonical form for the plant, H is completely known. Note that K_{11} corresponds to the unknown parameters in A, K_{12} corresponds to the unknown parameters in B_2, δG_1 corresponds to the unknown parameters in B_1, and $\delta G_2 = K_{12}$.

For closed-loop system identification, the partial derivative expressions in the sensitivity equations, equations (166)–(168), are modified as follows and the unknown parameter vector is defined as

$$
\gamma = \begin{bmatrix} vec(K_{11}) \\ vec(K_{12}) \\ vec(\delta G_1) \\ vec(\delta z_0) \end{bmatrix} .
\tag{184}
$$

For γ_i corresponding to the (j, k) element of K_{11},

$$
\frac{\partial K}{\partial \gamma_i} = e_j e_k^T
\tag{185}
$$

and

$$
\frac{\partial \delta G}{\partial \gamma_i} = 0, \quad \frac{\partial M}{\partial \gamma_i} = 0, \quad \frac{\partial \delta z_0}{\partial \gamma_i} = 0 ,
\tag{186}
$$

where $e_j e_k^T$ is a matrix of zeros except for a one in the (j, k) element. For γ_i corresponding to the (j, k) element of K_{12},

$$
\frac{\partial K}{\partial \gamma_i} = \begin{bmatrix} 0 & \frac{\partial(-K_{12}C_c)}{\partial \gamma_i} \\ 0 & 0 \end{bmatrix}
\tag{187}
$$

where

$$
\frac{\partial K_{12}C_c}{\partial \gamma_i} = -e_j e_k^T C_c ,
\tag{188}
$$

which is an $nxnc$ matrix of zeroes except for the jth row which is comprised of the kth row of C_c. Since $\delta G_2 = K_{12}$,

$$
\frac{\partial \delta G}{\partial \gamma_i} = \begin{bmatrix} 0 & \frac{\partial \delta G_2}{\partial \gamma_i} \\ 0 & 0 \end{bmatrix} ,
\tag{189}
$$

61

where $\frac{\partial \delta G_{12}}{\partial \gamma_i} = \frac{\partial K_{12}}{\partial \gamma_i}$ is zero except for a one in the (j, k) element. The terms $\frac{\partial M}{\partial \gamma_i}$ and $\frac{\partial \delta z_0}{\partial \gamma_i}$ are identically zero. For γ_i corresponding to the (j, k) element of δG_{11},

$$\frac{\partial \delta G}{\partial \gamma_i} = \begin{bmatrix} \frac{\partial \delta G_{11}}{\partial \gamma_i} & 0 \\ 0 & 0 \end{bmatrix}, \tag{190}$$

where $\frac{\partial \delta G_{11}}{\partial \gamma_i}$ is zero except for a one in the (j, k) element and all others are identically zero. Similarly, for γ_i corresponding to the jth element of δz_0, $\frac{\partial \delta z_0}{\partial \gamma_i}$ is a zero vector with a one in the jth element and all others are identically zero.

Note that this algorithm is not guaranteed to converge. Since the estimates are determined by minimizing the error in the closed-loop time response and not the error in the open-loop plant parameter estimates, the plant parameter estimates may not converge to the "true" plant parameters but still provide a good control design model.

6.3 Iterative Control Redesign Examples

The iterative closed-loop system identification and control design procedure implemented herein is patterned after the approach of reference 18 with one notable exception to be pointed out below.

Iterative closed-loop identification and control redesign algorithm:

1. Beginning with model $\hat{P}_i$, design a set of H_2 controllers of varying control authority.

2. Evaluate actual and estimated output and control costs and performance differential

3. Determine highest performance control design point which satisfies performance differential constraint threshold, denoted $C_{\hat{P},i}$.

4. Using closed-loop data from $T\left(P, C_{\hat{P},i}\right)$ and $\hat{P}_i$, do closed-loop system identification to determine $\hat{P}_{i+1}$.

5. Repeat until desired performance is attained.

This algorithm differs from the framework presented in reference 18 in that the amount of control authority increase between iterations is more formally quantified. Recognizing that small changes in controller authority tend to result in small changes in performance, a constant scaling factor was used in the control design step in reference 18 which was slightly increased each identification/control design iteration. Thus the control authority was gradually increased each iteration until an appropriate model and high authority control design was achieved. In the procedure introduced above, the performance is evaluated for a set of controllers with varying authority to ascertain the onset of performance differen-

tial due to model mismatch. Instead of numerous iterations of identification and control design, the emphasis is placed on evaluating a set of controllers designed for a common model. By explicitly evaluating the performance differential for each controller, large steps in control authority may be taken with each iteration, resulting in few identification/control design iterations. The output and control costs are evaluated in the same manner as was done for the building structure control example of section 5. Although the iterative procedure is not guaranteed to converge, the convergence may be checked at each iteration by evaluating the performance at each iteration.

6.3.1 Coupled Mass Example

As an example of the iterative identification and control procedure, the coupled two mass problem illustrated in figure 26 is used. This example problem highlights robust control issues as related to flexible space structures and was used as a benchmark problem in reference 64 (with $k_1 = 0$ and $d_1 = 0$). A disturbance acts on mass two and the control force is applied to first mass. The coefficient matrices are

$$
A = \begin{bmatrix}
0 & 0 & 1 & 0 \\
0 & 0 & 0 & 1 \\
-(k_1 + k_2)/m_1 & k_2/m_1 & -(d_1 + d_2)/m_1 & d_2/m_1 \\
k_2/m_2 & -k_2/m_2 & d_2/m_2 & -d_2 m_2
\end{bmatrix}
\tag{191}
$$

$$
B_1 = \begin{bmatrix} 0 \\ 0 \\ 0 \\ 1/m_2 \end{bmatrix}, \quad
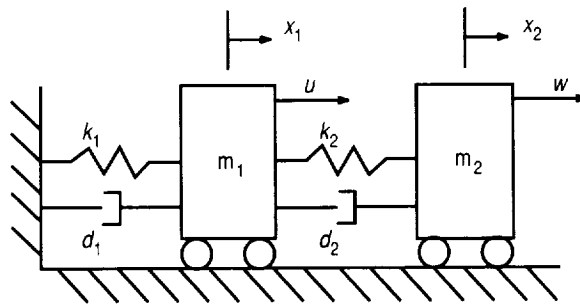B_2 = \begin{bmatrix} 0 \\ 0 \\ 1/m_1 \\ 0 \end{bmatrix}.
\tag{192}
$$

Figure 26. Coupled mass benchmark problem.

The state vector is $\bar{x} = [x_1, x_2, \dot{x}_1, \dot{x}_2]^T$ and the measurements are $y = [x_1, x_2]^T$, so

$$C_2 = \begin{bmatrix} 1 & 0 & 0 & 0 \\ 0 & 1 & 0 & 0 \end{bmatrix}.$$

(193)

Two cases will be considered—the first having open-loop stable and the second case having a rigid body mode. The stable system is described by $k_1 = k_2 = 1.2$, $m_1 = m_2 = 1.5$, $\zeta_1 = \zeta_2 = 0.1$ and the damping constant is computed by $d_i = 2\zeta_i \sqrt{k_i m_i}$.

The procedure begins with an initial plant for control design. As an extreme case, the initial plant is obtained by adding 50-percent error to k_1, k_2, ζ_1, and ζ_2 and 5-percent error for each of the two masses. After transforming the true $(A, [B_1 \ B_2], C_2)$ triple to observer canonical form, the resulting realization is

$$At \begin{bmatrix} 0 & -0.8000 & 0 & 0.8000 \\ 1.0000 & -0.1789 & 0 & 0.1789 \\ 0 & 0.8000 & 0 & -1.6000 \\ 0 & 0.1789 & 1.0000 & -0.3578 \end{bmatrix}$$

(194)

$$[B1t \ B2t] = \begin{bmatrix} 0.6667 & 0 \\ 0 & 0 \\ 0 & 0.6667 \\ 0 & 0 \end{bmatrix}, \quad C20 = \begin{bmatrix} 0 & 1 & 0 & 0 \\ 0 & 0 & 0 & 1 \end{bmatrix},$$

(195)

and the corresponding initial triple in observer canonical form is

$$A0 = \begin{bmatrix} 0 & -1.1429 & 0 & 1.1429 \\ 1.0000 & -0.3207 & 0 & 0.3207 \\ 0 & 1.1429 & 0 & -2.2857 \\ 0 & 0.3207 & 1.0000 & -0.6414 \end{bmatrix}$$

(196)

$$[B10 \ B20] = \begin{bmatrix} 0.6349 & 0 \\ 0 & 0 \\ 0 & 0.6349 \\ 0 & 0 \end{bmatrix}.$$

(197)

64

In observer canonical form, the C_2 matrix is fixed for a given set of observability indices and the columns of the A matrix with free elements corresponds to the columns of C_2 that have an element equal to one. Note that the resulting initial design plant elements varied by 79.28 percent and 42.86 percent in the A matrix, and 4.76 percent in the B_1 and B_2 matrices from the truth model.

A set of LQG controllers of varying authority were designed for the initial design plant using the weighting matrices

$$W = \begin{bmatrix} I_n & 0 \\ 0 & \rho I_{nu} \end{bmatrix}, \quad V = \begin{bmatrix} I_n & 0 \\ 0 & I_{ny} \end{bmatrix},$$ (198)

where ρ is used to vary the control authority. The performance of this set of controllers was then evaluated with both the design model and the truth model to assess the performance differential that results from the initial erroneous model. Recall from the beginning of this section that the performance differential is a measure of performance robustness. Figure 27 indicates a large performance difference at all control authority levels, so a controller with a moderate authority level ($\rho = 5$) is chosen for initial implementation.
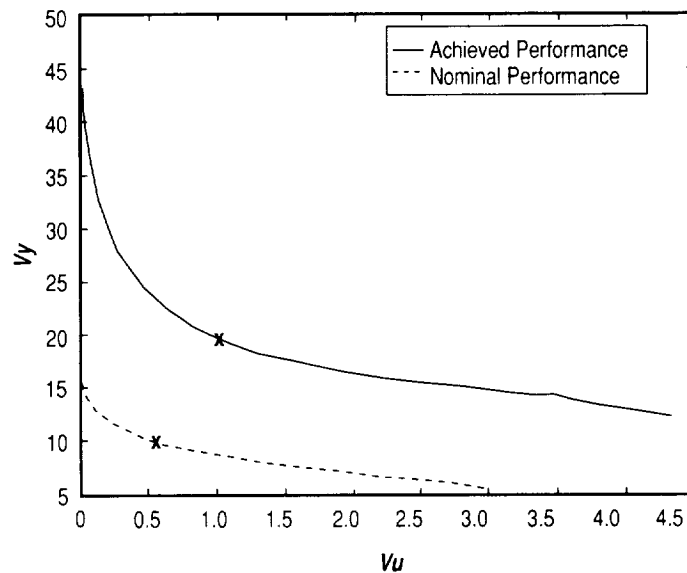
Figure 27. Performance differential using initial plant: Coupled mass problem.

Using the LQG controller designed for $\rho = 5$ with the initial design model, the closed-loop is excited with unit intensity, zero mean random noise low pass filtered at 25 Hz. The closed-loop measurements are corrupted with a low-intensity, random measurement noise (the standard deviation of the noise was equal to 20 percent of the standard deviation of the measurements). In reference 43, measurement noise is accounted for by averaging over multiple experiment sets. In this example, five sets of measurements are used and the five resulting sets of estimated system matrices are averaged.

Table 3 gives the initial, actual, and estimated parameters of the system matrices in observer canonical form. The significant error is clear as well as the convergence of the parameter estimates after 50 iterations. As with the combined open-loop algorithm, the first 25 iterations used the equation error method and the second 25 iterations used the output error method. The convergence over 50 iterations for the correction to the $A(4,3)$ parameter is shown in figure 28. This parameter corresponds to the largest element of γ (required the largest correction) at the first correction iteration. A slight discontinuity is evident at the 25th iteration when the algorithm switched from the equation error method to the output error method. However, this is removed after one iteration.

Table 3. Comparison of initial, actual, and estimated parameters
for open-loop stable coupled mass problem.

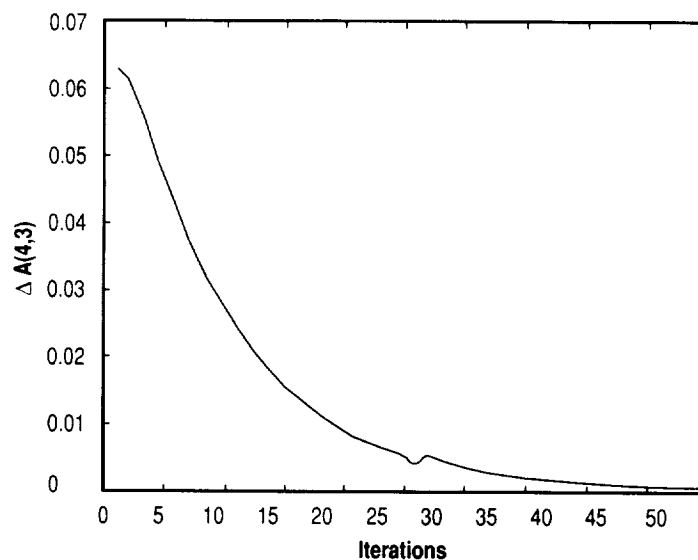| Initial Parameters	True Parameters	Estimated Parameters
−1.1429	−0.8000	−0.8240
−0.3207	−0.1789	−0.1832
1.1429	0.8000	0.8252
0.3207	0.1789	0.1993
1.1429	0.8000	0.8219
0.3207	0.1789	0.1720
−2.2857	−1.6000	−1.6531
−0.6414	−0.3578	−0.3815
0.6349	0.6667	0.6672
0	0	−0.0064
0	0	−0.0027
0	0	0.0016
0	0	−0.0004
0	0	0.0113
0.6349	0.6667	0.6733
0	0	0.0039

Figure 28. Convergence of $\Delta A(4,3)$.

Having refined the initial design model to obtain a more accurate model, a second set of LQG controllers is designed and the performance differential evaluated. Figure 29 shows that the gap between design performance and achieved performance is considerably decreased at all authority levels when compared to figure 27. The identified model results in robust performance (as defined at the beginning of this section in regard to performance differential) and good nominal performance. It bears pointing out that when the identification experiment was conducted without measurement noise, the achieved performance and design performance curves were indistinguishable, indicating that the difference in figure 29 is due to measurement noise. More averages and more iterations could possibly further diminish the performance differential. Another perspective is to compare the achieved performance for a set of LQG designs based on the initial plant model with the achieved performance for the designs based on the estimated model, shown in figure 30. The difference between the dashed line and the solid line indicates the performance increase attained by performing closed-loop system identification and controller redesign. Although the amount of performance sacrificed by designing the controller based on an initial open-loop design model depends on the specific plant and control design, figure 30 illustrates the fact that model error limits achievable performance and better performance can be obtained by refining the model to reduce the error. The design point corresponding to $\rho = 5$ which was used in the closed-loop system identification is indicated by 'x' on figure 30.
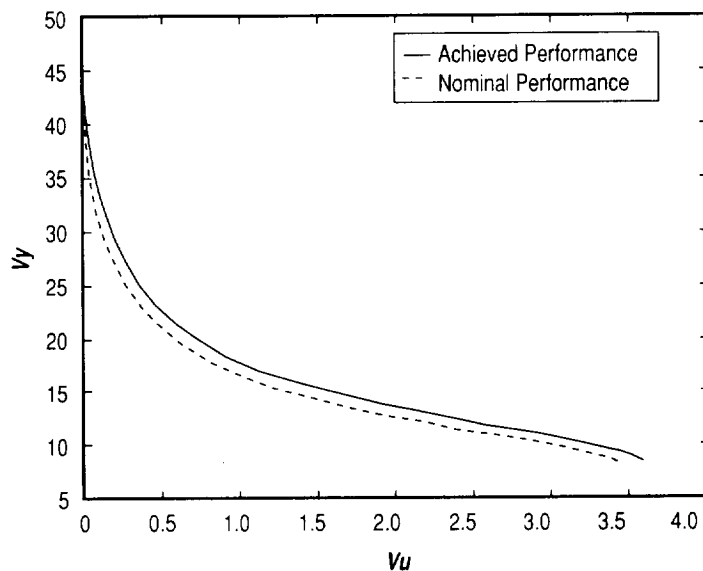
Figure 29. Performance differential using estimated plant: Coupled mass problem.

A more difficult identification problem is obtained by removing the spring and damper denoted k_1 and d_1 on figure 26, resulting in an unstable rigid body mode in the open-loop plant. Identification of open-loop unstable systems (such as spacecraft) is a difficult task which is a further motivation for closed-loop system identification. Using the same initial stiffness and damping error, table 4 indicates the convergence of the estimated system parameters after 50 iterations. Again, the measurements were noise-corrupted and the estimates were averaged after five identification experiments. Similar convergence of the parameter estimates was observed for this case as for the open-loop stable example.

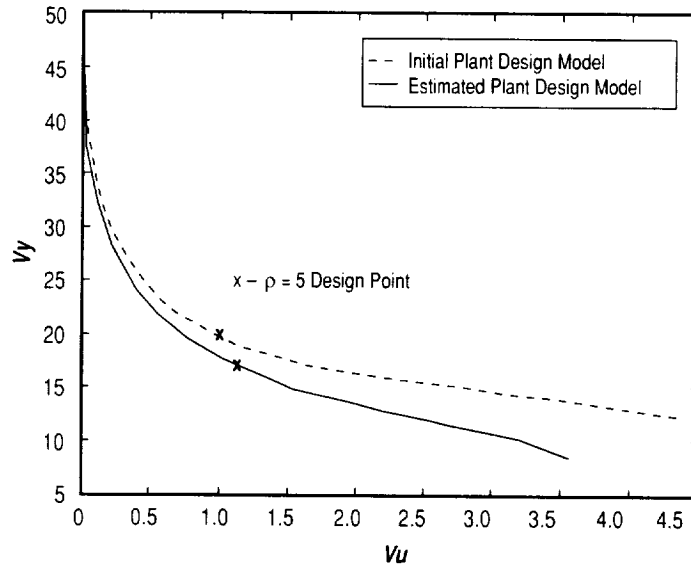Figure 30. Comparison of achieved performance: Coupled mass problem.

Table 4. Comparison of initial, actual, and estimated parameters
for open-loop unstable example.

Initial Parameters	True Parameters	Estimated Parameters
–1.1429	–0.8000	–0.8228
–0.3207	–0.1789	–0.1830
1.1429	0.8000	0.8253
0.3207	0.1789	0.1937
1.1429	0.8000	0.8228
0.3207	0.1789	0.1835
–1.1429	–0.8000	–0.8231
–0.3207	–0.1789	–0.1860
0.6349	0.6667	0.6637
0	0	0.0009
0	0	–0.0011
0	0	–0.0016
0	0	0.0016
0	0	0.0034
0.6349	0.6667	0.6678
0	0	0.0045

6.3.2 Building Control Example

A second example is the building structure used as a control design example in section 5. Using the six-state nominal design model as the truth model, the inputs are the ground acceleration and control force and the outputs are the relative displacements of the three floors, which results in 30 parameters to be estimated. An initial erroneous design model is obtained by adding 5-percent error to the natural frequency square terms and the B_1 and B_2 matrices. Although only 5-percent error is introduced, the maximum errors in the elements of the A, B_1, and B_2 matrices (in observer canonical form) are 72.2 percent, 9.9 percent, and 39.6 percent, respectively.

Using the initial model, a set of LQG controllers is designed using ρ to vary the control authority. For this example, filtered noise is used as input excitation and perfect measurements are assumed. Figure 31 indicates the performance differential resulting from controllers designed for the initial model, which is relatively constant at all control authority levels. A low authority controller is used for closed-loop system identification which results in an estimated plant with the performance differential shown in figure 32. For this estimated model, there is virtually no performance differential.
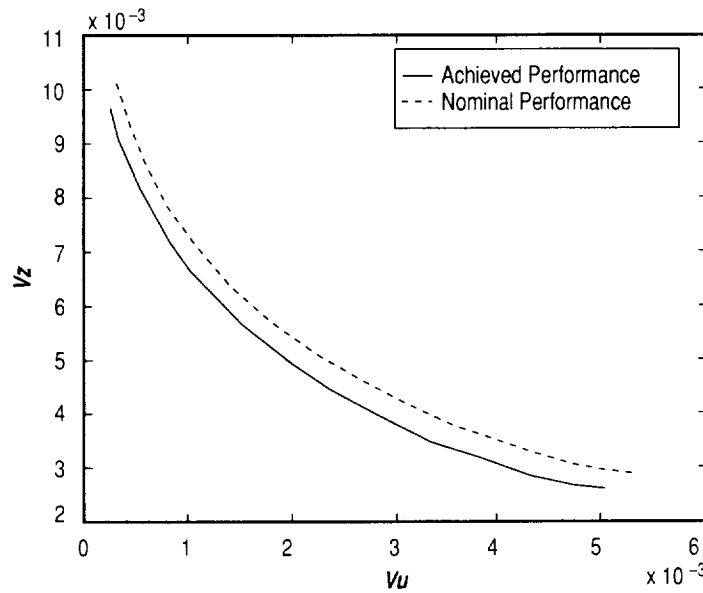
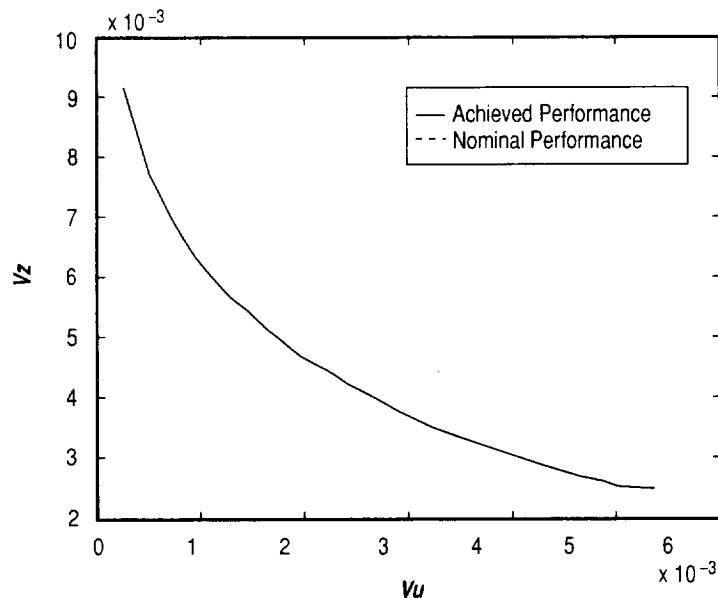Figure 31. Performance differential using initial plant: Building problem.

Figure 32. Performance differential using estimated plant: Building problem.

6.3.3 Discussion

Since the end objective is an iterative system identification and model-based control design procedure, additional constraints are placed on the input and output processes. The system identification is based on closed-loop test data which mandates that the generalized plant, equations (54)–(57), consist of actuated inputs and measured outputs only. Figure 33 illustrates this requirement where the disturbance inputs, w and w_p, act through the control input and sensor channels and the performance variables, z and z_p, must be linear combinations of the sensed variables, y, and the control inputs, u. Hence a constraint is placed on the generalized plant formulation by the system identification such that the columns of B_1 and B_p lie in the column space of B_2 and the rows of C_1 and C_p lie in the row space of C_2. With regard to the H_∞ subproblem, this requires the uncertainty representation to consist only of (input or output) multiplicative and additive uncertainty models, which implies that it is not possible, for example, to include parametric uncertainty such as mass or stiffness uncertainty in the generalized plant formulation. The matrices D_{21}, D_{2p}, D_{1p}, and D_{12} are obtained from the input/output uncertainty models and disturbances, and do not contain parameters to be estimated. Consequently, the plant matrices A, B_2, and C_2 are the only matrices to be estimated by closed-loop system identification. To relax this constraint would require introducing additional actuators and sensors for the sole purpose of system identification.
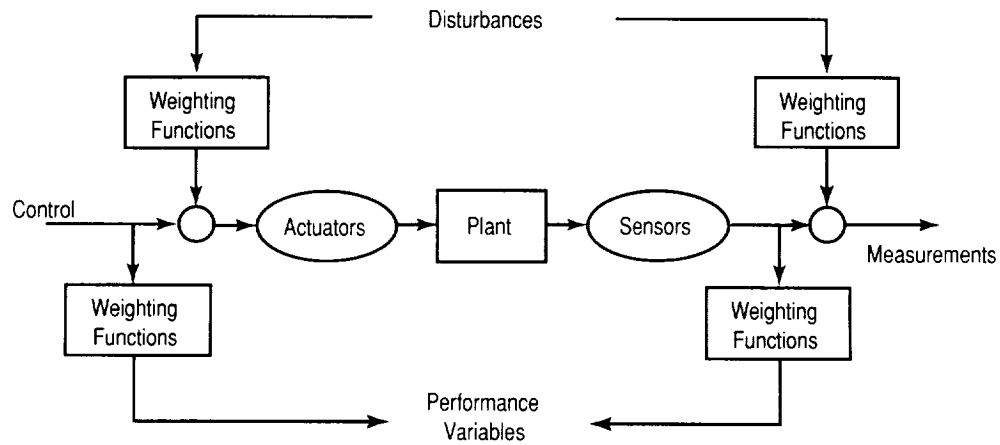
Figure 33. Input/output constraint relationships.

A brief discussion on the closed-loop system identification algorithm from a numerical implementation perspective is warranted. The stability of the algorithm is sensitive to several factors. The primary factor influencing convergence of the parameter estimation is the matrix inversion in the computation of $\hat{\gamma}$ (equation (164) or (165)). For this inverse to exist, the $(ny + nc) \times N_p$ sensitivity matrix f must have full row rank where $N_p = n*(nu + ny + nw)$ is the number of unknown parameters. Recall that the columns of f are time histories of the sensitivity equations, equations (166)–(168), which include the compensator state time histories. If the input is not sufficiently rich to excite the measurement and compensator states, then f will not have full rank. This difficulty is compounded as the number of parameters increases. If the matrix tends to singularity, the magnitude of the elements of $\hat{\gamma}$ diverge.

In order to alleviate the divergence of $\hat{\gamma}$ in the examples above, a relaxation factor was introduced that scaled $\hat{\gamma}$. Scaling $\hat{\gamma}$ by a relaxation factor of 0.5 typically was sufficient to produce smooth convergence as seen in figure 28. Without the relaxation factor, the estimates would overshoot and overcorrect, resulting in divergence of the parameter estimates. The relaxation factor in essence damped the overshoot of the correction steps at each iteration. This could possibly have been accomplished by using a pseudo-inverse of the matrix to zero the small singular values, but that would have introduced error. Using the relaxation factor did not introduce error but only slowed the convergence.

7. CONCLUSIONS AND RECOMMENDATIONS

This dissertation has shown that to achieve high performance control requires a control design methodology that maximizes performance while guaranteeing robust stability for a given model error. The mixed H_2 / H_∞ design procedure presented herein is well suited to this task when used to synthesize a set of controllers that explicitly trade between robustness and performance. Design examples have shown that fixed-order, mixed-norm design provides performance comparable to an H_2 design while overcoming a key deficiency of H_2 design by providing robust stability. When performance is defined by an H_2 measure in mixed-norm design, better performance is often obtained than the μ-synthesis for the same error bound. Synthesis of the mixed-norm controller set is accomplished using a homotopy algorithm which generates a trajectory of gain variations as plant parameters or performance specifications vary.

To improve performance often requires reducing model error through system identification. In many cases open-loop testing is not possible, and even when it is, often the most appropriate model for control design is obtained from closed-loop response data. A new method for refining a control design model from closed-loop response data is presented herein. Based on a prediction error method, the open-loop plant parameters are estimated in a canonical form. Examples have shown that higher performance can be obtained when the controller is redesigned based on the refined model.

A major shortcoming of the mixed-norm design procedure is the inherent computational burden associated with the homotopy algorithm. Basically a predictor-corrector method, the homotopy algorithm requires prediction step sizes that are typically quite small due to the ill-conditioning of the Hessian. In part, the numerical difficulties associated with the often ill-conditioned and indefinite Hessian are due to the use of canonical forms for the compensator dynamics. Transforming the controller to canonical form results in a more poorly conditioned realization which makes optimization of the controller parameters more difficult. Future research should investigate the use of over-parameterized realizations of the controller, as suggested in reference 49. By using a more robust optimization procedure that does not rely on inversion of the Hessian, larger step sizes and more efficient computation could possibly be attained. The robustness of the continuation algorithm developed herein could possibly be improved by using newer curve-tracking homotopy algorithms.[65] Another promising approach is to employ genetic algorithms which are insensitive to both ill-conditioning of the Hessian and saddle points in the search space. To improve the attainable performance, future developments should investigate the incorporation of real parameter uncertainty into the mixed-norm design procedure. Recent advancements in mixed real/complex μ synthesis are promising toward this end.[45] Computational efficiency may also be gained by taking advantage of developments in computer technology such as parallel architectures.

Much like the control design homotopy algorithm, a key shortcoming of the closed-loop system identification procedure is numerical sensitivity. The solution procedure presented herein requires

72

the inversion of a large data matrix which tends to be ill-conditioned. Ensuring full-rank of the data matrix requires sufficiently rich excitation in all of the modes to be identified which is often quite difficult in practice due to limitations such as sensor and actuator dynamics. Methods which do not involve matrix inversion such as genetic algorithms have potential for the closed-loop parameter estimation as well as control design. An additional benefit of genetic algorithms is that the system identification can be operating in the background as part of an autonomous identification/controller tuning process. Future research should be conducted to that end. Finally, the measurement noise properties (intensity, frequency spectrum, etc.) should be explicitly accounted for in the parameter estimation instead of the ad hoc use of ensemble averaging.

APPENDIX A—NUMERICAL OPTIMIZATION FOR ILL-CONDITIONED AND INDEFINITE HESSIANS

Many numerical optimization problems exist where analytical expressions for the function and its first and second derivatives are available. However, numerical determination of the minimum may be quite difficult. In particular, ill-conditioned and/or indefinite Hessians present a challenge for numerical optimization. A modification to the standard Newton optimization algorithm is presented here that effectively accommodates ill-conditioned, indefinite Hessians encountered in the synthesis of fixed-order optimal compensators. Synthesis of the optimal control law involves solution of a set of nonlinear coupled matrix equations that arise in a minimization problem with explicit first and second derivative expressions. However, an accurate initial estimate of the fixed-order compensator gains is often difficult to determine due to factors such as order reduction and transformation to certain parameterizations, which may result in an ill-conditioned or indefinite Hessian. Before describing the optimization procedure, preliminaries on quadratic optimization are presented. A more thorough treatment may be found in a text on numerical optimization such as references 66 and 67.

A.1 Background

In many optimization applications, the objective is to determine the parameter vector $x \in \mathfrak{R}^N$ which minimizes some function $f(x)$. It is assumed that the function is continuous with analytical expressions for the continuous first and second derivatives. The gradient vector and Hessian matrix are given by

$$g(x) = \nabla f(x) \tag{199}$$

and

$$G(x) = \nabla\left(\nabla f(x)^T\right) = \nabla^2 f(x) \ , \tag{200}$$

respectively, where the gradient operator is

$$\nabla(f) = \left[\frac{\partial f}{\partial x_1}, \frac{\partial f}{\partial x_2}, \mathrm{L} \ , \frac{\partial f}{\partial x_N}\right]^T \ . \tag{201}$$

Necessary conditions for a local minimizer, x^*, are that

$$g(x^*) = 0 \tag{202}$$

74

and

$$s^T G(x^*)s \geq 0 \quad s \in \mathfrak{R}^N \ .$$

(203)

The second order necessary condition, equation (203) is sufficient if

$$s^T G(x^*)s > 0 \quad \forall s \neq 0 \ .$$

(204)

The necessary condition requires the Hessian to be positive semidefinite while the sufficient condition requires that the Hessian be positive definite at the local minimum.

Numerical procedures are used to generate a sequence of points, $x^{(k)}$, with the objective of converging to the fixed solution point x^*. Given an estimate of the solution at the kth iteration, $x^{(k)}$, a one-dimensional line search in the direction $s^{(k)}$ is used to find the optimum step size, $\psi^{(k)}$, which minimizes

$$f\left(x^{(k+1)}\right) = f\left(x^{(k)} + \psi^{(k)}s^{(k)}\right) \ .$$

(205)

Typically, the function to be minimized will not be quadratic, but assuming a quadratic approximation (or a quadratic 'model') of the function is often effective for minimization. From the Taylor series expansion of a general function $f(x)$,

$$f(x + \delta) = f(x) + g(x)^T \delta + \frac{1}{2}\delta^T G(x)\delta + o\left(\delta^T \delta\right) \ .$$

(206)

the quadratic model may be obtained by truncating the terms above second order with the resulting error on the order of $\left\|\delta^T \delta\right\|$. Near a minimum, quadratic models accurately represent the function. Even when remote from the minimum, second order information provided by the quadratic model gives insight into the most fruitful search directions. Quadratic models also have the property of invariance under linear transformation which is important for scaling and preconditioning of the Hessian.

Based on the Taylor series approximation of a function truncated to second order, Newton's method defines the search directions of the quadratic model as

$$s^{(k)} = -\left(G^{(k)}\right)^{-1}g^{(k)} \ .$$

(207)

Another means of forming a quadratic model is to utilize search directions that are conjugate to the Hessian, given by

$$s^{(i)T}Gs^{(j)} = 0 \ .$$

(208)

The minimum of a quadratic function can be determined in at most N exact line searches along nonzero conjugate directions (Theorem 2.5.1, reference 66). Several options exist to select the conjugate directions, but one in particular is discussed below.

For the minimum of the quadratic model to exist in $\Re^N$ space, the Hessian must be positive definite. However, when $x^{(k)}$ is "far" from the minimizer x^*, the Hessian may not be positive definite. Ill-conditioning resulting from singularity or near-singularity of the Hessian is a particularly difficult situation which must be dealt with by the numerical optimization procedure. The two issues of indefiniteness and ill-conditioning of the Hessian are the motivation for the algorithm presented in the following section.

A.2 Partitioned Newton Optimization Algorithm

Ill-conditioning of the Hessian is a key difficulty in minimization of quadratic models. The condition number of a matrix is a measure of the closeness of the matrix to singularity and is defined as the ratio of the maximum singular value of the matrix to the minimum singular value, where the singular values of a matrix G are the square roots of the eigenvalues of $G^T G$. Since the eigenvalues of the Hessian are a measure of the curvature of the parameter space along directions defined by the corresponding eigenvectors, small magnitude eigenvalues indicate very slight curvature, or long "valleys" in the parameter space, which require large steps to achieve the minimum.

Choosing the eigenvectors of the Hessian as search directions guarantees that the search directions are orthonormal and conjugate to the Hessian, thereby forming a quadratic model of the type shown in equation (208).[67] When the $x^{(k)}$ is not "close" to the minimum, the Hessian may be indefinite. In this case, Newton's method with one line search in the direction given by equation (207) may not be effective. The directions with positive curvature must be searched independent of the directions with negative curvature to ensure minimization in each direction of the parameter space. Since the indefiniteness of the Hessian indicates that the current estimate, $x^{(k)}$, is remote from the minimum, searching along directions with negative curvature in the direction of decreasing cost may be effective for moving away from critical points such as saddle points.

An optimization scheme that is robust to ill-conditioned and indefinite Hessians is developed which applies Newton's method to a partitioned Hessian. For the symmetric Hessian G,

$$G\Phi = \Phi\Lambda \ ,$$

where the eigenvectors, ϕ_i, and eigenvalues, λ_i, comprise the matrices

$$\Phi = \begin{bmatrix} \phi_1 & \phi_2 & \text{L} & \phi_N \end{bmatrix} \tag{209}$$

and

$$\Lambda = \text{diag}\{\lambda_1, \lambda_2, \text{L}, \lambda_N\} \ . \tag{210}$$

76

The Hessian may be written

$$G = \Phi \Lambda \Phi^T$$

$$= \phi_1 \lambda_1 \phi_1^T + \phi_2 \lambda_2 \phi_2^T + L + \phi_N \lambda_N \phi_N^T \tag{211}$$

$$= \sum_{i=1}^{N} \phi_i \lambda_i \phi_i^T \quad.$$

Since the eigenvectors form a set of N conjugate directions, the minimization problem is to determine

$$\Psi^* = \arg\left[\min_{\Psi} f\left(x^{(k)} + \psi^{(1)}\phi_1 + \psi^{(2)}\phi_2 + L + \psi^{(N)}\phi_N\right)\right]$$

$$= \arg\left[\min_{\Psi} f\left(x^{(k)} + \Phi\Psi\right)\right] \tag{212}$$

where

$$\overline{\Psi} = \left\{ \Psi : \Psi = \begin{bmatrix} \psi^{(1)} & \psi^{(2)} & L & \psi^{(N)} \end{bmatrix}^T \right\} \quad. \tag{213}$$

This minimization problem consists of N one-dimensional line searches to determine the elements of $\Psi^* = \begin{bmatrix} \psi^{(1)*} & \psi^{(2)*} & L & \psi^{(N)*} \end{bmatrix}^T$. Instead of doing N one-dimensional line searches to determine Ψ^*, one could approximate the optimal step size in each direction with one scalar, $\overline{\psi}$, where

$$\overline{\psi} = \arg\min_{\psi} f\left(x^{(k)} + \psi \sum_{i=1}^{N} \phi_i\right) \quad. \tag{214}$$

In contrast with the search direction in Newton's method equation (207), which is a function of the inverse of the Hessian, the search direction formed from the Hessian eigenvectors is given by

$$s^{(k)} = \sum_{i=1}^{N} \phi_i \quad. \tag{215}$$

Although insensitive to near-singularity of the Hessian, this approximation of the step sizes would lead to similar difficulties as Newton's method in that directions with large curvature would dominate and progress would be restricted to a subspace of the parameter space.

A compromise between the approximation of equations (214) and the computational burden of the N one-dimensional line searches in equation (212) is to partition the search space into distinct subspaces with a line search for each subspace. This approach is implemented in the partitioned Newton optimization algorithm, which is formalized below.

By partitioning the eigenvalue and eigenvector matrices in equations (209)–(210) into five matrix partitions as

$$\Phi = \begin{bmatrix} \Phi_1 & \Phi_2 & \Phi_3 & \Phi_4 & \Phi_5 \end{bmatrix} \tag{216}$$

and

$$\Lambda = \text{block diag}\{\Lambda_1, \Lambda_2, L, \Lambda_5\} , \tag{217}$$

from equation (211) the inverse of the Hessian may be partitioned as

$$G^{-1} = \sum_{i=1}^{4} \Phi_i \Lambda_i^{-1} \Phi_i^T \tag{218}$$

and the Newton search directions analogous to equation (207) may be defined as

$$s^{(i)} = -\Phi_i \Lambda_i^{-1} \Phi_i^T g . \tag{219}$$

A.2.1 Algorithm

1. Given an initial estimate $x^{(0)}$, compute the eigenvectors and eigenvalues of the Hessian $G\left(x^{(0)}\right)$ and form Φ and Λ from equations (209)–(210).

2. Partition Φ and Λ according to equations (216)–(217) where:

   - Λ_1 is comprised of "large" positive eigenvalues,
   - Λ_2 is comprised of "small" positive eigenvalues,
   - Λ_3 is comprised of "small" negative eigenvalues,
   - Λ_4 is comprised of "large" negative eigenvalues,
   - Λ_5 is comprised of "near-zero" eigenvalues,

and Φ is compatibly partitioned. The partitions are determined by the intervals

$$\lambda_i > \lambda_{part} \Rightarrow \lambda_i \in \Lambda_1$$

$$\lambda_{tol} < \lambda_i \le \lambda_{part} \Rightarrow \lambda_i \in \Lambda_2$$

$$-\lambda_{part} < \lambda_i < -\lambda_{tol} \Rightarrow \lambda_i \in \Lambda_3$$

$$\lambda_i \le -\lambda_{part} \Rightarrow \lambda_i \in \Lambda_4$$

$$-\lambda_{tol} \le \lambda_i \le \lambda_{tol} \Rightarrow \lambda_i \in \Lambda_5 .$$

To preclude numerical problems due to near zero eigenvalues, λ_{tol} is defined to effectively set these small eigenvalues to zero by neglecting the partition Λ_5 in the search procedure.

3. Do four separate one-dimensional line searches to minimize x according to

$$x^{(i)} = x^{(i-1)} + \psi^{(i)} s^{(i)} ,$$

where

$$s^{(i)} = \Phi_i \Lambda_i^{-1} \Phi_i^T g, \quad \forall i = 1:4 ,$$

and the sign on $s^{(i)}$ is chosen to ensure descent of the cost function. These four searches constitute one iteration with $x^{(4)}$ used as the initial vector, $x^{(0)}$, for the next iteration.

Variations on this algorithm may be adopted where line searches are conducted in some of the individual directions comprising a partitioned eigenvector matrix, Φ_i, but with increased computation. Note that in well-conditioned cases where the Hessian eigenvalues are positive and larger than λ_{part}, this algorithm reduces to Newton's method. The following section presents example problems which demonstrate the utility of the partitioned Newton algorithm.

A.3 Examples

The examples in this section are specifically chosen to highlight ill-conditioned and indefinite Hessians. For the line searches, a golden section search is used and $\lambda_{part} = 1, \lambda_{zero} = 10^{-8}$. The stopping criteria for each test case is based on the relative change in cost between iterations and is given by

$$\frac{f\left(x^{(k-1)}\right) - f\left(x^{(k)}\right)}{f\left(x^{(k-1)}\right)} < 10^{-8} .$$

The first two examples are from reference 66, the third is from reference 67, and the fourth is an optimal control design.

Example 1:

$$f(x) = 100\left(x_2 - x_1^2\right)^2 + \left(1 - x_1\right)^2 .$$

This function is known as Rosenbrock's function and is a well-known test function for optimization methods. Located in a steep-sided parabolic valley, the minimum of this function occurs at $x^* = [1,1]^T$. The Hessian is singular when $x_2 - x_1^2 = 0.005$, so an extreme test case is to define the starting point as $x_0 = [0,0.005]^T$. From this initial point, Newton's method did not improve the cost and terminated after one iteration due to the singular Hessian. However, after 13 iterations, the partitioned Newton algorithm converged to the minimum, accurate to nine decimal places. Figure 34 graphically depicts the convergence achieved using the partitioned Newton algorithm.
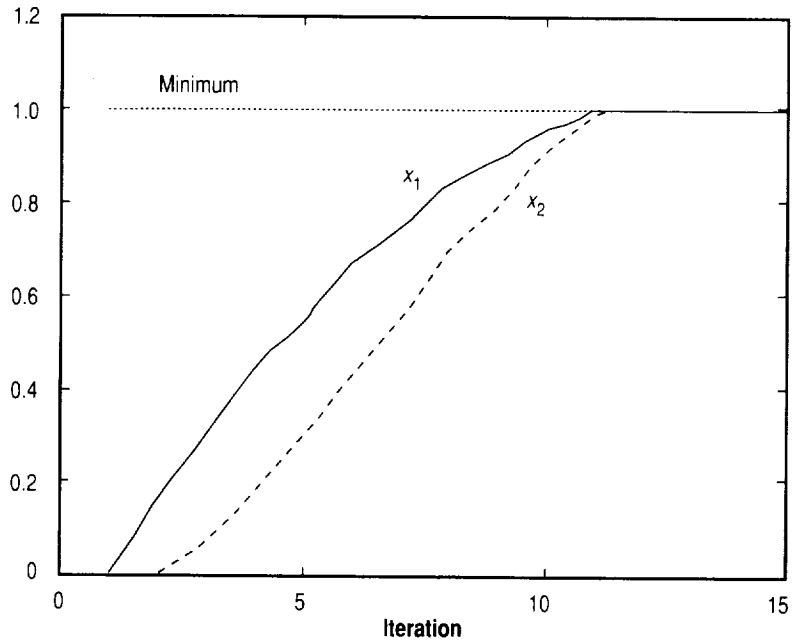
Figure 34. Convergence of Rosenbrock problem with partitioned Newton optimization.

Example 2:

$$f(x) = x_1^4 + x_1 x_2 + (1 + x_2)^2 .$$

For this example, an initial choice is

$$x_0 = [0,0]^T \Rightarrow g = [0,2]^T, \quad G = \begin{bmatrix} 0 & 1 \\ 1 & 2 \end{bmatrix} . \tag{220}$$

At this starting point, the Hessian is indefinite. The search direction from Newton's method is $s = [-2,0]^T$ which results in termination since no improvement can be made in the x_2 direction. The partitioned algorithm breaks this into two orthonormal search directions given by

$$\lambda_1 = 2.4142, \qquad s_1 = [-0.38268,-0.92388]^T$$

$$\lambda_2 = -0.4142, \qquad s_2 = [0.92388,-0.38268]^T .$$

Table 5 indicates the rapid convergence of the partitioned algorithm to the minimum, even though the Hessian is initially indefinite.

Table 5. Convergence of x for partitioned Newton method in example 2.

Iteration	x_1	x_2
0	0.0	0.0
1	0.6367312144637250	-1.075920796208131
2	0.7011674364048575	-1.3467638098297626
3	0.6959277688023086	-1.347963884399868
4	0.6958843926891740	-1.347942196344587
5	0.6958843897926642	-1.347942194896332

Example 3:

$$f(x) = 100\left(x_2 - x_1^2\right)^2 + \left(1 - x_1\right)^2 + 90\left(x_4 - x_3^2\right)^2 + \left(1 - x_3\right)^2$$

$$+ 10.1\left[\left(x_2 - 1\right)^2 + \left(x_4 - 1\right)^2\right] + 19.8\left(x_2 - 1\right)\left(x_4 - 1\right). \tag{221}$$

This example is known as Wood's function and is originally attributed to reference 68. Wood's function is much like Rosenbrock's function except with four parameters. Beginning at $x_0 = [3, -10, -5, 10]^T$, Newton's method did not converge to the minimum at $x^* = [1, 1, 1, 1]^T$ but terminated after 14 iterations at $x = [0.83, -2.31, -5.32, 25.84]^T$. Figure 35 indicates that the partitioned algorithm successfully found the minimizer x^*. The piecewise constant rate of convergence is indicated in figure 36. It is interesting to note that from x_0, the Hessian remained significantly indefinite with the minimum eigenvalue ranging from $-1.36e{-4}$ to -87.7 and the partitioned optimization algorithm continued to converge to the minimizer.
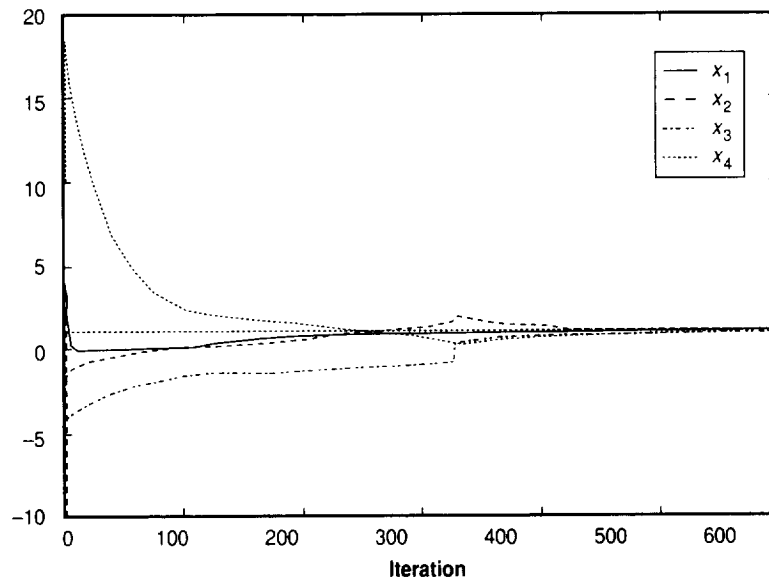

Figure 35. Convergence of Wood problem with partitioned Newton optimization.
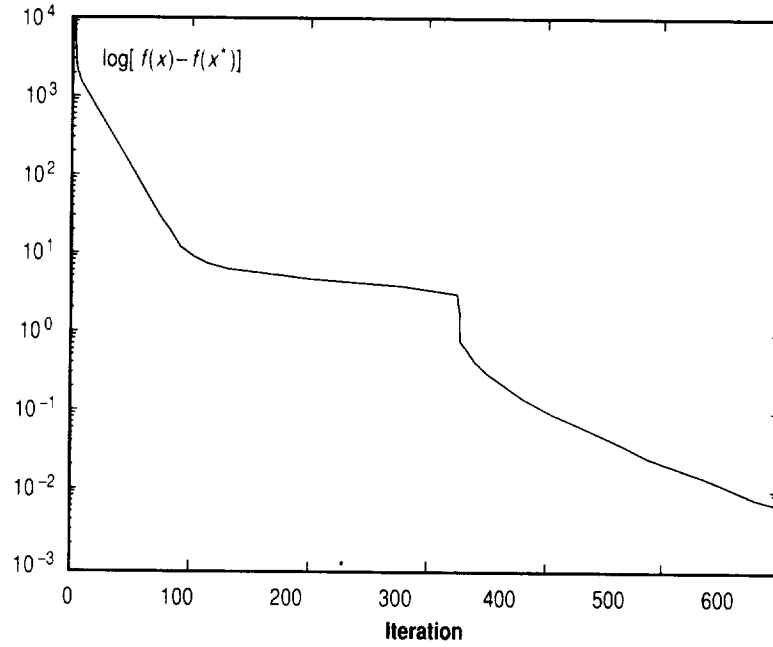
Figure 36. Rate of convergence of Wood problem with partitioned Newton optimization.

It should be pointed out that with some initial conditions for these functions, Newton's method converged more rapidly than the partitioned algorithm, but no case has been observed where the partitioned method did not converge.

Example 4:

The final example demonstrates the partitioned Newton optimization algorithm in the context for which it was developed, optimization of fixed-order dynamic compensators. The problem is to design an H_2 controller for the coupled mass problem introduced in section 6. Section 3 presents the formulation of the fixed-order H_2-optimal control problem with the gradient and Hessian expressions developed as a special case of the fixed-order mixed H_2 / H_∞ control problem. This optimization algorithm comprises the local correction step of the homotopy algorithm introduced in section 4.

For this example, the plant is described by equations (191)–(192) for A and B_2, respectively, with $k_1 = k_2 = 1.2$, $m_1 = m_2 = 1.5$, and $\zeta_1 = \zeta_2 = 0.1$. The remaining plant matrices are

$$B_1 = \begin{bmatrix} I & 0 \end{bmatrix}, \quad C_1 = \begin{bmatrix} I & 0 \end{bmatrix}^T, \quad D_{11} = 0, \quad D_{12} = \begin{bmatrix} 0 & \rho I \end{bmatrix}, \quad D_{21} = \begin{bmatrix} 0 & I \end{bmatrix}, \quad D_{22} = 0 \quad , \tag{222}$$

where ρ is used to vary the control authority.

In order to illustrate the distinction between the partitioned Newton algorithm and Newton's method, an initial controller is selected to be remote from the minimum. The desired controller is for $\rho = 0.01$ and the initial controller is selected as the exact solution for the lower authority case

is for $\rho = 0.01$ and the initial controller is selected as the exact solution for the lower authority case with $\rho = 10$. Convergence is defined to occur when the relative change in cost between iterations is less than 5×10^{-7}.

Figure 37 illustrates the convergence of the gradient toward zero with the partitioned Newton algorithm as well as the termination of the Newton optimization remote from the minimum. Figure 38 presents the comparison of the convergence of the (2,1) element of the controller gain matrix, G, to the exact value with both the partitioned Newton method and the Newton method. Clearly, the Newton optimization does not converge to the correct value. For this example, the difficulty in convergence is due to the near-singularity of the Hessian which produces large erroneous correction steps with Newton's method. These results strongly indicate the deficiencies of an optimization algorithm that uses second order information and assumes a positive definite Hessian (such as Newton's method). The partitioned Newton algorithm presented herein is better suited for these problems by accounting for ill-conditioned and indefinite Hessians.
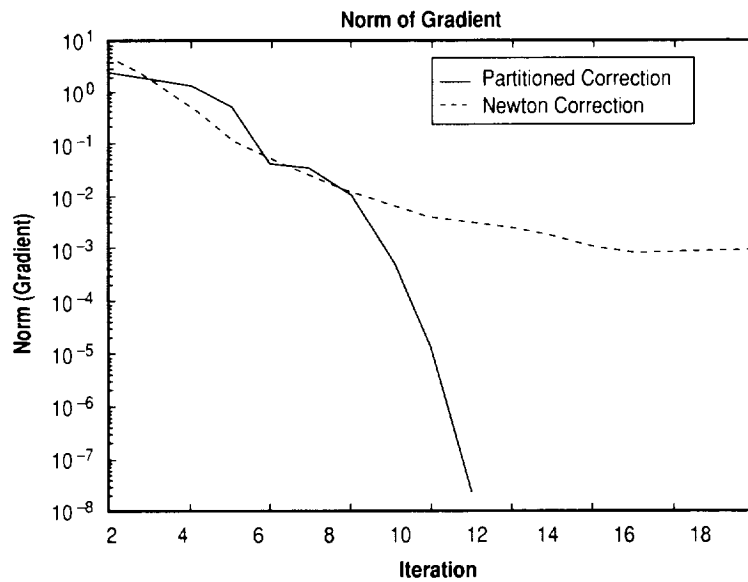

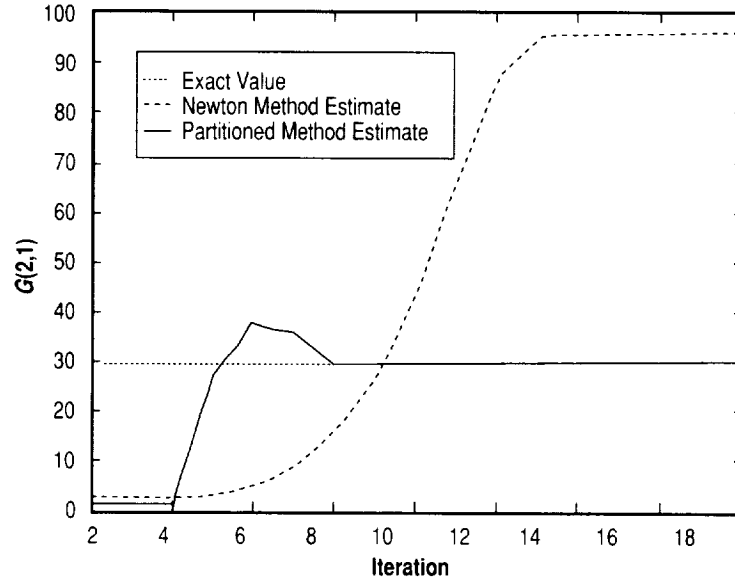Figure 37. Convergence of gradient for control design.

Figure 38. Convergence of control gain estimate.

The initial and exact final controller gains for the controller in the controller canonical form (defined in equation (35)) are

$$G_0 = \begin{bmatrix} 0.4073 & -0.6215 & -0.0003 & -0.3032 \\ 2.3727 & 4.1798 & 4.3888 & 2.2904 \end{bmatrix} \tag{223}$$

$$G_{exact} = \begin{bmatrix} 8.3899 & -37.0769 & -1.2240 & -13.8905 \\ 29.5261 & 40.7987 & 27.6252 & 9.8040 \end{bmatrix} . \tag{224}$$

Using the partitioned Newton method, after 11 iterations the percent error in each element is

$$G_{error} = \begin{bmatrix} 0.0562 & 0.0650 & 0.1305 & 0.0671 \\ 0.0637 & 0.0613 & 0.0608 & 0.0637 \end{bmatrix} \text{ percent} . \tag{225}$$

The Newton method terminated after 18 iterations with percent error

$$G_{error} = \begin{bmatrix} 224 & 215 & 698 & 195 \\ 223 & 253 & 245 & 275 \end{bmatrix} \text{ percent} . \tag{226}$$

84

REFERENCES

1. Bernstein, D.S.; and Haddad, W.M.: "LQG Control With an H_∞ Performance Bound: A Riccati Equation Approach." *IEEE Transactions on Automatic Control*, Vol. 34, pp. 293–305, March 1989.

2. Sharkey, J.P.; Nurre, G.S.; Beals, G.P.; and Nelson, J.D.: "A Chronology of the On-Orbit Pointing Control System Changes on the Hubble Space Telescope and Associated Pointing Improvements." In *Proceedings of The AIAA Guidance, Navigation and Control Conference*, Hilton Head, SC, August 1992.

3. Skelton, R.E.: "Model Error Concepts in Control Design." *International Journal of Control*, Vol. 49(5), pp. 1725–1753, 1989.

4. Doyle, J.C.: "Analysis of Feedback Systems With Structured Uncertainties." In *Proc. IEE-D 129*, pp. 242–250, 1982.

5. Doyle, J.C.: "Lecture Notes on Advances in Multivariable Control." Technical Report, ONR/ Honeywell Workshop on Advances in Multivariable Control, Minneapolis, MN, October 1984.

6. Doyle, J.C.; and Chu, C.C.: "Robust Control of Multivariable and Large Scale Systems." Technical Report, AFOSR. Final Technical Report for Contract No. F49620–84–C–0088, March 1986.

7. Bernstein, D.S.; and Hyland, D.C.: "Optimal Projection for Uncertain Systems (OPUS): A Unified Theory of Reduced-Order Robust Control Design." In *Large Space Structures: Dynamics and Control*, S.N. Atluri and A.K. Amos, editors, pp. 263–302. Springer-Verlag, New York, 1988.

8. Collins, Jr., E.G.; Haddad, W.M.; and Ying, S.S.: "Reduced-Order Dynamic Compensation Using the Hyland and Bernstein Optimal Projection Equations." *Journal of Guidance, Control, and Dynamics*, Vol. 19(2), pp. 407–417, 1996.

9. Ridgely, D.B.; Canfield, R.A.; Walker, D.E.; and Smith, L.D.: "The Fixed Order Mixed H_2 / H_∞ Control Problem: Development and Numerical Solution." *The International Journal of Robust and Nonlinear Control*. Submitted for publication.

10. Haddad, W.M.; and Bernstein, D.S.: "Generalized Riccati Equations for the Full- and Reduced-Order Mixed-Norm H_2 / H_∞ Standard Problem." *Systems & Control Letters*, Vol. 14, pp. 185–197, 1990.

11. Bernstein, D.S.; Haddad, W.M.; and Nett, C.N.: "Minimal Complexity Control Law Synthesis, Part 2: Problem Solution via H_2 / H_∞ Optimal Static Output Feedback." In *Proceedings of The American Control Conference*, pp. 2506–2511, 1989.

12. Rotea, M.A.; and Khargonekar, P.P.: " H_2-Optimal Control With an H_∞ Constraint: The State Feedback Case." *Automatica*, Vol. 27(2), pp. 307–316, 1991.

13. Jacques, D.R.; Ridgely, D.B.; Canfield, R.A.; and Spillman, M.S.: "A MATLAB™ Toolbox for Fixed Order, Mixed-Norm Control Synthesis." *Control Systems Magazine*, Vol. 16(5), October 1996.

14. Sweriduk, G.D.; and Calise, A.J.: "A Differential Game Approach to the Mixed H_2 / H_∞ Problem." In *Proceedings of The AIAA Guidance, Navigation and Control Conference*, pp. 1072–1081, 1994.

15. Davis, L.D.; Collins, Jr., E.G.; and Haddad, W.M.: "Discrete-Time, Mixed-Norm H_2 / H_∞ Controller Synthesis." *Optimal Control Application and Methods*, Vol. 17(2), pp. 107–122, 1996.

16. Ge, Y.; Collins, Jr., E.G.; and Bernstein, D.S.: "Probability-One Homotopy Algorithms for Full- and Reduced-Order H_2 / H_∞ Controller Synthesis." *Optimal Control Application and Methods*, Vol. 17, pp. 187–208, 1996.

17. Balas, G.J.; and Doyle, J.C.: "Robust Control of Flexible Modes in the Controller Crossover Region." In *Proceedings of The American Control Conference*, June 1989.

18. Schrama, R.J.P.: "Accurate Identification for Control: The Necessity of an Iterative Scheme." *IEEE Transactions on Automatic Control*, Vol. 37(7), pp. 991–994, July 1992.

19. Liu, K.; and Skelton, R.E.: "Closed Loop Identification and Iterative Controller Design." In *Proceedings of The IEEE Conference on Decision and Control*, pp. 482–487, December 1990.

20. Phan, M.; Juang, J.N.; Horta, L.G.; and Longman, R.W.: "System Identification From Closed-Loop Data With Known Output Feedback Dynamics." *Journal of Guidance, Control, and Dynamics*, Vol. 17(4), pp. 661–669, 1994.

21. Bosse, A.B.: "Identification of Flexible Structures Under Closed Loop Control." Ph.D. thesis, The University of Cincinnati, Cincinnati, OH, January 1993.

22. Huang, J.K.; Lee, H.C.; Schoen, M. P.; and Hsiao, M.H.: "State-Space System Identification From Closed Loop Frequency Response Data." *Journal of Guidance, Control, and Dynamics*, Vol. 19(6), pp. 1378–1380, November 1996.

23. Van Den Hof, P.M.J.; and Schrama, R.J.P.: "Identification and Control—Closed Loop Issues." *Automatica*, Vol. 31(12), pp. 1751–1770, 1995.

24. Ljung, L.: "System Identification: Theory for the User." Prentice-Hall, Inc., Englewood Cliffs, NJ, 1987.

25. Zang, Z.; Bitmead, R.; and Gevers, M.: "H_2 Iterative Model Refinement and Control Robustness Enhancement." In *Proceedings of The IEEE Conference on Decision and Control*, pp. 279–284, 1991.

26. Hansen, F.R.; and Franklin, G.F.: "On a Fractional Representation Approach to Closed Loop Experiment Design." In *Proceedings of The American Control Conference*, pp. 1319–1320, 1988.

27. Hansen, F.R.; Franklin, G.F.; and Kosut, R.: "Closed Loop Identification via the Fractional Representation: Experiment Design." In *Proceedings of The American Control Conference*, pp. 1422–1427, 1989.

28. Schrama, R.J.P.: "An Open Loop Solution to the Approximate Closed-Loop Identification Problem. In *Proceedings of 9th IFAC/IFORS Symposium of Identification and System Parameter Estimation*, pp. 1602–1607, 1991.

29. Schrama, R.J.P.: "Approximate Identification and Control Design." Ph.D. thesis, Delft University of Techology, The Netherlands, 1992.

30. Anderson, B.D.O.; and Kosut, R.L.: "Adaptive Robust Control: On-Line Learning." In *Proceedings of The IEEE Conference on Decision and Control*, pp. 297–298, 1991.

31. Van Den Hof, P.M.J.; Schrama, R.J.P.; de Callafon, R.A.; and Bosgra, O.H.: "Identification of Normalized Coprime Factors from Closed Loop Experiment Data." In *Proceedings of The IEEE Conference on Decision and Control*, 1995.

32. Francis, B.A.: "A Course in H_∞ Control Theory." Springer-Verlag, Berlin, 1987.

33. Doyle, J.C.; Glover, K.; Khargonekar, P.P.; and Francis, B.A.: "State-Space Solutions to Standard H_2 and H_∞ Control Problems." *IEEE Transactions on Automatic Control*, Vol. 34(8), pp. 831–847, August 1989.

34. Maciejowski, J.M.: "Multivariable Feedback Design." Addison Wesley, 1989.

35. Morari, M.; and Zafiriou, E.: "Robust Process Control." Prentice-Hall, Inc., 1989.

36. Haddad, W.M.; Collins, Jr., E.G.; and Moser, R.: "Structured Singular Value Controller Synthesis Using Constant D-Scales Without D–K Iteration." *International Journal of Control*, Vol. 63(4), pp. 813–830, 1996.

37. Haddad, W.M.; How, J.P.; Hall, S.R.; and Bernstein, D.S.: "Extensions of Mixed-μ Bounds to Monotonic and Odd Monotonic Nonlinearities Using Absolute Stability Theory." In *Proceedings of The IEEE Conference on Decision and Control*, Tucson, AZ, 1992.

38. Haddad, W.M.; How, J.P.; Hall, S.R.; and Bernstein, D.S.: "Extensions of Mixed-μ Bounds to Monotonic and Odd Monotonic Nonlinearities Using Absolute Stability Theory." *International Journal of Control*, Vol. 60(5), pp. 905–951, 1994.

39. How, J.P.; Haddad, W.M.; and Hall, S.R.: "Application of Popov Controller Synthesis to Benchmark Problems With Real Parameter Uncertainty." *Journal of Guidance, Control, and Dynamics*, Vol. 17(4), pp. 759–768, July/August 1994.

40. Haddad, W.M., and Bernstein, D.S.: "Parameter-Dependent Lyapunov Functions and the Popov Criterion in Robust, Analysis and Synthesis. *IEEE Transactions on Automatic Control*, Vol. AC–40, pp. 536–543, 1995.

41. Collins, Jr., E.G.; Haddad, W.M.; Watson, L.T.; and Sadhukhan, D.: "Probability-One Homotopy Algorithms for Robust Controller Synthesis With Fixed-Structure Multipliers." *International Journal of Robust and Nonlinear Control*, Vol. 7, pp. 165–185, 1997.

42. Kramer, F.S.; and Calise, A.J.: "Fixed-Order Dynamic Compensation for Multivariable Linear Systems." *Journal of Guidance, Control, and Dynamics*, Vol. 11(1), pp. 80–85, 1988.

43. Denery, D.G.: "Identification of System Parameters From Input-Output Data With Application to Air Vehicles." Ph.D. thesis, Stanford University, May 1971.

44. Mustafa, D.: "Relations Between Maximum Entropy/H_∞ Control and Combined H_∞/LQG Control." *Systems & Control Letters*, Vol. 12, pp. 193–203, 1989.

45. Buschek, H.: "Synthesis of Fixed-Order Controllers With Robustness to Mixed Real/Complex Uncertainties." Ph.D. thesis, The Georgia Institute of Technology, Atlanta, GA, February 1995.

46. Whorton, M.S.; Calise, A.J.; and Hsu, C.C.: "A Study of Fixed Order Mixed Norm Designs for a Benchmark Problem in Structural Control." *Earthquake Engineering and Structural Dynamics*, accepted for publication.

47. Walker, D.E.; and Ridgely, D.B.: "Mixed H_2 / μ Optimization." *Journal of Guidance, Control, and Dynamics*, submitted for publication.

48. Whorton, M.S.; Buschek, H.; and Calise, A.J.: "Development of Homotopy Algorithms for Fixed Order Mixed H_2 / H_∞ Controller Synthesis." NASA TP–3507, September 1994.

49. Collins, Jr., E.G.; Davis, L.D.; and Richter, S.L.: "Design of Reduced-Order H_2 Optimal Controllers Using a Homotopy Algorithm." *International Journal of Control*, Vol. 61(1), pp. 97–126, 1996.

50. Mercadal, M.: "Homotopy Approach to Optimal, Linear Quadratic, Fixed Architecture Compensation." *Journal of Guidance, Control, and Dynamics*, Vol. 14(6), pp. 1224–1233, 1991.

51. Richter, S.L.; and DeCarlo, R.A.: "Continuation Methods: Theory and Applications." *IEEE Transactions on Circuits and Systems*, Vol. CAS–30(6), pp. 347–352, June 1983.

52. Collins, Jr., E.G.; Haddad, W.M.; and Ying, S.S.: "Nearly Nonminimal Linear Quadratic Gaussian Reduced-Order Control Design Initialization." *Journal of Guidance, Control, and Dynamics*, Vol. 19(1), pp. 259–262, 1996.

53. Cannon, Jr., R.H.; and Rosenthal, D.E.: "Experiments in Control of Flexible Structures With Noncolocated Sensors and Actuators." *Journal of Guidance, Control, and Dynamics*, Vol. 7(5), pp. 546–553, 1984.

54. Seinfield, D.R.; Haddad, W.M.; Bernstein, D.S.; and Nett, C.N.: "H_2 / H_∞ Controller Synthesis: Illustrative Numerical Results via Quasi-Newton Methods." In *Proceedings of The American Control Conference*, Boston, MA, June 1991.

55. Spencer, Jr., B.F.; Dyke, S.J.; and Deoskar, H.S.: "Benchmark Problems in Structural Control." In *Proceedings of the ASCE Structures Conference*, 1997.

56. Balas, G.J.; Doyle, J.C.; Glover, K.; Packard, A.; and Smith, R.: "μ-Analysis and Synthesis Toolbox." *The Mathworks*, 1993.

57. Balas, G.J.: "Robust Control of Flexible Structures: Theory and Experiments." Ph.D. Thesis, The California Institute of Technology, Pasadena, CA, 1990.

58. Juang, J.N.; Cooper, J.E.; and Wright, J.R.: "An Eigensystem Realization Algorithm Using Data Correlation (ERA/DC) for Modal Parameter Identification." *Control Theory and Advanced Technology*, Vol. 4(1), 1988.

59. Junag, J.N.; Horta, L.G.; and Phan, M.: "System/Observer/Controller Identification Toolbox." NASA Technical Memorandum 107566, February 1992.

60. Anderson, J.B.; Driskill, T.C.; Jefferson, P.; and Lassiter, J.O.: "Controls, Astrophysics, and Structures Experiment in Space (CASES) Mast Modal Survey Test Report." Technical Report LSS (CASES)–DEV–ED92–001, NASA MSFC, February 1992.

61. Rice, S.C.: "CSI GTF Finite Element Report." Technical Report, Logicon Control Dynamics, January 1993.

62. Luenberger, D.G.: "Canonical Forms for Linear Multivariable Systems." *IEEE Transactions on Automatic Control*, Vol. AC–12(3), pp. 290–293, June 1967.

63. Kailath, T.: "Linear Systems." Prentice-Hall, Inc., 1980.

64. Wie, B.; and Bernstein, D.S.: "Benchmark Problems for Robust Control Design." *Journal of Guidance, Control, and Dynamics*, Vol. 15(5), pp. 1057–1059, 1992.
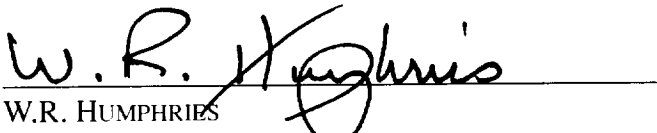
65. Watson, L.T.; Sosonkina, M.; Melville, R.C.; Morgan, A.P.; and Walker, H.F.: "Hompack90: A Suite of Fortran 90 Codes for Globally Convergent Homotopy Algorithms." *ACM Transactions on Mathematical Software*, to appear.

66. Fletcher, R.: "Practical Methods of Optimization, Volume 1." John Wiley & Sons, NY, 1980.

67. Brent, R.P.: "Algorithms for Minimization Without Derivatives." Prentice-Hall, Englewood Cliffs, NJ, 1973.

68. Collville, A.R.: "A Comparative Study of Nonlinear Programming Codes." Technical Report 320–2949, IBM New York Scientific Center, 1968.

APPROVAL

HIGH PERFORMANCE, ROBUST CONTROL OF FLEXIBLE SPACE STRUCTURES
(MSFC Center Director's Discretionary Fund Final Report, Project No. 96–23)

M.S. Whorton

The information in this report has been reviewed for technical content. Review of any information concerning Department of Defense or nuclear energy activities or programs has been made by the MSFC Security Classification Officer. This report, in its entirety, has been determined to be unclassified.

W.R. HUMPHRIES
DIRECTOR, STRUCTURES AND DYNAMICS LABORATORY

REPORT DOCUMENTATION PAGE

Form Approved
OMB No. 0704-0188

1. AGENCY USE ONLY *(Leave Blank)*	2. REPORT DATE May 1998	3. REPORT TYPE AND DATES COVERED Technical Memorandum

4. TITLE AND SUBTITLE	5. FUNDING NUMBERS
High Performance, Robust Control of Flexible Space Structures (MSFC Center Director's Discretionary Fund Final Report, Project No. 96–23)	

6. AUTHORS

M.S. Whorton

7. PERFORMING ORGANIZATION NAMES(S) AND ADDRESS(ES)	8. PERFORMING ORGANIZATION REPORT NUMBER
George C. Marshall Space Flight Center Marshall Space Flight Center, Alabama 35812	M–865

9. SPONSORING/MONITORING AGENCY NAME(S) AND ADDRESS(ES)	10. SPONSORING/MONITORING AGENCY REPORT NUMBER
National Aeronautics and Space Administration Washington, DC 20546–0001	NASA/TM—1998–207945

11. SUPPLEMENTARY NOTES

Prepared by Structures and Dynamics Laboratory, Science and Engineering Directorate

12a. DISTRIBUTION/AVAILABILITY STATEMENT	12b. DISTRIBUTION CODE
Unclassified–Unlimited Subject Category 18 Nonstandard Distribution	

13. ABSTRACT *(Maximum 200 words)*

Many spacecraft systems have ambitious objectives that place stringent requirements on control systems. Achievable performance is often limited because of difficulty of obtaining accurate models for flexible space structures. To achieve sufficiently high performance to accomplish mission objectives may require the ability to refine the control design model based on closed-loop test data and tune the controller based on the refined model. A control system design procedure is developed based on mixed H_2/H_∞ optimization to synthesize a set of controllers explicitly trading between nominal performance and robust stability. A homotopy algorithm is presented which generates a trajectory of gains that may be implemented to determine maximum achievable performance for a given model error bound. Examples show that a better balance between robustness and performance is obtained using the mixed H_2/H_∞ design method than either H_2 or mu-synthesis control design. A second contribution is a new procedure for closed-loop system identification which refines parameters of a control design model in a canonical realization. Examples demonstrate convergence of the parameter estimation and improved performance realized by using the refined model for controller redesign. These developments result in an effective mechanism for achieving high-performance control of flexible space structures.

14. SUBJECT TERMS		15. NUMBER OF PAGES
robust control, mixed H_2/H_∞ control theory, parameter optimization, homotopy methods		100
		16. PRICE CODE A05

17. SECURITY CLASSIFICATION OF REPORT	18. SECURITY CLASSIFICATION OF THIS PAGE	19. SECURITY CLASSIFICATION OF ABSTRACT	20. LIMITATION OF ABSTRACT
Unclassified	Unclassified	Unclassified	Unlimited